C.2

TECHNICAL REPORT
NATICK/TR-93/002

AD A257 953

METHODS FOR IMPROVED AIRBAG PERFORMANCE FOR AIRDROP

by
Calvin K. Lee

October 1992

Final Report
October 1989 - September 1991

UNITED STATES ARMY NATICK
RESEARCH, DEVELOPMENT AND ENGINEERING CENTER
NATICK, MASSACHUSETTS 01760-5000

AERO-MECHANICAL ENGINEERING DIRECTORATE

DISCLAIMERS

The findings contained in this report are not to be construed as an official Department of the Army position unless so designated by other authorized documents.

Citation of trade names in this report does not constitute an official endorsement or approval of the use of such items.

DESTRUCTION NOTICE

For Classified Documents:

Follow the procedures in DoD 5200.22-M, Industrial Security Manual, Section II-19 or DoD 5200.1-R, Information Security Program Regulation, Chapter IX.

For Unclassified/Limited Distribution Documents:

Destroy by any method that prevents disclosure of contents or reconstruction of the document.

REPORT DOCUMENTATION PAGE

Form Approved
OMB No. 0704-0188

1. AGENCY USE ONLY (Leave blank)	2. REPORT DATE	3. REPORT TYPE AND DATES COVERED
	October 1992	Final Report, Oct 89 - Sep 91

4. TITLE AND SUBTITLE

Methods for Improved Airbag Performance for Airdrop

5. FUNDING NUMBERS

PE: 1L162786
PR: D283
WU: AH002
AG CODE: T/B1346

6. AUTHOR(S)

Calvin K. Lee

7. PERFORMING ORGANIZATION NAME(S) AND ADDRESS(ES)

U.S. Army Natick Research, Development and Engineering Ctr
Kansas Street, ATTN: SATNC-UE
Natick, MA 01760-5017

8. PERFORMING ORGANIZATION REPORT NUMBER

NATICK/TR-93/002

9. SPONSORING/MONITORING AGENCY NAME(S) AND ADDRESS(ES)

10. SPONSORING/MONITORING AGENCY REPORT NUMBER

11. SUPPLEMENTARY NOTES

12a. DISTRIBUTION/AVAILABILITY STATEMENT

Approved for public release,
distribution is unlimited.

12b. DISTRIBUTION CODE

13. ABSTRACT (Maximum 200 words)

Airbags are currently being investigated as a ground impact energy absorber for U.S. Army airdrops. Simple airbags with constant vent areas have been studied previously by numerous investigators. In this research effort, a method of controlling the vent area and a method of injecting gas into a simple airbag to improve its performance, i.e., to decrease its peak G force, were analytically and experimentally investigated. In addition, augmented simple airbags using paper honeycomb as an auxiliary energy absorber were also experimentally investigated. Complex airbags using vent-control and gas-injection and augmented airbags were found to decrease the peak G forces of simple airbags by 30%. Results of these investigations are presented in this report.

14. SUBJECT TERMS			15. NUMBER OF PAGES
Airbags	Test and evaluation	Energy absorbers	116
Soft landing	Impact attenuation	Ground impact	16. PRICE CODE
	Airdrop Operations		

17. SECURITY CLASSIFICATION OF REPORT	18. SECURITY CLASSIFICATION OF THIS PAGE	19. SECURITY CLASSIFICATION OF ABSTRACT	20. LIMITATION OF ABSTRACT
Unclassified	Unclassified	Unclassified	Unlimited

TABLE OF CONTENTS

LIST OF FIGURES

LIST OF FIGURES (Cont'd)

LIST OF FIGURES (Cont'd)

LIST OF TABLES

PREFACE

The present investigation, Advanced Pneumatic Techniques for Impact Energy Absorption, was conducted by the author in the Engineering Technology Division of the Aero-Mechanical Engineering Directorate (AMED) from October 1, 1989 to September 30, 1991 under Program Element: 1L162786, Project No. D283, Work Unit: AH002, and Aggregate Code: T/B1346.

Airbags are being considered by the U.S. Army as an alternative to the paper honeycomb currently used for soft landing of airdropped payloads. This report summarizes some of the 6.2 work effort conducted to achieve this goal.

Numerous AMED personnel contributed to this work effort. They include Nicholas P. Rosato, John R. Doucette, and Joseph Silva. In addition, Professor Francis Lai of University of Massachusetts, Lowell, MA and Eric Michelson of Canton High School, Canton, MA also contributed to this work. The valuable contributions of all these workers are greatly appreciated.

The citation of trade names in this report does not constitute official endorsement or approval of use of an item or product.

LIST OF SYMBOLS

a	acceleration
A_v	air vent area
C_D	discharge coefficient
g	gravitational acceleration
G	retardation force on payload from airbag
h	airbag height
H	drop height
l	airbag length
$\dot{m}_e$	gas exhaust rate at vent area
$\dot{m}_i$	gas injection rate
$\overline{\dot{m}_i}$	time-averaged gas injection rate
M	payload mass
P_i	initial tank air pressure
P_f	final tank air pressure
P	air pressure
q	air velocity at vent area
t	time
t_f	amount of time to compress the entire airbag height (stroke time)
t_i	gas injection time
u	vertical payload descent velocity
w	airbag width

y	free drop height
ρ	air density

Subscripts

o	time zero when airbag touches ground
v	at vent area
p	peak value

METHODS FOR IMPROVED AIRBAG PERFORMANCE FOR AIRDROP

Introduction

The steady descent velocity of a payload airdropped by U.S. Army parachutes is about 28 ft/s (Fig. 1). During ground impact at this velocity, an energy absorber is needed to dissipate some of the impact energy and to provide structural protection for the payload. The U.S. Army currently uses paper honeycomb as the energy absorber. Strategic positioning of paper honeycomb between the payload, such as a vehicle, and the platform is a time-consuming and labor intensive process[1] (Fig. 2). Airbags are presently being investigated by the U.S. Army as an alternative impact energy absorber for airdrop.[2,3,4]

An airbag, in its simplest form, is a fabric enclosure with a constant vent opening. When the bag is attached to the underside of an airdrop platform and compressed at ground impact, its air pressure increases from one atmosphere as air is vented through the fixed vent opening (Fig. 3A). The high-pressure air decelerates the payload by applying a retarding force via the platform. A one-dimensional analysis of simple airbags was given by Browning.[5] One major problem of simple airbags is that a large portion of the airbag stroke (height) is used to compress the air from atmospheric pressure to a peak pressure. This often results in a bag height that is susceptible to ground winds and payload tipover during ground impact. Furthermore, the pressure-time or retardation force - time profile is an inefficient triangular shape (as compared to the efficient rectangular shape provided by paper honeycomb).[2,3]

Three methods are currently being investigated to improve the performance of simple airbags for Army airdrop. The first method involves controlling the air release rate by decreasing the air vent area during the airbag stroke (Fig. 3B). This method was mentioned[5] and theoretically studied.[4] But it has never been examined experimentally. The second method requires injecting gas into the airbag during the stroke (Fig. 3C). In the present study, analytical and experimental investigations of complex airbags using vent-control and gas-injection were conducted. The third method introduces and combines an auxiliary energy absorber with a simple airbag. This method was experimentally investigated using paper honeycomb as the auxiliary energy absorber. In addition, simple airbags with constant vents were also investigated for comparison with the three methods. Results of these investigations are presented in this report.

General Approach

Simple airbags are generally constructed in a vertical circular cylindrical shape. Multiples of these airbags are connected to the underside of a platform to provide cushioning for the payload. From a complex-airbag viewpoint, it is complicated and impractical to provide multiple air-vent or gas-injection controls for multiple complex airbags. In addition, if multiple airbags are to be used where paper honeycomb is being used now, i.e., between the payload (such as a vehicle) and the platform, circular cylindrical airbags will most likely not be the appropriate shape. With these thoughts in mind, the author chose rectangular-shaped airbags, which can be used either below the platform or between the payload and the platform, for the present investigation.

Fig. 4A shows a rectangular airbag with initial height h_o, length 1, and width w, supporting a payload mass M via a platform. The entire system is descending vertically with a velocity u_o.

Before ground impact, the air pressure inside the airbag is at atmospheric pressure P_o. During ground impact (Fig. 4B), the airbag is compressed to height h, and the increased air pressure P decelerates the payload velocity to u. For a simple airbag, the vent area A_v is constant. For a vent-control complex airbag, A_v is a function of time t and the gas injection rate, $\dot{m}_i$, is zero. For a gas-injection complex airbag, $\dot{m}_i$ is finite and A_v is constant.

As an initial investigation, the one-dimensional approach and assumptions employed by Browning[5] were used in the present airbag study. The two ordinary differential equations governing the motion of a simple airbag as shown in Fig. 4 are:

Air flow equation:

$$\rho_V A_V q C_D = -\frac{d}{dt}(\rho h w l) \tag{1}$$

Payload motion equation:

$$M\frac{d^2h}{dt^2} = -Mg + (\frac{P}{P_o} - 1)P_o w l \tag{2}$$

Eq. (1) describes the amount of air being vented as the airbag is compressed. Eq. (2) describes the deceleration of the payload provided by the airbag. For a given simple airbag/payload system and its steady descending velocity before ground impact, the two unknowns in Eqs. (1) and (2) are bag height, h(t), and air pressure, P(t). Theoretical performance of simple airbags was studied by Browning[5] based on these two equations; experimental work was also conducted by other investigators.[6,7]. For the present simple airbag study, emphasis was toward Army airdrop application and comparison with complex and augmented airbags. Analysis of complex airbags

was based on modifications of Eqs. (1) and (2).

The standard size of a section of Army Type V aluminum airdrop platform is 9-ft wide and 2-ft long. Sections of platform are connected lengthwise in an airdrop operation to form various lengths of platform to accommodate different payloads. Typical platform linear loading densities for airdrop are about 1000 lbs to 2000 lbs per linear foot (lengthwise). If the entire projected area of a 9-ft x 4-ft platform is used for an airbag to support a payload, the corresponding airbag loading density is 111 lbs/ft^2 to 222 lbs/ft^2. This range of loading densities falls into the desired surface loading densities of airbags[5]. These practical considerations were used in the present investigation.

Simple Airbags

Analysis

As mentioned earlier, rectangular-shaped airbags were studied. Using a one-dimensional analysis for such a geometry would at best be an approximation of the actual processes of airbag compression and payload deceleration. Therefore, the purpose of the analysis was to obtain qualitative results to guide the experiments and to provide some guidelines for future airbag work.

Eqs. (1) and (2) presented earlier are the two basic equations required to solve for the motion of a payload supported by a simple airbag with constant vents. For a given simple-airbag/payload system and its initial ground impact velocity, i.e., known ρ_v, A_v, C_D, h_o, w, l, M, P_o, and u_o, the two equations govern the performance of the airbag in terms of the two unknowns h(t) and P(t). Of particular importance in airbag performance is the force that the compressed air in the airbag imparts on the payload as it is being decelerated. This force should not be higher than the force that would cause structural damage of the payload. This imparted force,

called the G force, is measured in terms of the gravitational acceleration g, i.e., $G = (d^2h/d^2t)/g$. For Army airdrop using paper honeycomb, this G force is generally about 30 g's. In addition to the G force, the air pressure P is also important because it is related to the structural integrity of the airbag fabric. Therefore, the G and P time profiles are emphasized in this report.

The method developed by Shampine and Watts[8] for solving ordinary differential equations was used for solving Eqs. (1) and (2). A computer program based on this method was written to integrate numerically Eqs. (1) and (2) for a given airbag system and its initial condition. For a given airbag system, a set of A_v values were chosen based on Browning and other airbag studies for numerical integration. Solutions of G (t), P(t), and u(t) were sought for the given A_v values. As discussed in Browning, in addition to the G force, the u time profile also has to be examined for possible payload rebound if A_v is too large. Therefore, an optimum A_v is a vent opening that yields a good balance between the G and u profiles. Typically, this corresponds to a payload landing velocity equal to about 30% of the initial payload velocity u_o.

A 9-ft x 4-ft, an 8-ft x 4-ft, and a 4-ft x 4-ft platform area were chosen for the analytical study. Specifics of the airbags and payloads, the initial conditions for the cases studied, and the optimum A_v values determined are tabulated in Table 1. The corresponding analytical results of G and P profiles are shown in Figs. 5-18. Peak G forces, G_p, and peak P values, P_p, from these G and P profiles are also shown in Table 1.

Table 1

Simple Airbag Analytical Results

Case No	Bag Size ft x ft x ft(h_o)	y ft	M lb_m	A_v ft^2	G_p g	P_p psig
1 (Fig. 5)	9x4x2	7	1490	1.56	9.10	3.10
2 (Fig. 6)	9x4x2	7	2490	1.00	10.6	5.68
3 (Fig. 7)	9x4x2	13	2490	1.56	11.8	6.44
4 (Fig. 8)	9x4x3	7	1490	1.78	6.86	2.35
5 (Fig. 9)	9x4x3	7	2490	1.22	7.41	4.17
6 (Fig. 10)	9x4x3	13	1490	2.22	9.02	3.01
7 (Fig. 11)	9x4x3	13	2490	1.78	8.40	4.81
8 (Fig. 12)	8x4x4	7	1390	1.33	7.19	2.60
9 (Fig. 13)	8x4x3	13	4000	1.5	6.67	6.68
10 (Fig. 14)	8x4x3	13	8000	1.5	4.30	9.39
11 (Fig. 15)	8x4x4	13	4000	1.5	5.75	6.01
12 (Fig. 16)	8x4x7	13	8000	1.5	3.10	7.18
13 (Fig. 17)	8x4x8	13	12000	1.5	2.32	8.70
14a (Fig. 18)	4x4x1	7	315	0.62	23.3	--
14b (Fig. 18)	4x4x1	7	315	1.04	11.4	--
14c (Fig. 18)	4x4x1	7	315	1.32	7.0	--

For a circular cylindrical airbag, its height generally should not exceed its diameter to avoid the payload tipover problem[5]. Following this guideline, the height of the present rectangular airbag should not exceed 4 feet. Results in Figs. 13 and 15 show that satisfactory performance is provided by 4-ft or under, simple airbags supporting a 4000-lb or less payload. As the payload weight increases to 8000 lbs, the 4-ft height becomes insufficient and results in a high 18 ft/s payload ground impact velocity as shown in Fig. 14C. If the height is increased to 7 feet, the payload landing velocity is decreased to 12 ft/s (Fig. 16C). Similarly, for a 12,000-lb_m payload, an 8-ft high airbag is required for a 12 ft/s payload landing velocity (Fig. 17C). However, for an airbag higher than 4 feet, the airbag compression process will most likely not be vertical; the

calculation becomes academic and gives optimistic results. Cushioning heavy payloads is a main problem for simple airbags. One method to circumvent this is to install a blowout patch at the air vent that will break at a selected air pressure. Before the breakage of the blowout patch, the air pressure is rapidly built up so that the airbag height can be decreased for a heavy payload. Currently, such an airbag system is used by the Soviets.

The 4-ft x 4-ft x 1-ft airbag study was mainly conducted for comparison with the gas-injection complex airbag study (to be presented later). Results in Fig. 18 illustrate the effects of A_v on G and u profiles mentioned earlier. As A_v increases from 0.62 ft^2 to 1.32 ft^2, G_p decreases but the landing velocity increases. Therefore, of the three A_v values, 1.04 ft^2 is the best value that yields a moderately low G_p force and an acceptible landing velocity.

Experiments

Neoprene-coated nylon has been mainly used to construct airbags. For the present investigation, a high strength/weight ratio polyurethane-coated Kevlar(R) was fabricated to construct the airbags. Its specifications are as follows: areal density - 24.3 oz/yd^2, thickness - 0.03 in, tensile strength - 490 lbs_f at 10% elongation in the fill direction and 670 lbs_f at 6.5% elongation in the warp direction, tear strength - 120 lbs_f.

The experimental set-up for the constant-vent simple airbag study is shown in Fig. 19. A 9-ft x 4-ft surface area, 1-in thick, and 490-lb_m aluminum slab was used as the platform. A 9-ft (w) x 4-ft(l) x 3-ft (h_o) Kevlar airbag was constructed and attached to the aluminum platform along its boundaries. Two 16-in x 12-in rectangular openings were cut from the aluminum platform as air vents for the airbag. Two rectangular sliding gates were installed on the two openings for manual settings of the vent size for the constant-vent study. A weight slab of 1000

lbs or 2000 lbs was bolted to the platform at the center as the payload for the airbag. Along with the aluminum platform, the total payload/platform weight was 1490 lbs or 2490 lbs. An accelerometer was glued to the payload to measure its acceleration. A pressure transducer was installed under the platform to measure the airbag air pressure.

For each of the two payload weights, free drop experiments were conducted from 7-ft to 13-ft drop heights to obtain 21 to 29 ft/s airbag ground impact velocities. In a typical experiment, the total vent area was set at a selected value. The entire airbag system was lifted to a selected height as shown in Fig. 20. The entire system was then released to impact the ground. The G force on the payload from the airbag and the air pressure P were measured during the experiment. For each drop height, experiments were conducted with several air vent sizes to determine the optimum A_v that yielded the lowest peak G force. Drop conditions for all the experiments and the optimum A_v values are shown in Table 2. Their corresponding G and P profiles are shown in Figs. 21-28. Peak G and P values obtained from these profiles are tabulated in Table 2. Results in Table 2 are plotted in Fig. 29.

It is seen that for the same payload, as the drop height or ground impact velocity increases, G_p and A_v increase. For the two payload weights, the G force levels are acceptable. However, one should note that the measurements were made in laboratory conditions. In actual airdrop conditions, ground winds and horizontal motion of the payload will most likely cause higher G forces then those measured. Although a 4000-lb payload (1000-lb per linear foot of platform) has not been dropped, based on the measurements in Fig. 29, the 9' x 4' x 3' simple airbag would most likely be able to cushion a 4000-lb payload with G force levels comparable to those provided by paper honeycomb. For a 8000-lb payload, the G force levels would most likely be excessively high.

Table 2

Simple Airbag Drop Test Conditions and Results

Drop No.	y ft	M lb_m	A_v ft_2	G_p g	P_p psig
		Airbag Size: 9'(w) x 4'(l) x 3'(h_o)			
1	7	1490	1.78	10.2	3.05
2	9	1490	2.0	11.5	3.62
3	11	1490	2.2	12.7	3.87
4	13	1490	2.2	18.0	5.19
5	7	2490	1.22	11.5	5.19
6	9	2490	1.56	11.9	5.11
7	11	2490	1.56	13.0	5.77
8	13	2490	1.78	18.0	8.16
		Airbag Size: 8'(w) x 4'(l) x 4'(h_o)			
9	7	1390	1.33	13.8	4.27

Comparison between the analytical results and the experimental results for the same airbag and drop conditions, i.e., case no. 4 in Table 1 and drop no. 1 in Table 2, case no. 5 and drop no. 5, case no. 6 and drop no. 4, and case no. 7 and drop no. 8, the measured G forces and air pressure are higher than those predicted from analysis. Therefore, the analytical results presented earlier should be used with caution.

Vent-Control Airbags

Analysis

The purpose of this analysis was to study the feasibility of vent-control complex airbags and to obtain some qualitative results to guide the experiments. The following analytical approach was used. For a vent-control airbag, the vent area, A_v, in Eq. (1) is no longer a constant, but an unknown to be solved as a function of time, t. If a velocity profile, u(t) or dh/dt, of the payload

after airbag ground impact is chosen and input in Eqs. (1) and (2), then the two unknowns $A_v(t)$ and P(t) can be sought to satisfy the assumed u(t). For this approach to generate useful solutions to guide the experiments, the payload mass, its descent velocity, the airbag dimensions and the assumed u(t) have to be compatible, e.g., sufficient airbag height for a given payload mass and descent velocity. This background information was obtained from simple airbag performance.[5]

After reviewing the simple airbag performance[5], the following fourth order polynomial was chosen for u(t) for the vent-control airbag:

$$u=dh/dt=u_o[-(\frac{t}{t_f})^4+2(\frac{t}{t_f})^2-1] \qquad (3)$$

Eq. (3) satisfies the initial condition: $u = -u_o$ when the airbag impacts the ground at t=0. The final boundary condition for u is u=0 at the end of the airbag stroke when the payload/platform touches the ground at $t=t_f$. Furthermore, the maximum deceleration $a_{max}=(du/dt)_{max}=(8\sqrt{3/9})(u_o/t_f)$. Therefore, for a given u_o, a_{max} has to be selected to calculate t_f in order to proceed with numerical integration of Eqs. (1) and (2) from t=0. For the current analysis, a_{max} = 10 g's was selected. The ordinary differential equation solver code developed by Shampine and Watts[8] was again used to determine $A_v(t)$ to satisfy the chosen u(t) given by Eq.(3).

Specifics of the vent-control airbags, payloads, and the initial conditions for the cases studied are tabulated in Table 3. The corresponding analytical results of G, P, and u profiles are shown in Figs. 30-34. Peak G forces, G_p, and peak P values, P_p, from the G and P profiles are shown in Table 3. These results show that to obtain the desired u(t) profile and a peak G force less than

10 g's, the vent area, A_v, has to decrease with respect to time from an open to a closed position during the compression stroke of the airbag. Comparison between the results in Table 3 and the simple airbag results in Table 1 for the same airbags and drop conditions, i.e., cases no. 1, 4, 5, and 8 in Table 1 and cases no. 1, 2, 3, and 4 in Table 3, respectively, shows that lower peak G forces are provided by the vent-control method.

To illustrate the detailed performance differences between a simple airbag and a complex airbag using vent-control or gas injection (presented later), case no. 9 in Table 1 (or case no. 5 in Table 3) has been chosen, i.e., an 8-ft(w) x 4-ft(l) x 3-ft(h_o) airbag supporting a 4000-lb payload with a 28 ft/s descent velocity. To satisfy the desired u profile (Eq. (3)) using vent-control, Fig. 34B shows that A_v has to be rapidly opened from a closed position and then closed linearly with time at a rate of 13.6 ft^2/s throughout the remaining airbag stroke. The corresponding G profile in Fig. 34A shows slower G-force time rise rates and a 29% lower G_p as compared to those of the constant-vent case. The payload ground impact velocity is approximately zero (as required by Eq. (3)), also lower than that of the constant-vent case.

Table 3

Vent-Control Airbag Analytical Results

Case No	Bag Size ft x ft x ft(h_o)	y ft	M lb_m	G_p g	P_p psig
1 (Fig. 30)	9x4x2	7	1490	5.68	1.91
2 (Fig. 31)	9x4x3	7	1490	3.79	1.38
3 (Fig. 32)	9x4x3	7	2490	3.86	2.33
4 (Fig. 33)	8x4x4	7	1390	2.79	1.15
5 (Fig. 34)	8x4x3	13	4000	6.8	6.8

Experiments

The experimental set-up for the vent-control complex airbag study is shown in Fig. 35. An 8-ft(w) x 4-ft(l) x 4-ft(h_o) Kevlar airbag was attached to a 9-ft x 4-ft Type V platform. A payload was bolted to the center of the platform. A 12-in x 16-in opening was cut from the platform as the air vent for the airbag. An accelerometer was glued to the payload to measure its acceleration. A pressure transducer was connected to the airbag to measure its air pressure. A pneumatic/electronic system was designed and constructed to control the air vent size. Details of the design were reported by Rosato.[9] Major components of the system, such as the sliding gate to control the vent size, the air supply tank, the air cylinder and the associated valves, are shown in Fig. 36.

A schematic of the vent-control system is shown in Fig. 37. The size of the 12-in x 16-in air vent, K, is controlled by the rectangular sliding gate, I, which moves in the 12-in length direction. The sliding gate is connected to the piston of the air cylinder, F. The piston drives and translates the sliding gate to close the vent area, K, when high pressure air flows in from the air supply

tank, A, through the solenoid valve, D, and the check valve, E. The solenoid valve is connected to the system control circuit, G, which also monitors the position of the sliding gate, I, through the valve position feedback pot, H. The firing signal to activate D through G comes from either the airbag air pressure, L, or the midair trip wire triggering switch assembly, M and N.

In a typical experiment, the 12-in x 16-in air vent is fully opened first and the airbag/payload system is positioned at a desired height above the ground by a crane. The entire system is then released. After the system freefalls for a certain distance, the airbag falls on the tripwire to release it from the midair triggering switch, thereby sending a firing signal to the system control circuit. It immediately energizes the solenoid valve in a open position to release the high pressure air from the air supply tank through the check valve to the air cylinder. The high pressure air in the air cylinder then pushes the piston and the sliding gate to close the air vent. When the sliding gate fully closes the air vent, the valve position feedback pot sends a signal to the system control circuit, which in turn deenergizes the solenoid valve to release the high pressure air inside the air cylinder to the atmosphere through the check valve and the solenoid valve.

As shown in Fig. 36, the air vent was not located symmetrically at the center of the platform but on one side of it. Vertical drop tests from various heights and payload weights showed that the maximum drop height and payload weight for satisfactory vertical airbag compression was 7 ft (corresponding to u_o = 21.2ft/s) and 1,000 lbs, respectively. Consequently, drop tests were conducted for this drop condition to examine the performance of the airbag operated with a constant vent and with the controlled vent.

Drop tests were conducted with various constant vent sizes to determine the optimum value. It was found that a 192-in^2 (12-in x 16-in) air vent yielded the lowest peak G force. The corresponding G force and air pressure time profiles are shown in Fig. 38.

As indicated by the analytical results in Figs. 30-34, A_v has to be rapidly closed immediately after the airbag impacts the ground and before the peak G force or the maximum air pressure is reached. This was achieved as shown in Fig. 38 where the controlled A_v time profile is compared with the G force time profile for the constant-vent drop test. When this vent control was applied to the airbag, its performance was much improved. Fig. 39 shows the resulting G force profile; Figs. 40 and 41 show the G force and the air pressure comparison between the constant- vent and the vent-control drop tests. It is seen that by controlling the air vent, the profiles become flatter, resulting in a 37% decrease in G_p. These results confirm the improved airbag performance provided by vent-control.

Gas-Injection Airbags

Analysis

Qualitative results were also pursued from analysis to guide the gas-injection airbag experiments. For a complex airbag with gas injection, the air flow Eq. (1) becomes:

$$\rho_v A_v q C_D = -\frac{d}{dt}(\rho h w l) + \frac{dm_i}{dt} \tag{4}$$

where dm_i/dt is the gas injection rate term and A_v is a constant as mentioned earlier. The payload motion equation remains the same as Eq. (2). As in the vent-control analysis, the same payload velocity profile u(t) expressed by Eq. (3) was assumed. However, the unknowns in

Eqs. (2) and (4) are now A_v, $\dot{m}_i$ (gas injection rate) and P. They were solved by the following procedure. Based on the results from the constant-vent and vent-control airbags, a series of A_v values were assumed to initiate the numerical integration of Eqs. (2) and (4). For each assumed A_v, $\dot{m}_i$ and P were pursued to obtain the assumed u(t). As expected, extremely small or excessively large A_v values did not give satisfactory results. Optimum combinations of A_v and m_i for a given airbag/payload system were determined by comparing the resulting u(t) with the assumed u(t). Through this procedure, A_v and $\dot{m}_i$ were then determined. In addition, gas exhaust rate $\dot{m}_e$ from A_v was also calculated.

Specifics of the gas-injection (based on air) airbags, payloads, and the initial conditions for the cases studied are tabulated in Table 4. The corresponding analytical results of G and P profiles are shown in Figs. 42-47. Peak G forces, G_p, and peak P values, P_p, from the G and P profiles are also shown in Table 4.

Table 4

Air-Injection Airbag Analytical Results

Case No	Bag Size ft x ft x ft(h_o)	y ft	M lb_m	G_p g	P_p psig
1 (Fig. 42)	9x4x2	7	1490	8.27	2.66
2 (Fig. 43)	9x4x2	7	2490	5.69	3.23
3 (Fig. 44)	9x4x2	13	1490	14.6	4.5
4 (Fig. 45)	9x4x2	13	2490	10.6	5.62
5 (Fig. 46)	8x4x3	13	4000	6.46	6.40
6 (Fig. 47)	4x4x1	7	315	11.6	1.71

Comparison between the results in Table 4 and the simple airbag results in Table 1 for the same airbags and drop conditions, i.e., cases no. 1, 2, 3, and 9 in Table 1 and cases no. 1, 2, 4, and 5 in Table 4, respectively, shows that lower peak G forces are provided by the gas-injection method.

As mentioned earlier, case no. 9 in Table 1 (or case no. 5 in Table 4) was chosen to illustrate the performance differences between a simple airbag and a complex airbag using vent-control or gas-injection. To satisfy the desired u profile (Eq. (3)) using air-injection, Fig. 46B shows that $\dot{m}_i$ increases with time as the airbag is being compressed. Note that 1 lb/s of air at standard condition is 790 ft^3/min, a considerable amount of air flow. As a result of the air injection, Fig. 46A shows that both the G and u profiles are improved (a lower peak G force and a lower payload ground impact velocity) when compared to those of the constant-vent airbag. Comparison of the simple airbag and the complex airbag with vent-control or air-injection is shown in Fig. 48. It is seen that vent-control and air-injection airbags have similar performance, which is better than that of the simple airbag.

Experiments

The airbag used for the vent-control study was found through preliminary experiments to be too large for the amount of compressed air available from an existing compressed air tank at Natick. Consequently, a smaller airbag/platform system as shown in Fig. 49 was contructed for the gas-injection study.

A 4-ft (w) x 4-ft (l) x 1-ft (h_o) coated Kevlar airbag (A in Fig. 50) was constructed and attached to a 4-ft x 4-ft x 1-in (thickness) aluminum platform (B). The platform has four vent openings (C) at four corners for symmetrical air venting. The four vent openings are equipped with manual sliding gates (D) to adjust the vent size for constant-vent airbag study. Two 100-1b weights (E) are strapped to the platform as the payload. Air injection is provided at the center of the platform via a 1.5-in I.D. (inside diameter) and 27-ft long flexible high pressure hose (F). The hose is connected to a 2.4-ft^3 capacity compressed air tank (G). An AC (alternating current) operated normally closed solenoid valve (H) is installed at the end of the flexible hose. The solenoid valve controls the air injection flow via a 1-7/8-in I.D. metal air inlet pipe (I) connected to the platform. A timing-control circuit (J) controls the operation of the solenoid valve, H. The circuit J also controls another solenoid valve (K) that operates the mechanical release device (L) for the airbag/platform system. An accelerometer (M) was glued to the center of the platform to measure the acceleration (G force) of the payload/platform. Airbag air pressure is measured by a pressure transducer (N).

In a typical air-injection experiment, compressed air up to 80 psig is delivered to the compressed air tank, G (and the flexible hose F). Time sequence between the solenoid valves, H and K (air injection before or after airbag/platform release), and the time duration of air

injection (solenoid valve H) are set by the timing-control circuit, J. The desired fixed air vent size, C, is set by the sliding gates, D. The airbag/platform system is hoisted to 7 feet above ground level. An experiment begins by manually activating the time-control circuit, J, first. The two solenoid valves, H and K, are then activated according to the sequence and time duration set by the timing-control circuit, J. Subsequently, the airbag/platform is released and compressed air is injected into the airbag. After a 7-ft freefall, the airbag/platform system impacts the ground with a downward velocity of 21 ft/s. During the airbag compression stroke, its air pressure, P, and the deceleration or the G force of the platform/payload are measured and recorded for analysis.

Before air-injection experiments were conducted, the airflow characteristics of the air-injection system were studied first. The study involved calculating the average air mass flow (injection) rate, m_i, of the compressed air supply tank, G, from (1) tank air pressure and injection time measurements, and (2) exhaust air velocity measurements at the air vents of the airbag. Results are described below.

The air supply tank was pressurized to an initial air pressure, P_i, first. A selected injection time, t_i, was set by the timing-control circuit. It then activated the solenoid valve, H, to inject the compressed air into the airbag hung stationary in the air with the four vents fully opened. At the end of the injection time, t_i, air injection was terminated and the final tank air pressure, P_f, was measured. The ideal gas law was used to determine the initial and the final air mass in the tank using P_i and P_f. The difference between the two mass valves, Δm, divided by t_i gives the average air injection rate, $\overline{\dot{m}_i}$. Table 5 shows all the measurements and the calculated average air injection rates, $\overline{\dot{m}_i}$. It is seen that the m_i values are in the same order of magnitude

as those predicted from the analysis (Fig. 47D).

In addition to the tank air pressure measurements, exhaust air velocities at the air vents and the airbag air pressure were also measured. Some measurements were made with the four air vents fully opened and some were made with only one air vent fully opened. The measurements are shown in Fig. 51. It is seen that airbag air pressure and exhaust air velocity continued to rise after air was injected into the airbag. Air continued to flow out of the airbag after air injection was terminated, even beyond 0.66 second that corresponds to the amount of time for a 7-ft freefall. The three exhaust air velocity profiles in Fig. 51 were integrated over time to calculate the average exhaust air mass flow rates. Results are also shown in Table 5. These results agree well with the air injection rates shown in the same Table.

Table 5

Air Injection Rates

P_i psig	P_f psig	t_i sec	Δm lb_m	$\dot{m}_i$ lb_m/sec
50	35	0.2	0.24	1.07
	30	0.3	0.285	0.951
	25	0.4	0.357	0.892
	24	0.5	0.428	0.856
60	45	0.2	0.214	1.07
	40	0.3	0.285	0.951
	30	0.4	0.428	1.07
70	55	0.2	0.214	1.07 (1.03)*
	45	0.3	0.357	1.19 (1.24)*
	40	0.4	0.428	1.07 (1.01)*
80	50	0.3	0.428	1.43

*Determined from the exhaust air velocity measurements at the 25-in^2 air vent.

Before air injection experiments were investigated, constant-vent experiments were conducted first. In these experiments, the airbag/platform system was dropped from a 7-ft height to obtain a 21 ft/s ground impact velocity. The air vent size was varied from 70-in^2 to 150-in^2 in an increment of 20-in^2. Air pressure, P, and G force were measured for each constant-vent size. The peak G force, G_p, was found to decrease from A_v = 70-in^2 to 130-in^2 where G_p reached the minimum and then it increased from A_v = 130-in^2 to 150-in^2, indicating 130-in^2 to be the optimum A_v. The corresponding G and P profiles for A_v = 130-in^2 are shown in Fig. 52, which is the best performance a constant-vent can offer for the present airbag and drop condition.

The gas-injection analysis presented earlier shows that air is to be injected when the airbag is being compressed. This guideline was followed in the early air-injection experiments. Air injection time, t_i, was set to inject air into the airbag at various times during airbag compression. When air was injected this way, a change in the initial rise of the G force profile and a decrease in G_p were not observed. The part of the G profile that was affected was the decreasing part of the G profile after G_p as shown in Fig. 53. In the analysis, gas mixing was assumed to be instantaneous and local flow conditions inside the airbag were not considered. In reality, it takes time for the centrally injected air to mix with the air inside the airbag. To allow for this mixing time, air was then injected into the airbag prior to its compression. This was accomplished by controlling the two solenoid valves, H and K (Fig. 50), with the timing-control circuit, J. A series of experiments were conducted this way. They are described below.

In this series of experiments, air was injected prior to airbag/platform release from a height of seven feet. Air-injection time, t_i, varied from 0.1 to 0.5 second and compressed air pressure, P_i, was set from 50 to 90 psig as shown in Table 6. To illustrate the experimental procedure, for

the experiment with P_i = 80 psig and t_i = 0.2 s, compressed air was injected into the airbag for 0.2 s before it was released from seven ft. At the end of the 0.2 s, air-injection was terminated and the airbag/platform was released to freefall for seven ft (0.66 s). Payload deceleration and airbag air pressure were measured during the experiment. As shown in Fig. 51, the supplied compressed air continued to flow out of the airbag well into the 0.66-s time range after termination of air injection. Therefore, although air was injected prior to airbag compression, its effect was felt during airbag compression and resulted in decreased peak G forces as shown in Table 6.

Table 6

Air-Injection Airbag Experimental Results

Airbag size: 4'(w) x 4'(l) x 1'(h_o)
Payload platform mass: 315 lb_m
A_v = 1.04 ft^2

Air Injection Time
(Seconds)

Tank air pressure at beginning of air injection	0.1		0.2		0.3		0.4		0.5	
psig	G_p g	P_p psig	G_p g	P_p psig	G_p g	P_p psig	G_p g	P_p psig	G_p g	P_p psig
50	--	--	31.6	5.07	23.7	4.51	25.9	4.89	26.3	4.76
60	--	--	22.7	4.26	23.0	4.51	23.3	4.54	--	--
63	--	--	--	--	--	--	26.0	5.07	--	--
70	--	--	25.7	4.74	26.1	4.80	24.9	5.26	--	--
80	30	5.33	30.3	5.35	25.9	5.14	--	--	31.8	5.63
80	29.1	5.12	25.3	4.75	28.9	5.58	--	--	--	--
90	--	--	43.3	8.16	--	--	--	--	--	--

Simple airbag
(no air injection)

A_v, ft^2	G_p,g	P_p, psig
0.903	44.82	5.93
0.903	47.6	5.14
0.903	49.9	5.89

Table 6 shows the measured peak G force, G_p, and peak airbag pressure, P_p, of the airbag using air-injection along with the measurements obtained earlier for the airbag using the optimum constant vent (130-in^2). Comparison of the two methods of operation shows that lower G_p values were obtained using air-injection. Comparison of the G and P profiles is shown in Figs. 52 and 54. It is seen that air-injection resulted in a slower initial rise in the profiles and a longer airbag stroke time. Thus, lower g values were obtained using air-injection. These experimental results qualitatively agree with the analytical results presented earlier.

For comparison purposes, experiments using paper honeycomb as the sole impact energy absorber were also conducted. For these experiments, the airbag was removed from the platform, and two blocks of paper honeycomb were taped to the underside of the platform directly below the two 100-lb payloads. By use of paper honeycomb design guidelines[10] and by experimentation with different paper honeycomb sizes, two blocks of 18-in x 7-in (cross-section) x 16-in (height) blocks were found to be the optimum size for the 315-lb payload/platform. The corresponding G force profile is shown in Fig. 55 along with the G force profile for the air-injection airbag obtained earlier. The peak G force is about the same for both profiles. The well-known overall rectangular-shaped G profile of paper honeycomb is evident. The typical, relatively slow initial rise of the airbag G profile is also evident.

Augmented Airbags

Previous complex airbag experiments using vent-control and air-injection methods showed that they decreased the peak G force of simple airbags with constant vents. But they did not increase the initial slow rise of the G profile. To achieve this, an auxiliary energy absorber is necessary to augment the airbag. Paper honeycomb was chosen for this purpose. Impact energy attenuation characteristics of augmented airbags using paper honeycomb were then investigated.

Two extensions as shown in Fig. 56 were added to the platform to hold two relatively small pieces of paper honeycomb on two sides of the airbag. The additional weight of the two extensions resulted in a 420-lb total weight of the payload/platform. In order to increase the initial slope of the airbag G profile, paper honeycomb had to be crushed first when the bottom of the airbag impacted the ground or slightly before that instant. Therefore, the paper honeycomb had to be at least 1-ft thick or slightly thicker so that it would extend beyond the bottom of the airbag to absorb most of the initial impact energy. Paper honeycomb design guidelines[10] showed that a 390-in^2 (cross-section) x 3-in (height) was necessary for cushioning a 420-lb payload landing with a 21 ft/s velocity. Smaller blocks of paper honeycomb were experimented in conjunction with the airbag (Fig. 56). Additionally, 100% honeycomb (without the airbag) and simple airbag experiments were also conducted to compare their performance with the augmented airbag.

Table 7

Augmented Airbag Experimental Results

Airbag size = 4'(w)x4'(l)x1'(h_o)
Payload/platform mass = 420 lb_m
Drop height = 7'

EXPERIMENT	A_v in^2	G_p g	P_p psig
1. Augmented simple airbag	110	21.3	3.33
with 50-in^2 x 12-in paper honeycomb	110	23.7	3.08
2. Simple airbag with	50	30.1	6.81
constant vent	70	32.8	6.17
3. Paper honeycomb only (no airbag)			
192 in^2 x 6 in	--	31.3	--
252 in^2 x 6 in	--	29.2	--
4. Air-injection airbag	110	21.3	3.35
with 50 in^2 x 12 in^2 paper	130	22.4	3.73
honeycomb (m_i at 70 psig for 0.35 s)			

Four groups of experiments as shown in Table 7 were conducted. Results from two best experiments with low peak G forces from each group are tabulated in Table 7 and the corresponding G and P profiles are shown in Figs. 57-60. Figs. 57 and 58 show the typical triangular-shaped profiles of the simple airbag with constant air vents. Fig. 59 illustrates the more rapid initial rise in the G profile of paper honeycomb. When paper honeycomb and the simple airbag were combined together, much improved overall rectangular-shaped G and P profiles were obtained, as shown in Figs. 57-59. Consequently, as shown in Table 7, the peak G force of about 33 g's for both the simple airbag and the paper honeycomb was reduced to about 24 g's by using the augmented airbag. The cross-sectional area of the paper honeycomb used as the auxiliary energy absorber for the simple airbag was about 1/4 to 1/5 of that of the 100% paper honeycomb. Fig. 60 shows the G and P profiles of the paper honeycomb augmented airbag with air-injection. Results were similar to those in Figs. 57-59, for the augmented airbag without air-injection.

Airdrop Applications

In view of the improved performance of air-injection airbags and paper honeycomb-augmented airbags, they can be effectively utilized for airdrop applications. One highly simplified arrangement is conceptually shown in Fig. 61. Two rails of paper honeycomb are positioned longitudinally along the two sides of a platform as shown in Figs. 61A and 61B. Because of the high crushing strength of paper honeycomb (6,100 lb_f/ft^2), it can be sized so that it provides a drive-on capability for one to drive a vehicle on it and to rig the vehicle onto the platform. Between the two rails of paper honeycomb is a single or a series of airbags with constant vents (shown deflated in Figs. 61A and 61B). Figs. 61A and 61B show the rigged vehicle ready for airdrop. As the entire vehicle/platform system impacts the ground, the paper honeycomb absorbs the initial impact energy as shown in Fig. 61C. Simultaneously the airbags are inflated by air injection (source not shown in Fig. 61C) to further absorb the impact energy as it was demonstrated by the augmented airbag experiments presented earlier. After the airbags are compressed and deflated, and the entire system is stablized, one can then derig the vehicle and drive it off the platform. Thus, a drive-on/drive-off capability, simple rigging/derigging, and quick ground mobility are provided by such a paper honeycomb-augmented airbag system.

Summary and Conclusion

For a 4-ft deep rectangular-shaped simple airbag installed below a 9-ft x 4-ft Type V airdrop platform, a 4000-lb payload is about the maximum weight that the airbag can support to yield similar G forces as those yielded by paper honeycomb. Complex airbags using vent-control and gas-injection, and augmented airbags using paper honeycomb are found to improve the performance of simple airbags by decreasing the peak G force.

Current Army transport aircraft, such as the C-130, does not have sufficient space between the platform and the aircraft floor for airbag installation. Furthermore, airbags below a platform will always have the payload tipover problem. Based on these unfavorable factors along with the improved performance provided by the complex and augmented airbags, future airbag investigations should be toward using these enhanced performance airbags between the payload and the platform. A series of airbags equipped with gas-injection and an auxiliary energy absorber (such as paper honeycomb) as shown in Fig. 61 would be the arrangement to pursue.

REFERENCES

1. Covington, C. and Shield, R., "Fragility Studies", Structural Mechanics Research Laboratory, University of Texas, Austin, TX 1960. Contract reports to Quartermaster Research and Engineering Command, Natick, MA

2. Lee, C.K., "Performance of a Single Balloon-Skirt Airbag in Vertical Drops", Natick Technical Report TR-88/059, U.S. Army Natick Research, Development and Engineering Center, Natick, MA, July 1988 (AD A198 240)

3. Nykvist, W., "Balloon-Skirt Airbags as Airdrop Shock Absorbers: Performance in Vertical Drops", Natick Technical Report TR-82/626, U.S. Army Natick Research Development, and Engineering Center, Natick, MA, December 1981 (AD A118 228)

4. Ross, E.W., "Control Systems for Platform Landing Cushioned by Air Bags", Natick Technical Report TR-88/021, U.S. Army Natick Research, Development and Engineering Center, Natick, MA, July 1987 (AD A196 154)

5. Browning, A.C., "A Vertical Approach to Air Bag Shock Absorber Design", Technical Note No. Mech. Eng. 369, Royal Aircraft Establishment, Farmborough, England, February, 1963

6. Tomcsak, S., "Decelerator Bag Study", Technical Report WADC-TR-59-775, Wright-Patterson Air Force Base Contract AF 33(600)-30825 to Goodyear Tire and Rubber Co., Akron, OH, June 1960 (AD 243 159)

7. Turnbow, J., and Ogletree, W., "The Energy Dissipation Characteristics of Airbags", U.S. Army QMR&E Command Contract DA 19-129-QM-1383 to University of Texas Structural Mechanics Research Laboratories, Austin, TX, August 1959 (AD 228 787)

8. Shampine, L.F. and Watts, H.A., "Design of User Oriented Package of ODE Solvers", Sandia Report No. SAND 79-2374, Sandia National Laboratories, Albuquerque, NM, 1979

9. Rosato, N., "Design Development of an Airbag Vent Control Mechanism", Paper No. 91-WA-DE-1, presented at the ASME (American Society of Mechanical Engineers) Winter Annual Meeting, December 1-8, 1991, Atlanta, GA

10. Gionfriddo, M.P., "Impact Energy Attenuation", presented at the 1990 Parachute Systems Technology Short Course sponsored by University of Minnesota, Framingham, MA, June 11-15, 1990

This document reports research undertaken at the US Army Natick Research, Development and Engineering Center and has been assigned No. NATICK/TR-93/082 in the series of reports approved for publication.

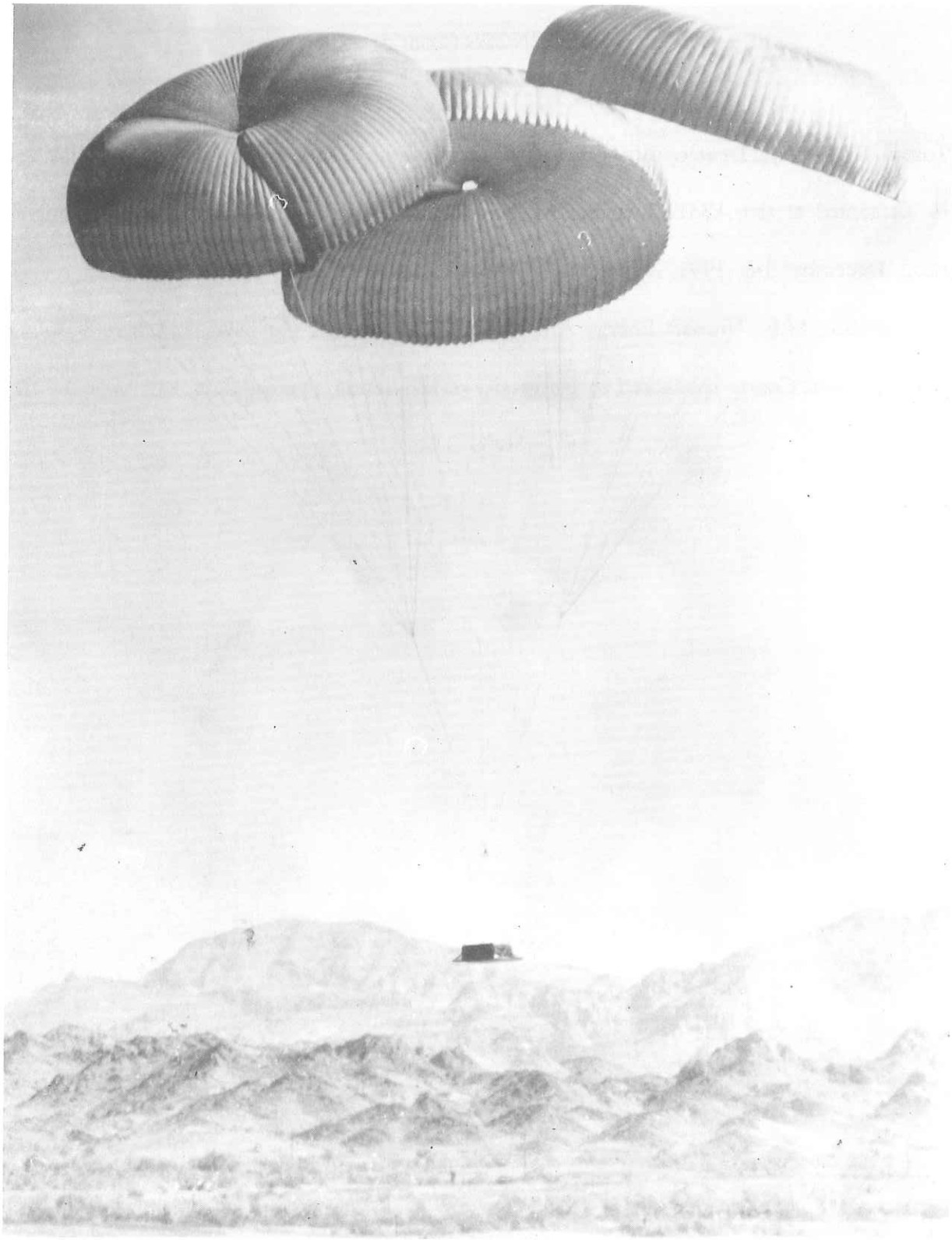

Figure 1. Photograph Showing Steady Descent of a Payload Airdropped Using U.S. Army Parachutes

Figure 2. Photograph Showing a U.S. Army Vehicle Cushioned by Paper Honeycomb and Mounted on a Platform for Airdrop

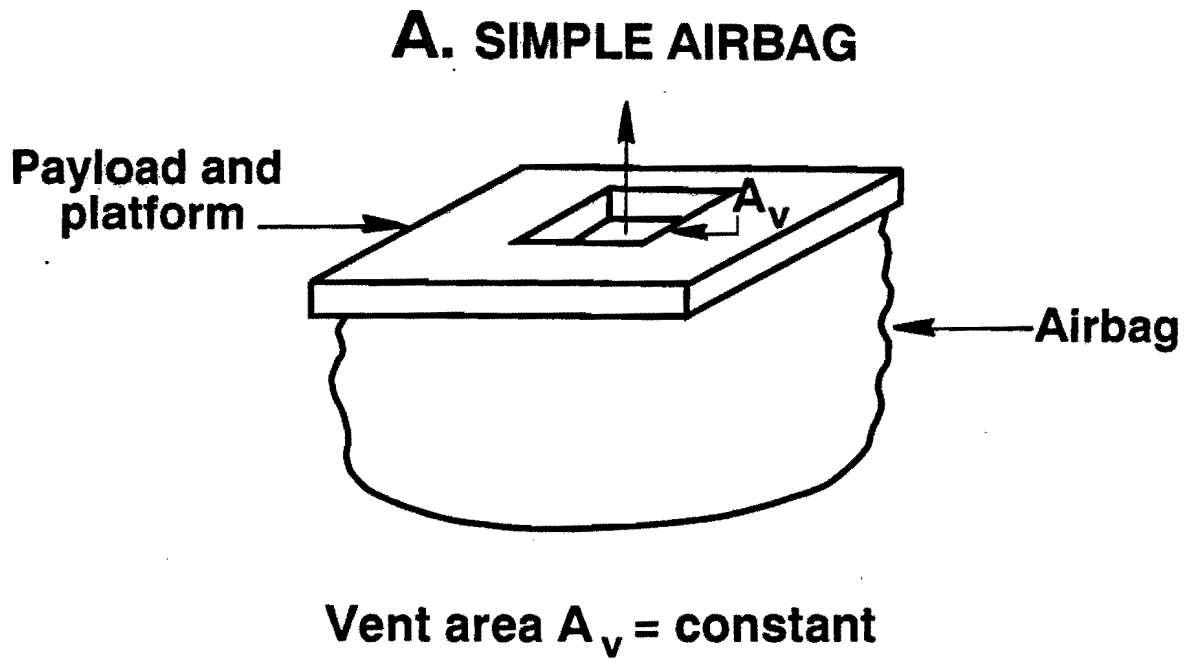

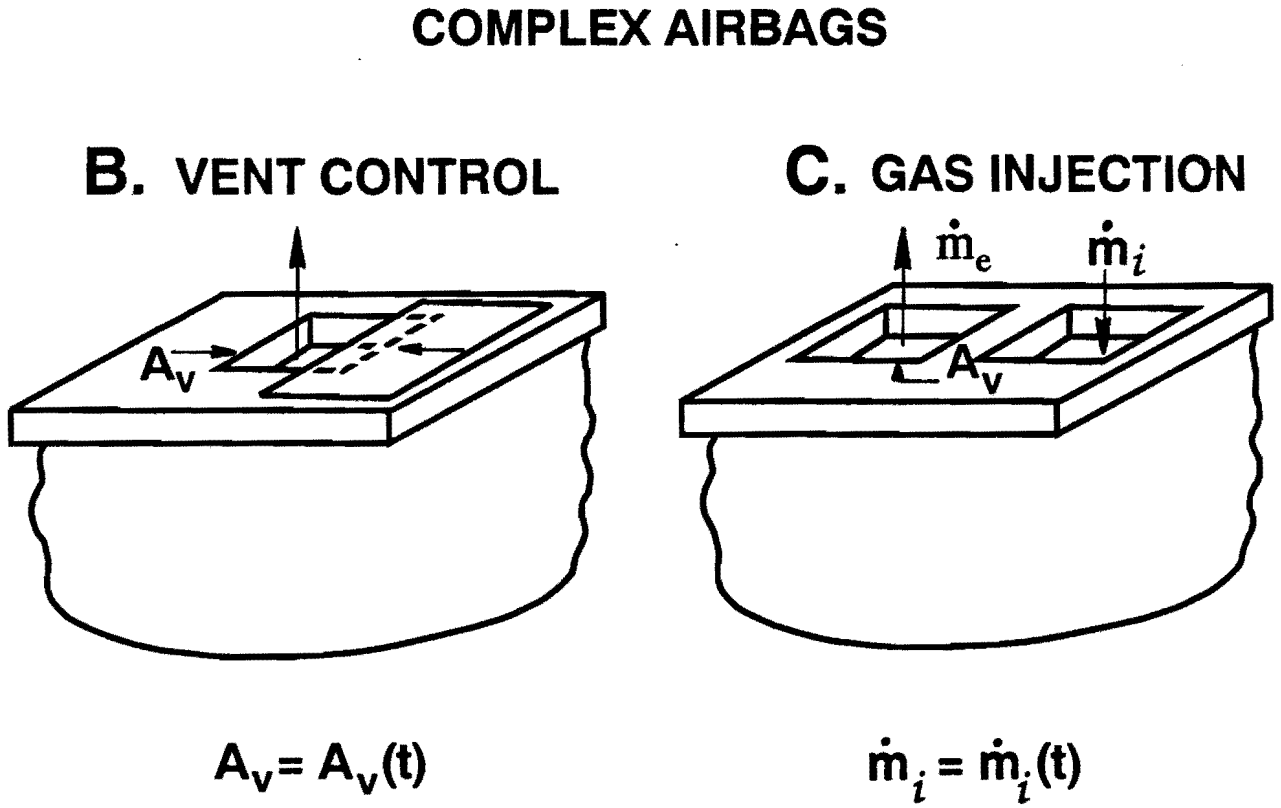

Figure 3. Schematics Showing a Simple Airbag and Concepts of Complex Airbags

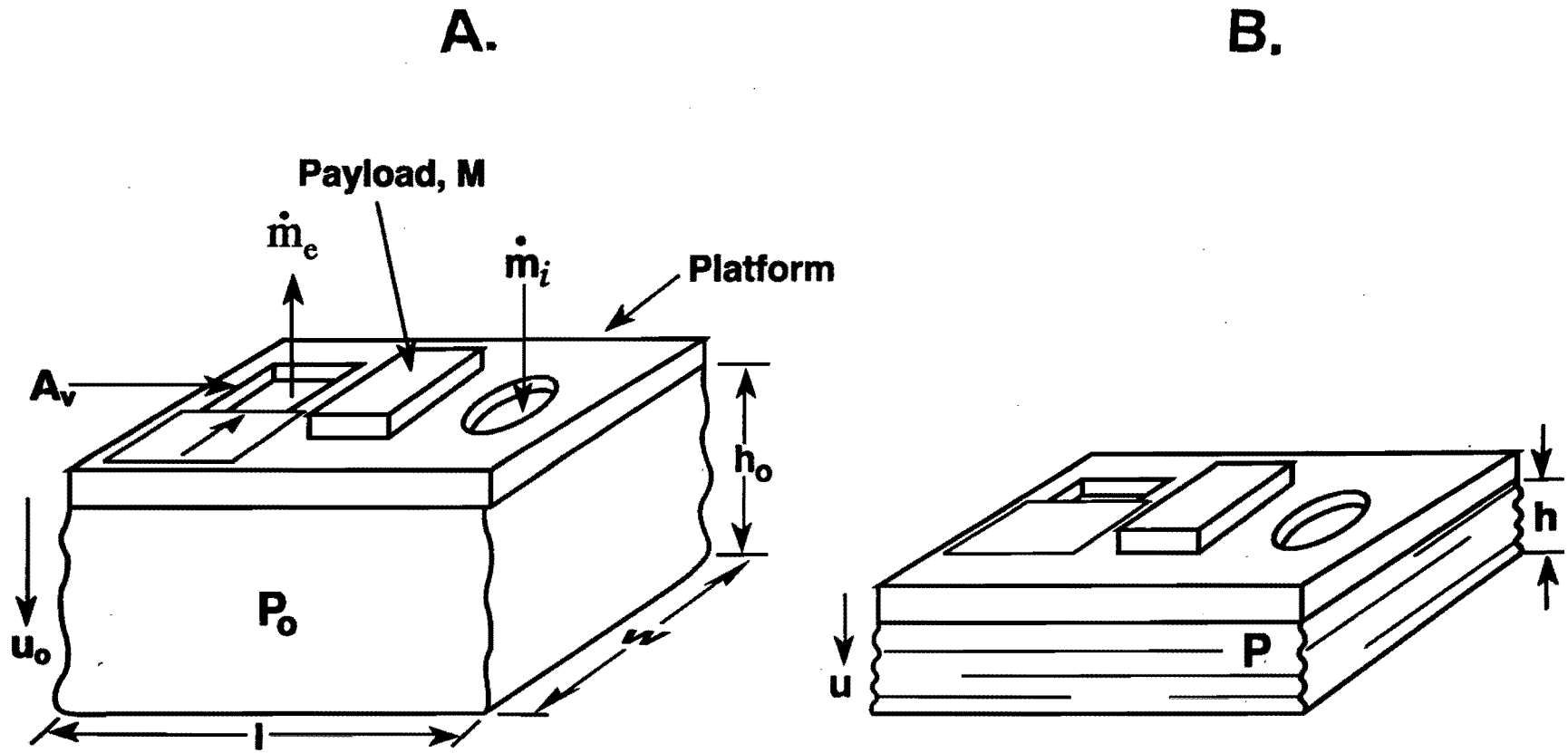

Figure 4. Schematics Showing the Compression of an Airbag and Physical Variables

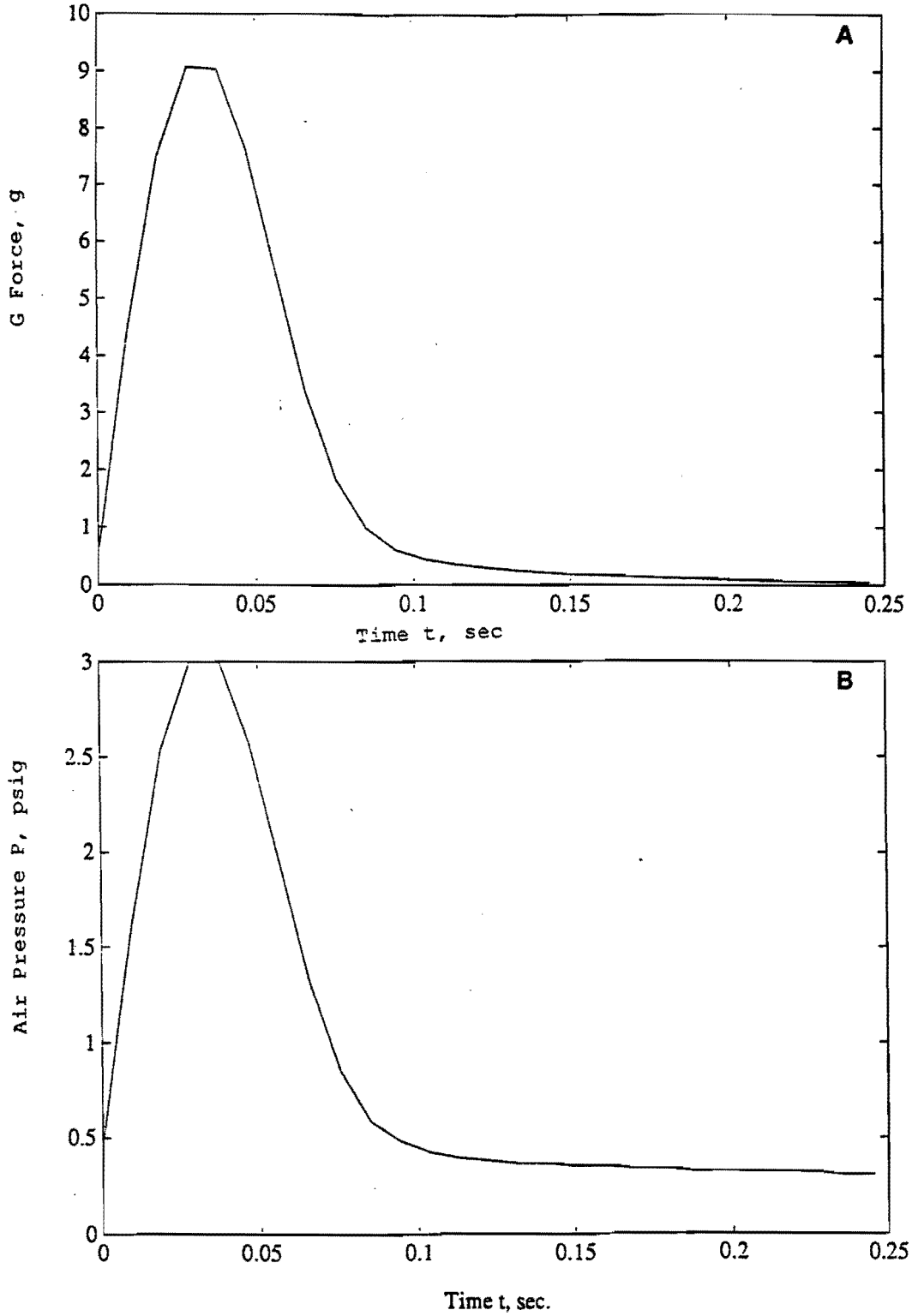

Analytical Results of Simple Airbags

Figure 5. 9'(1) x 4'(w) x 2'(h_o), H = 7' M = 1490 lbs, A_v = 1.56 ft^2; A. G force, B. Air pressure

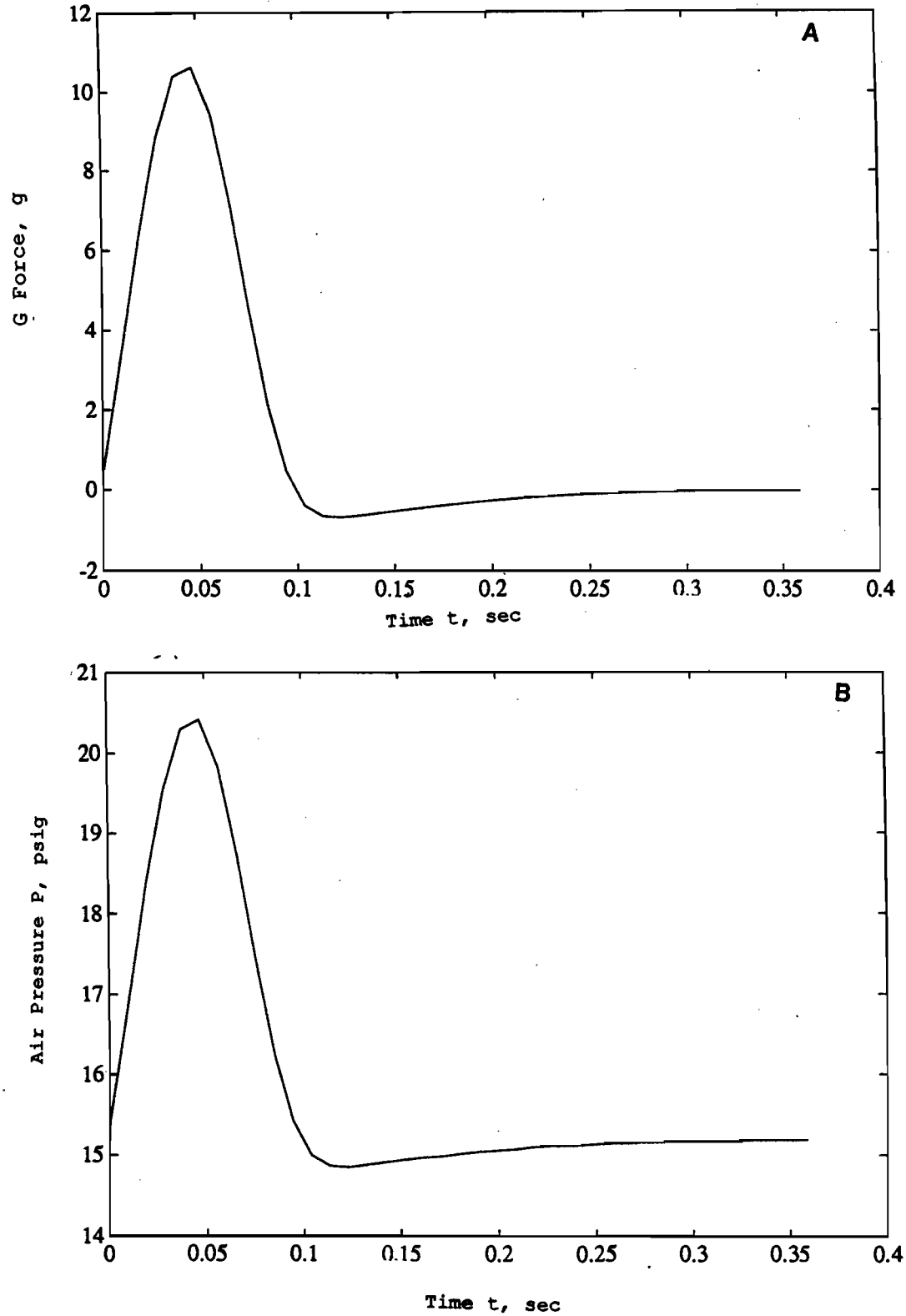

Analytical Results of Simple Airbags

Figure 6. 9' x 4' x 2', H = 7', M = 2490 lbs, A_v = 1 ft^2; A. G Force, B. Air pressure

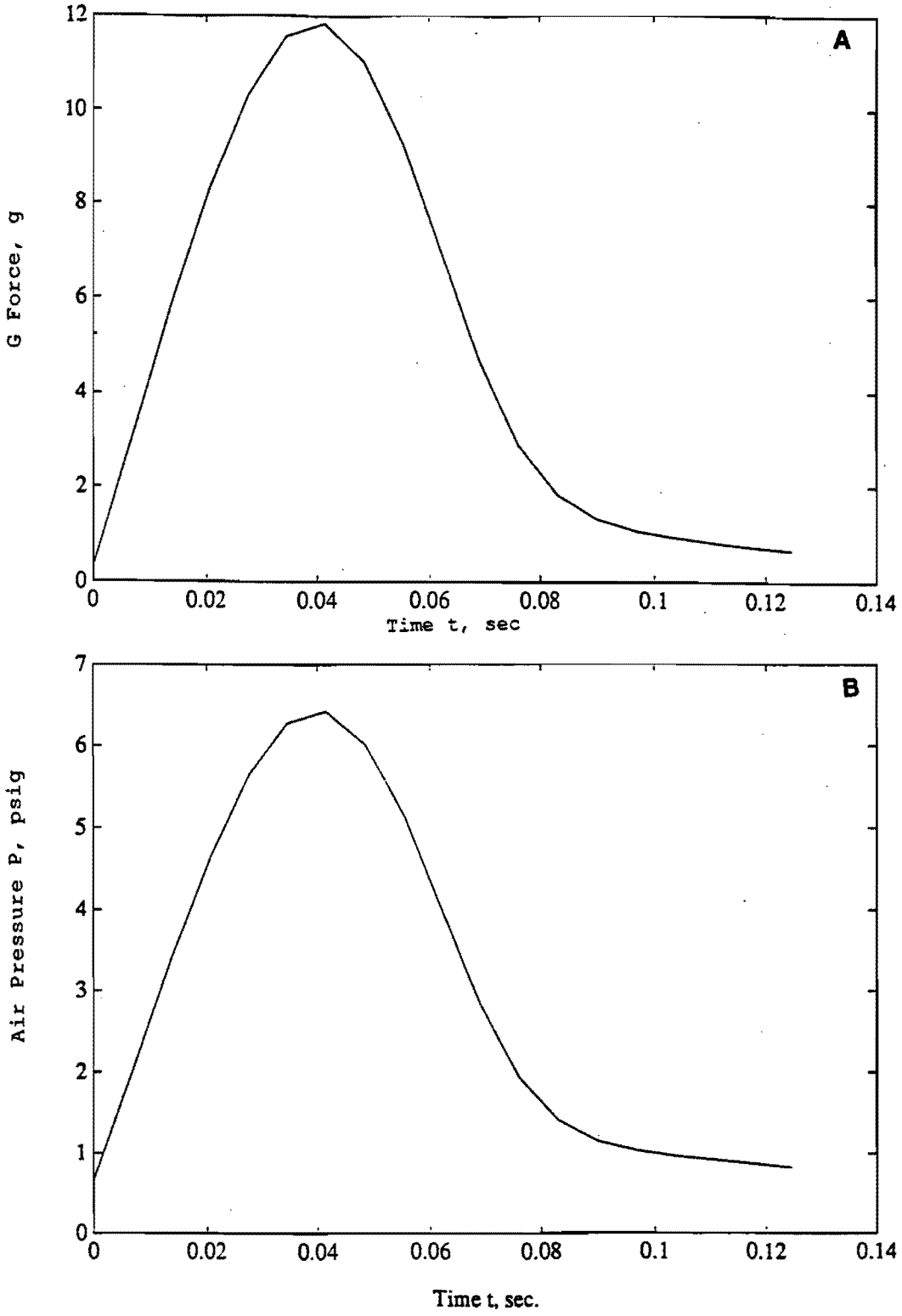

Analytical Results of Simple Airbags

Figure 7. 9' x 4' x 2', H = 13', M = 2490 lbs, A_v = 1.56 ft^2; A. G force, B. Air pressure

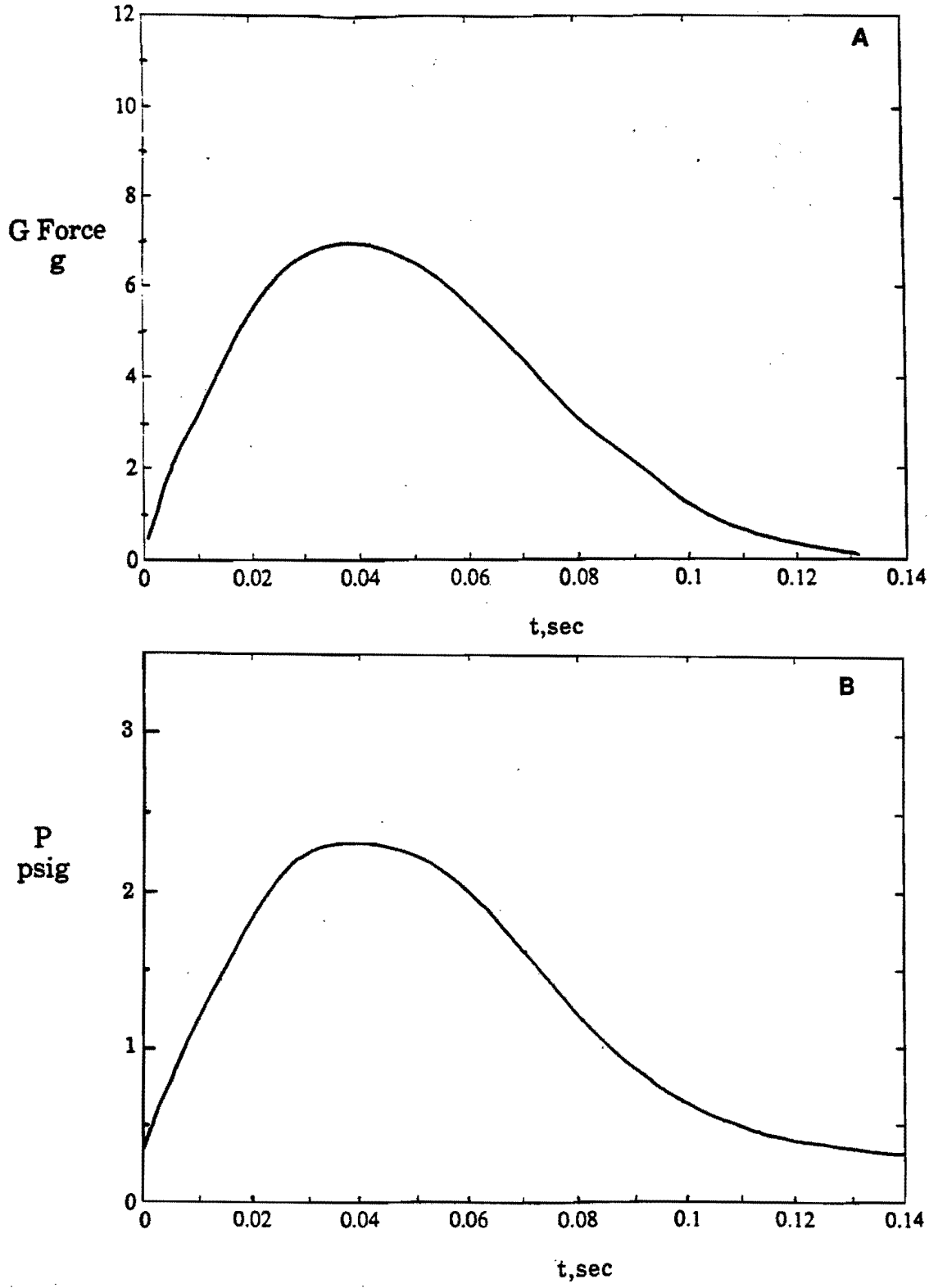

Analytical Results of Simple Airbags

Figure 8. 9' x 4' x 3', H = 7', M = 1490 lbs, A_v = 1.78 ft^2; A. G force, B. Air pressure

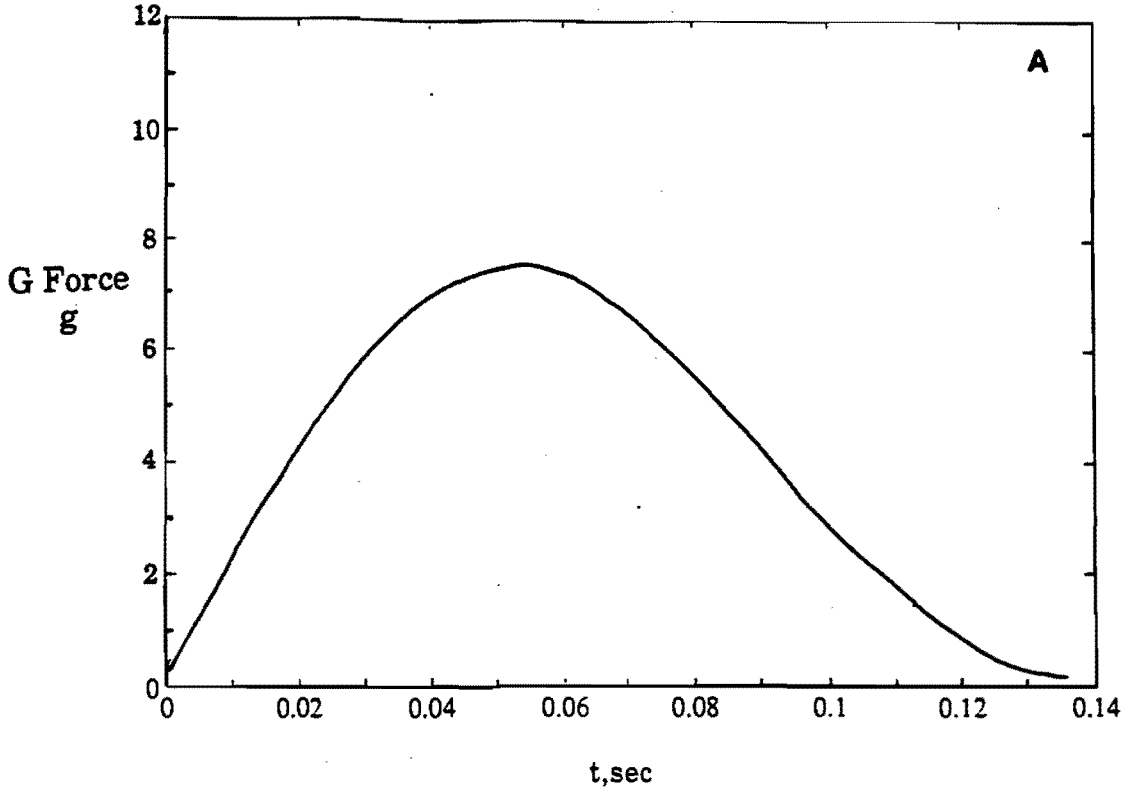

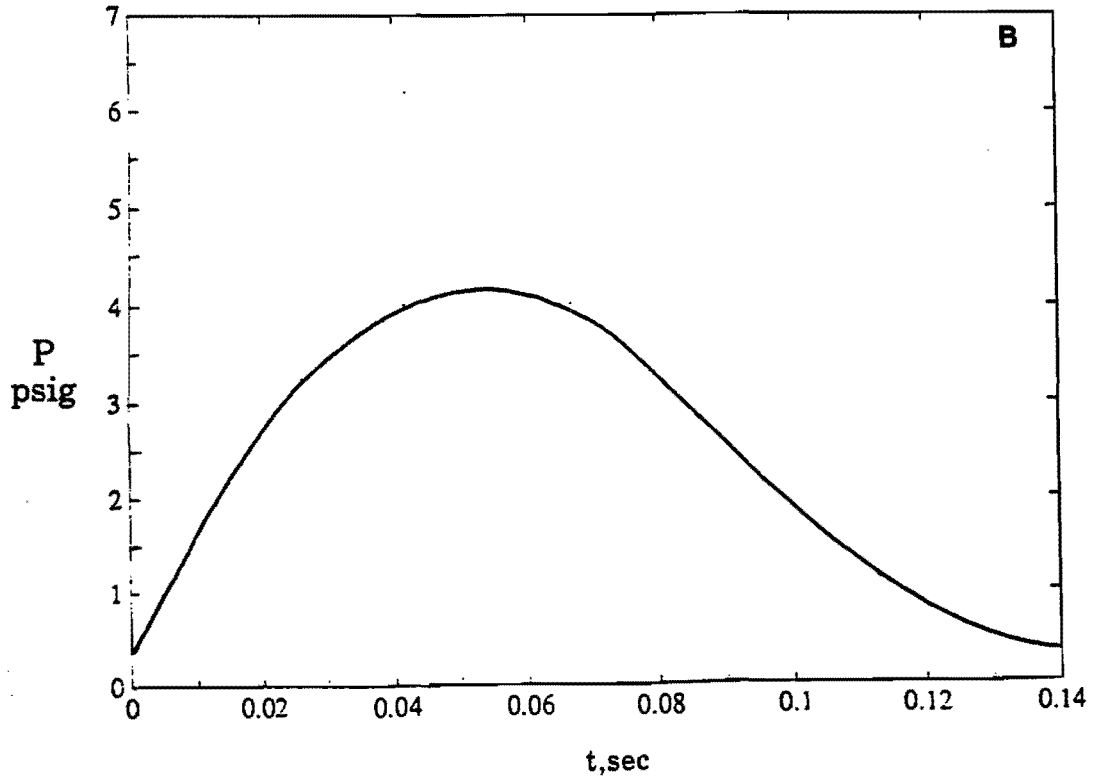

Analytical Results of Simple Airbags

Figure 9. 9' x 4' x 3', H = 7', M = 2490 lbs, A_v = 1.22 ft^2; A. G force, B. Air pressure

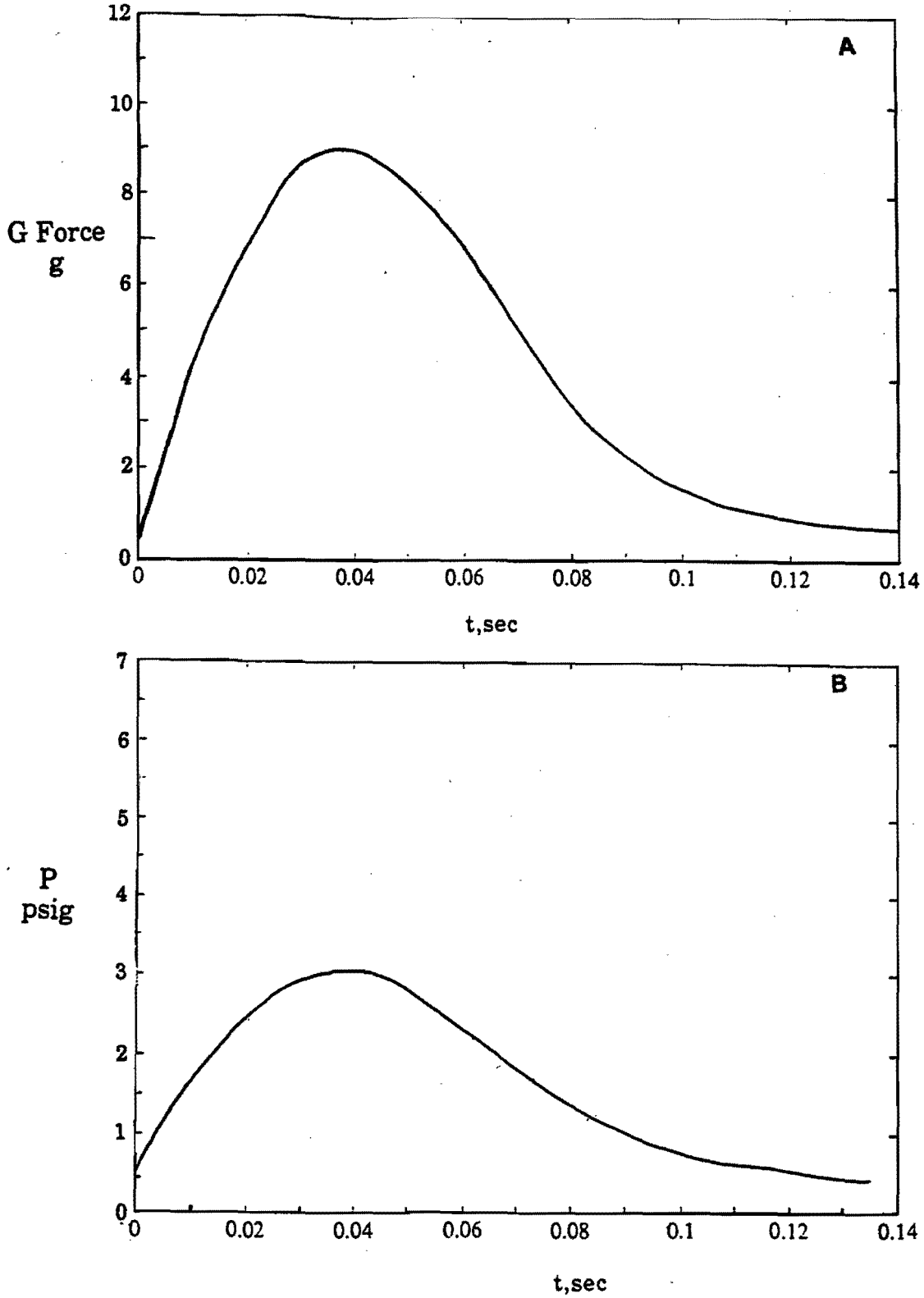

Analytical Results of Simple Airbags

Figure 10. 9' x 4' x 3', H = 13', M = 1490 lbs, A_v = 2.22 ft^2; A. G force, B. Air Pressure

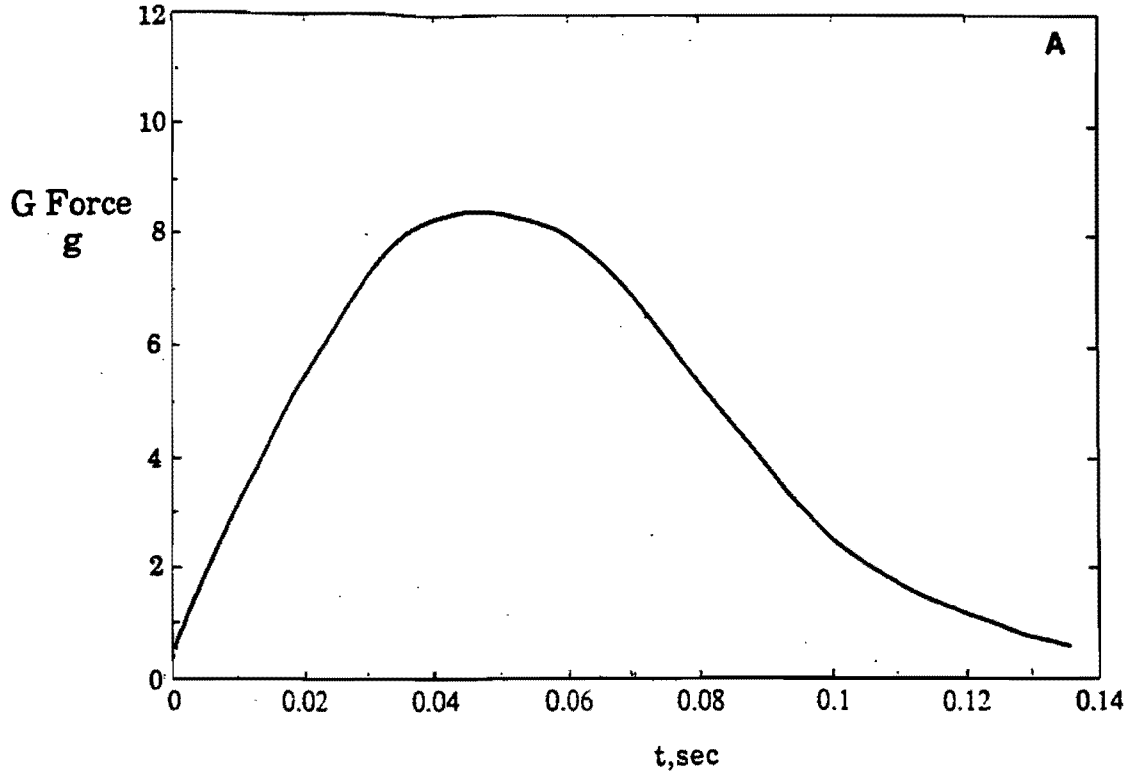

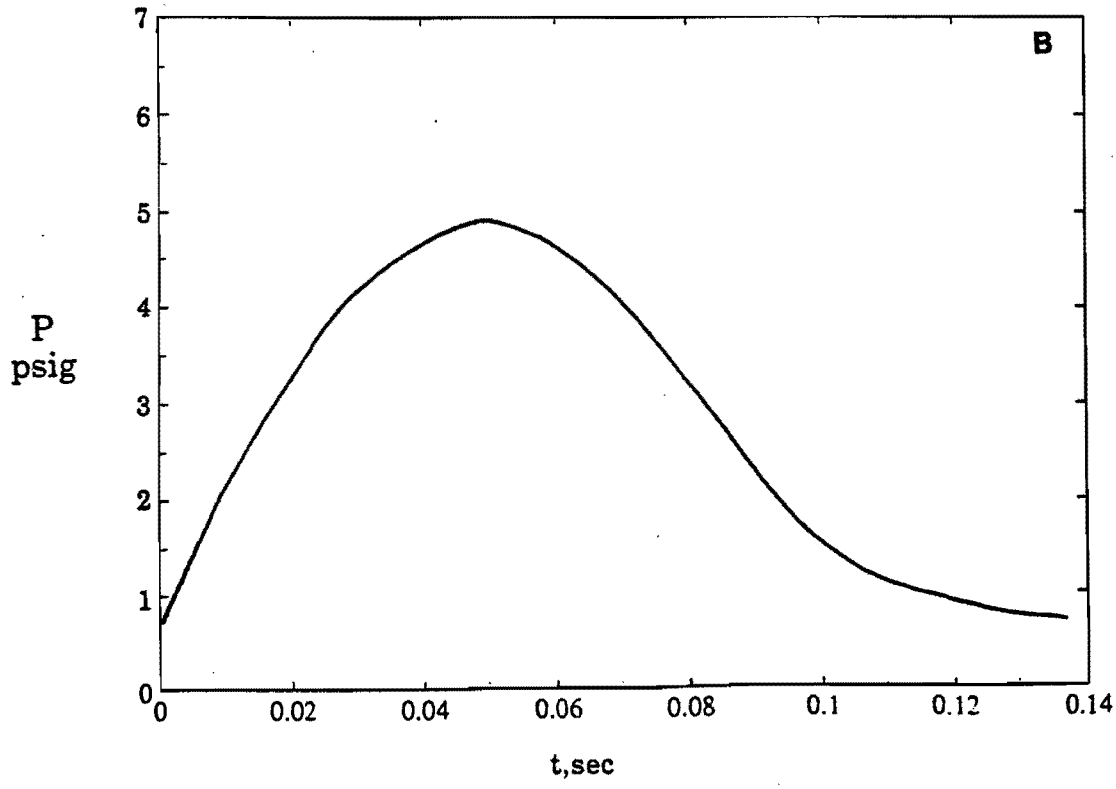

Analytical Results of Simple Airbags

Figure 11. 9' x 4' x 3', H = 13', M = 2490 lbs, A_v = 1.78 ft^2; A. G force, B. Air pressure

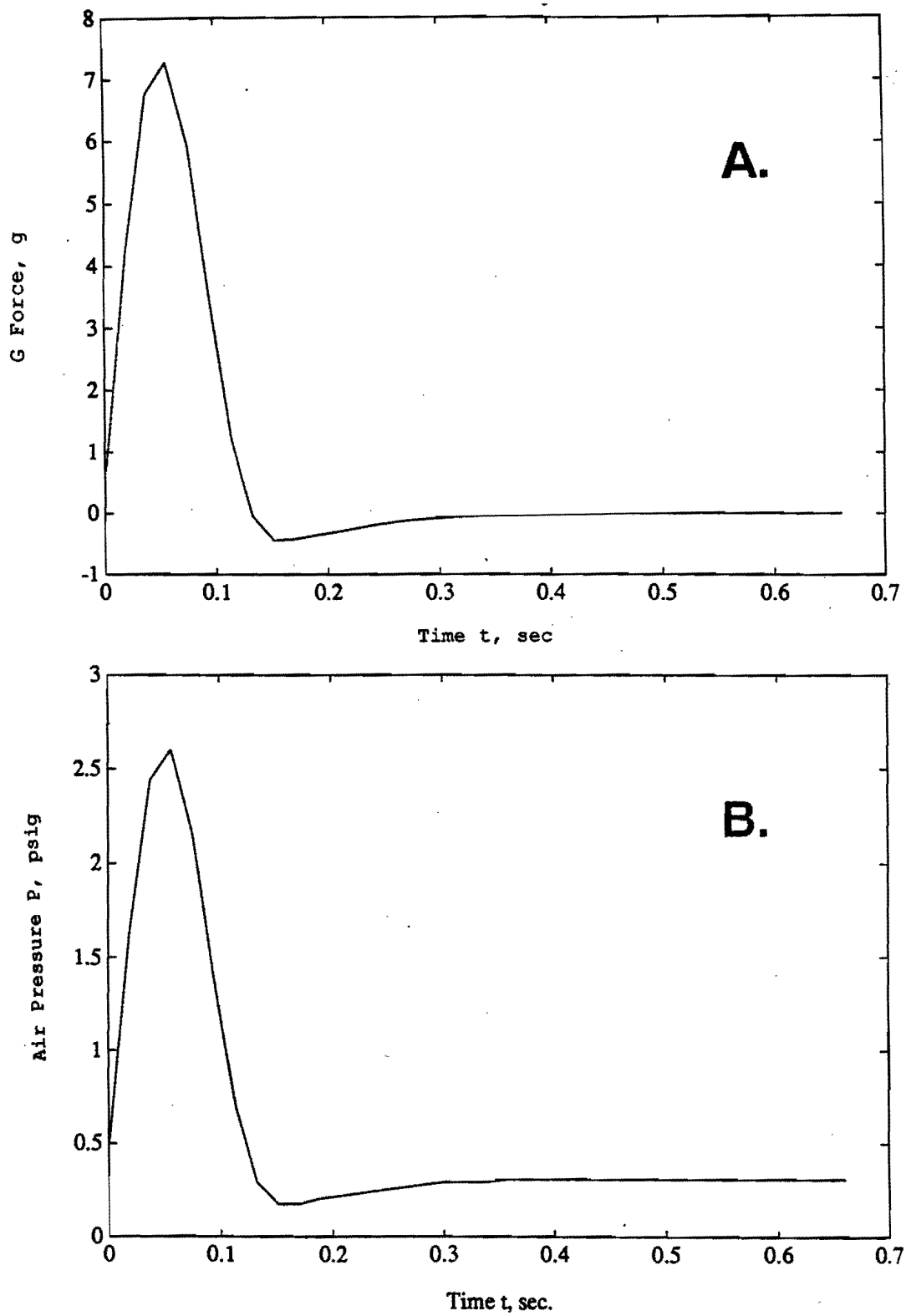

Analytical Results of Simple Airbags

Figure 12. 8' x 4' x 4', H = 7', M = 1390 lbs, A_v = 1.39 ft^2; A. G force, B. Air pressure

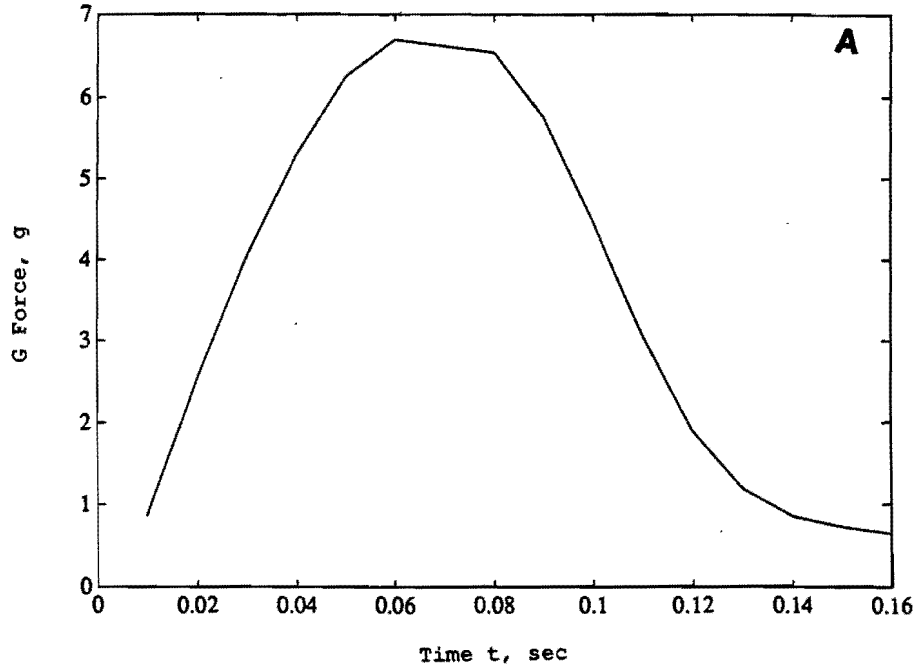

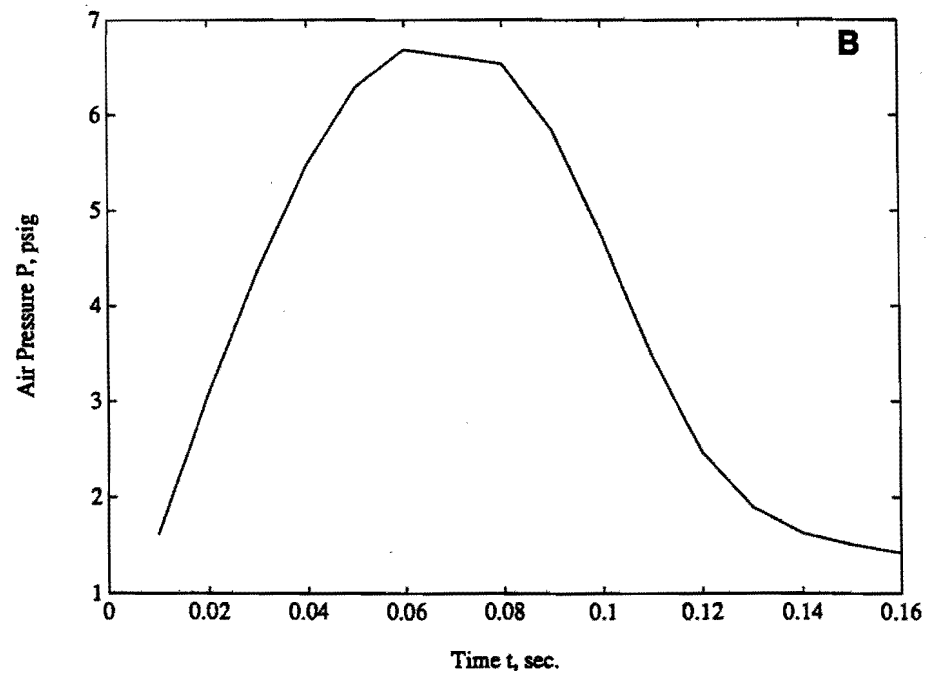

Analytical Results of Simple Airbags

Figure 13. 8' x 4' x 3', H = 13', M = 4000 lbs, A_v = 1.5 ft^2; A. G force, B. Air pressure

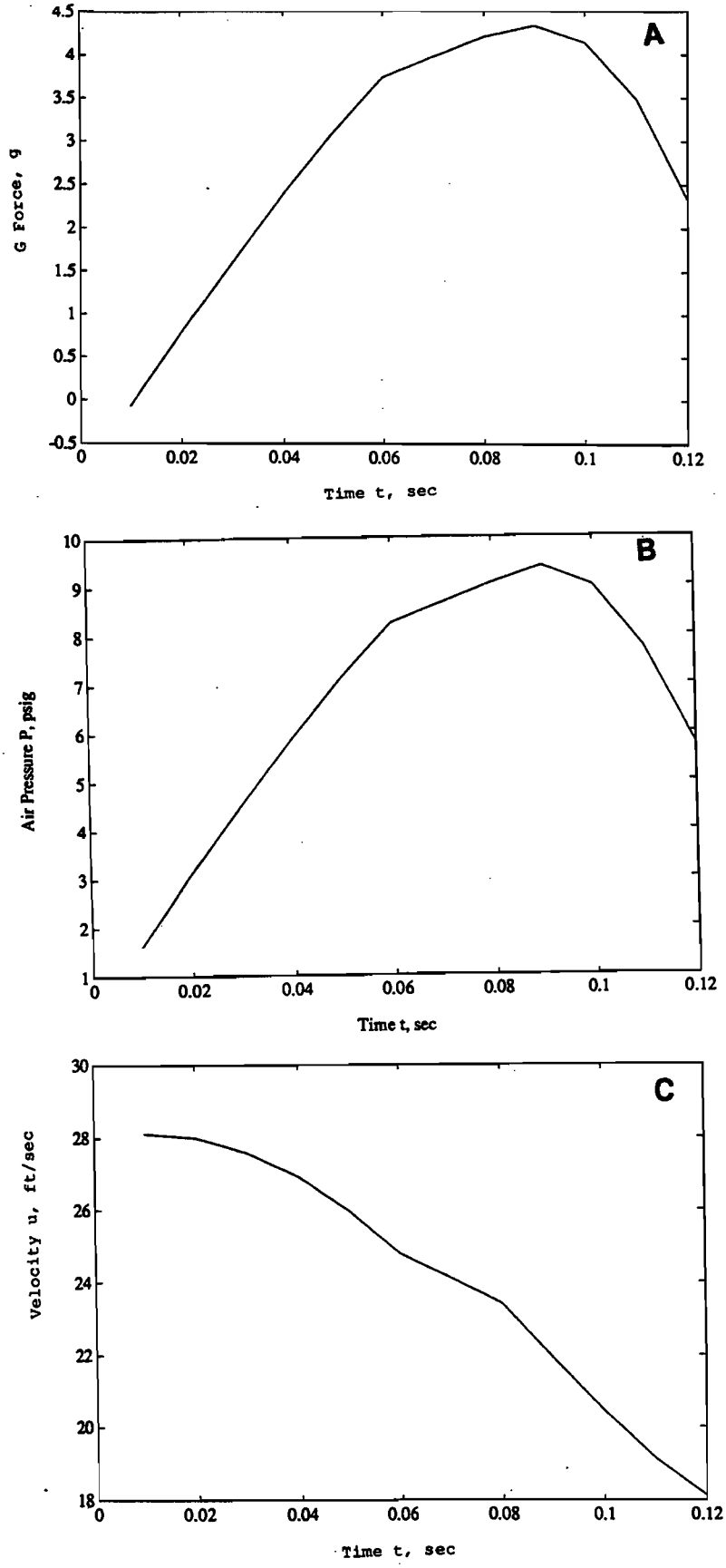

Analytical Results of Simple Airbags

Figure 14. 8' x 4' x 3', H = 13', M = 8000 lbs, A_v = 1.5 ft^2; A. G force, B. Air pressure, C. Velocity

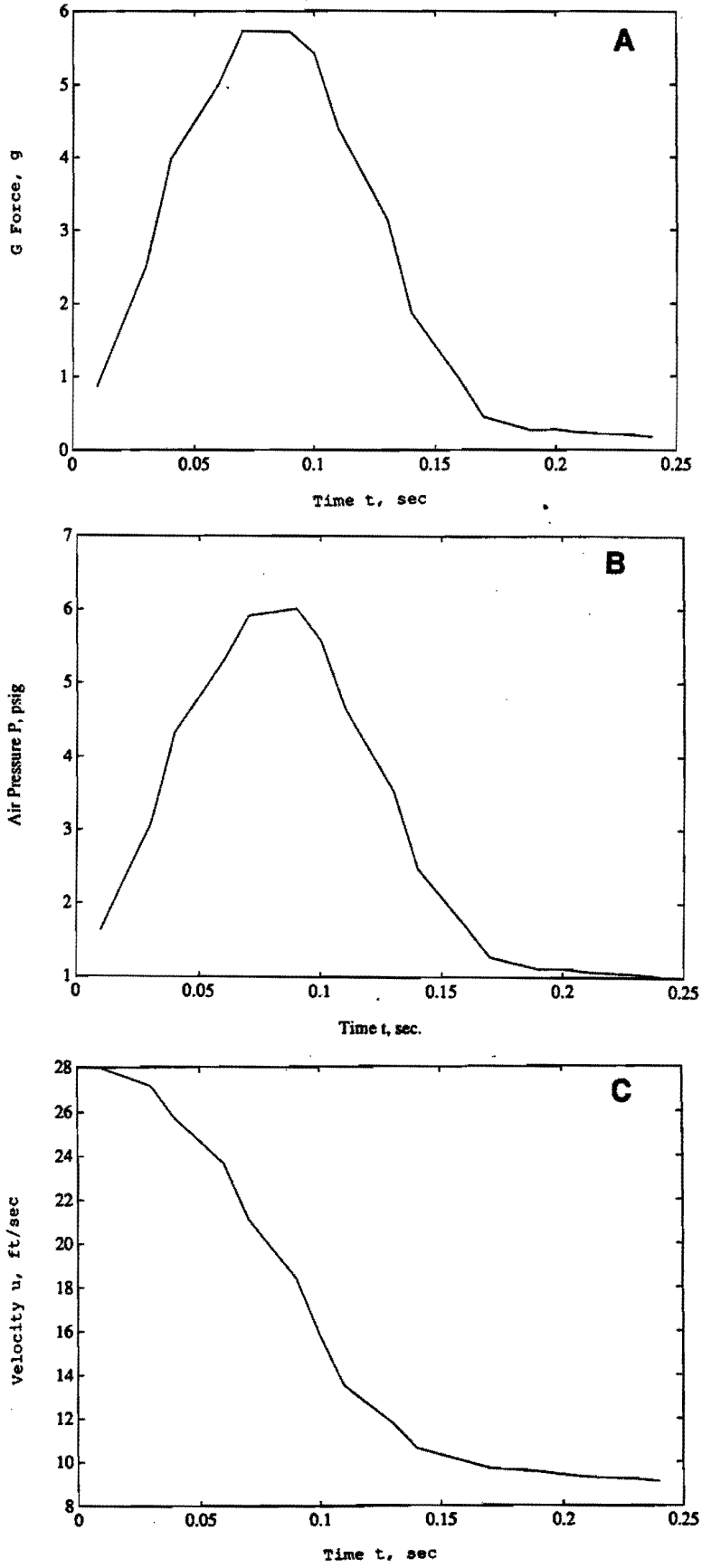

Analytical Results of Simple Airbags

Figure 15. 8' x 4' x 4', H = 13', M = 4000 lbs, A_v = 1.5 ft^2; A. G force, B. Air pressure, C. Velocity

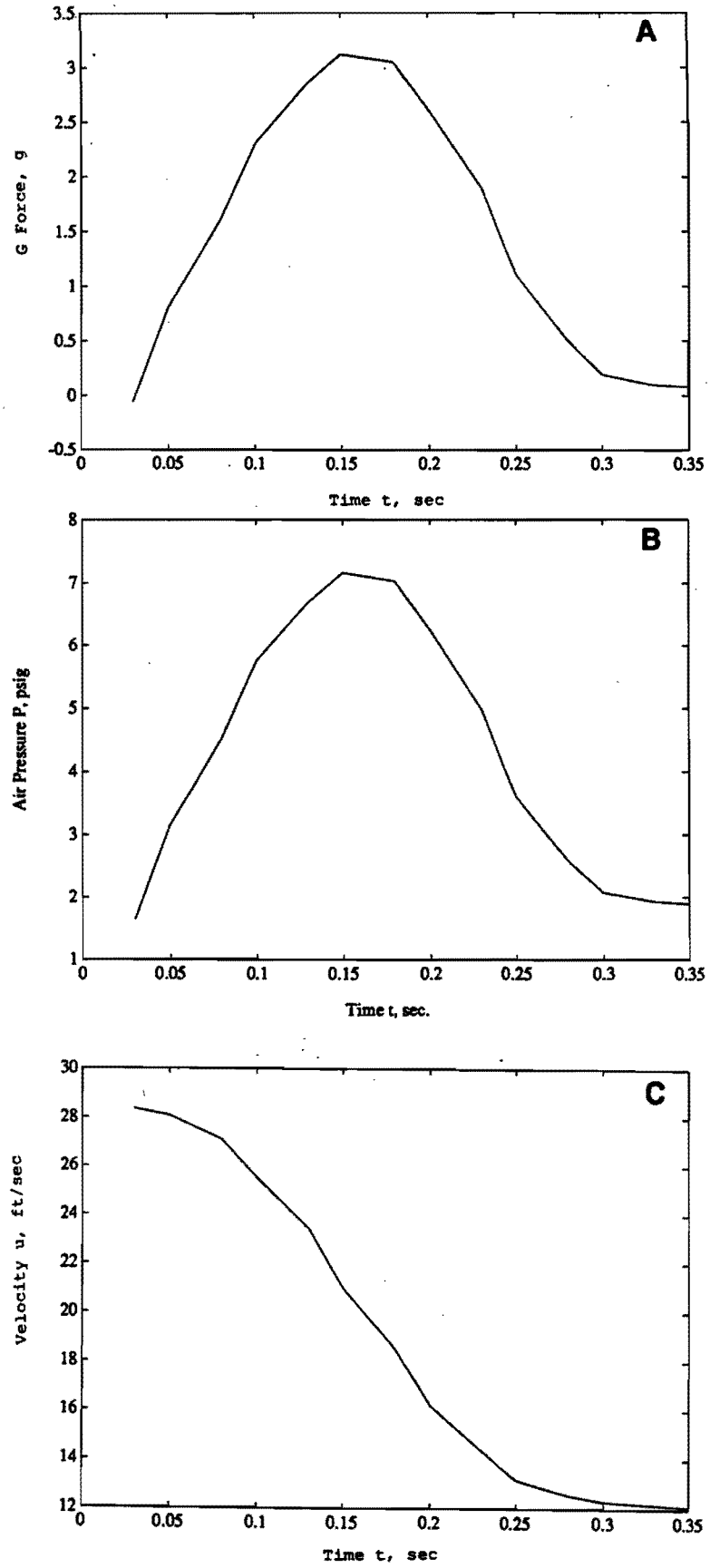

Analytical Results of Simple Airbags

Figure 16. 8' x 4' x 7', H = 13', M = 8000 lbs, A_v = 1.5 ft^2; A. G force, B. Air pressure, C. Velocity

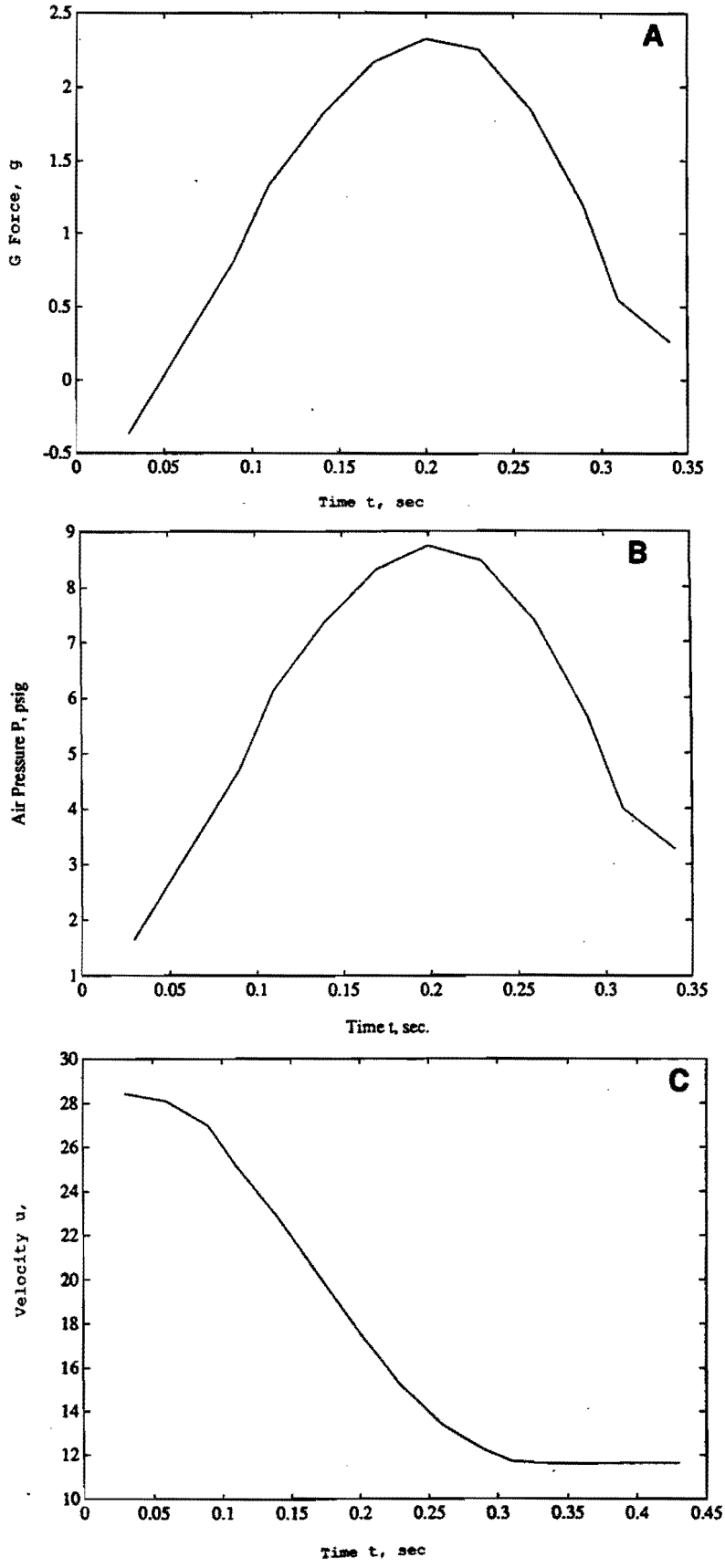

Analytical Results of Simple Airbags

Figure 17. 8' x 4' x 8', H = 13', M = 12000 lbs, A_v = 1.5 ft^2; A. G force, B. Air pressure, C. Velocity

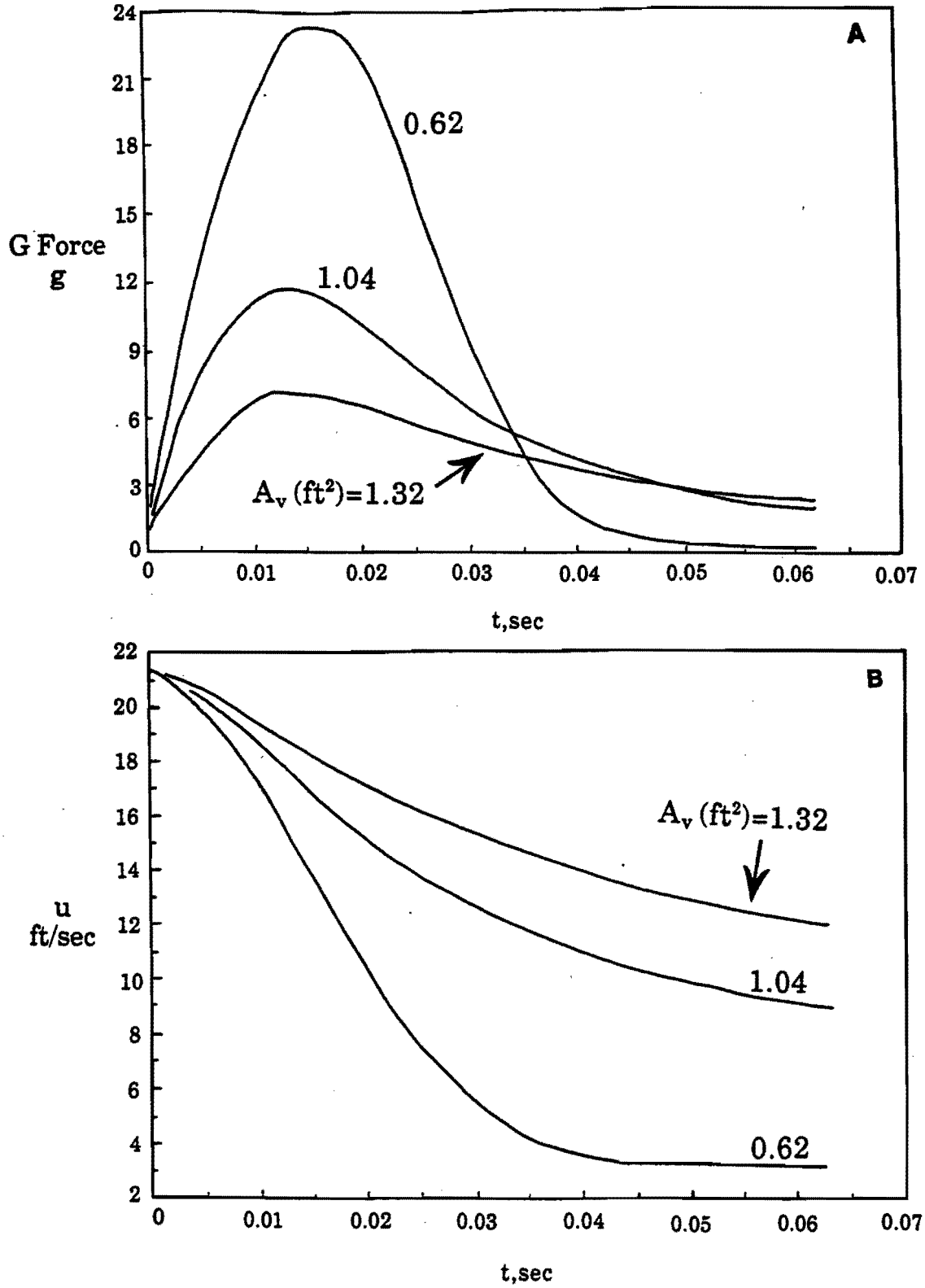

Analytical Results of Simple Airbags
Figure 18. 4' x 4' x 1', H = 7', M = 315 lbs, A. G force, B. Velocity

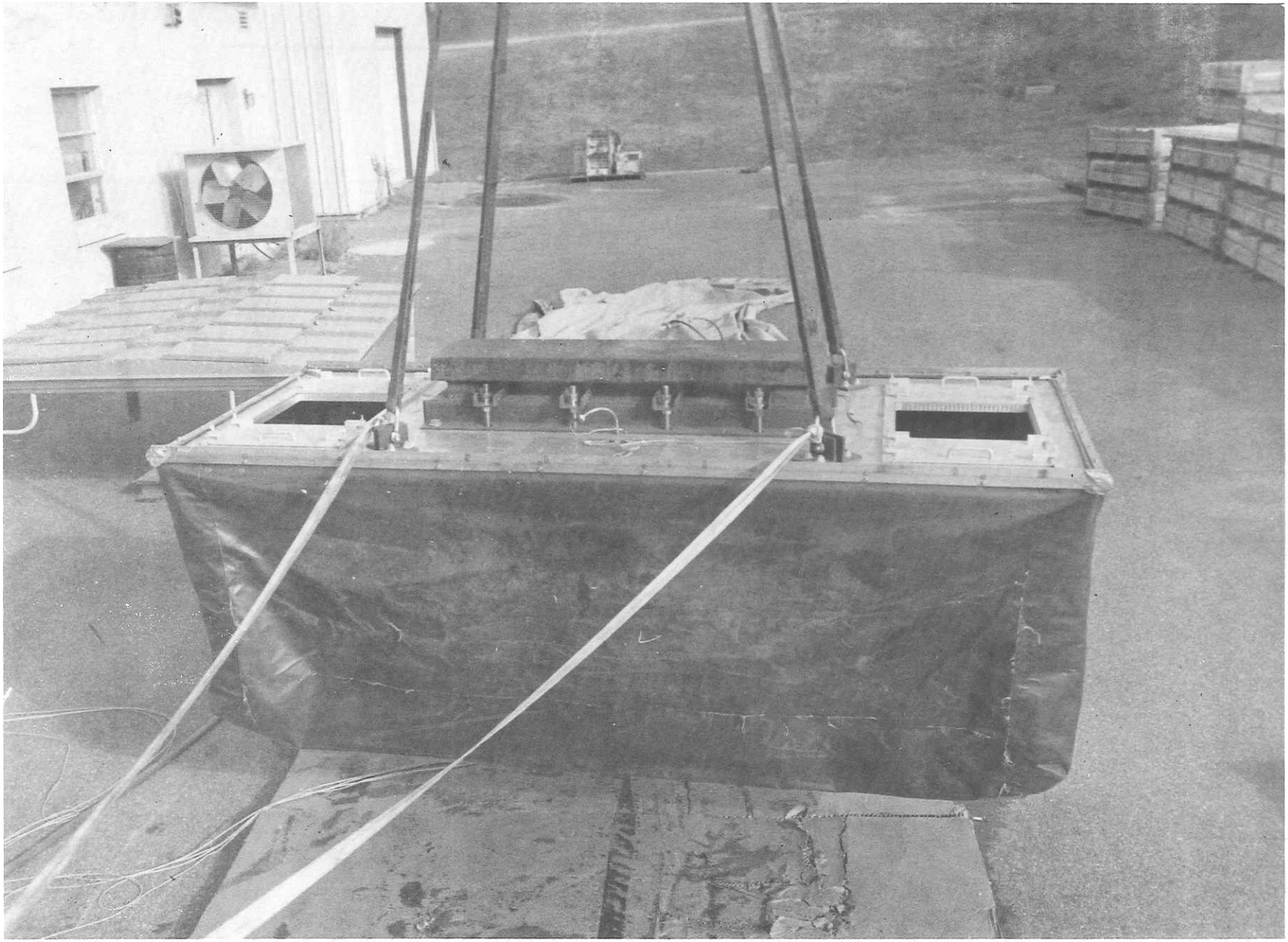

Figure 19. Photograph Showing the 9' x 4' x 4' Simple Airbag with Two Vent Openings and a Payload

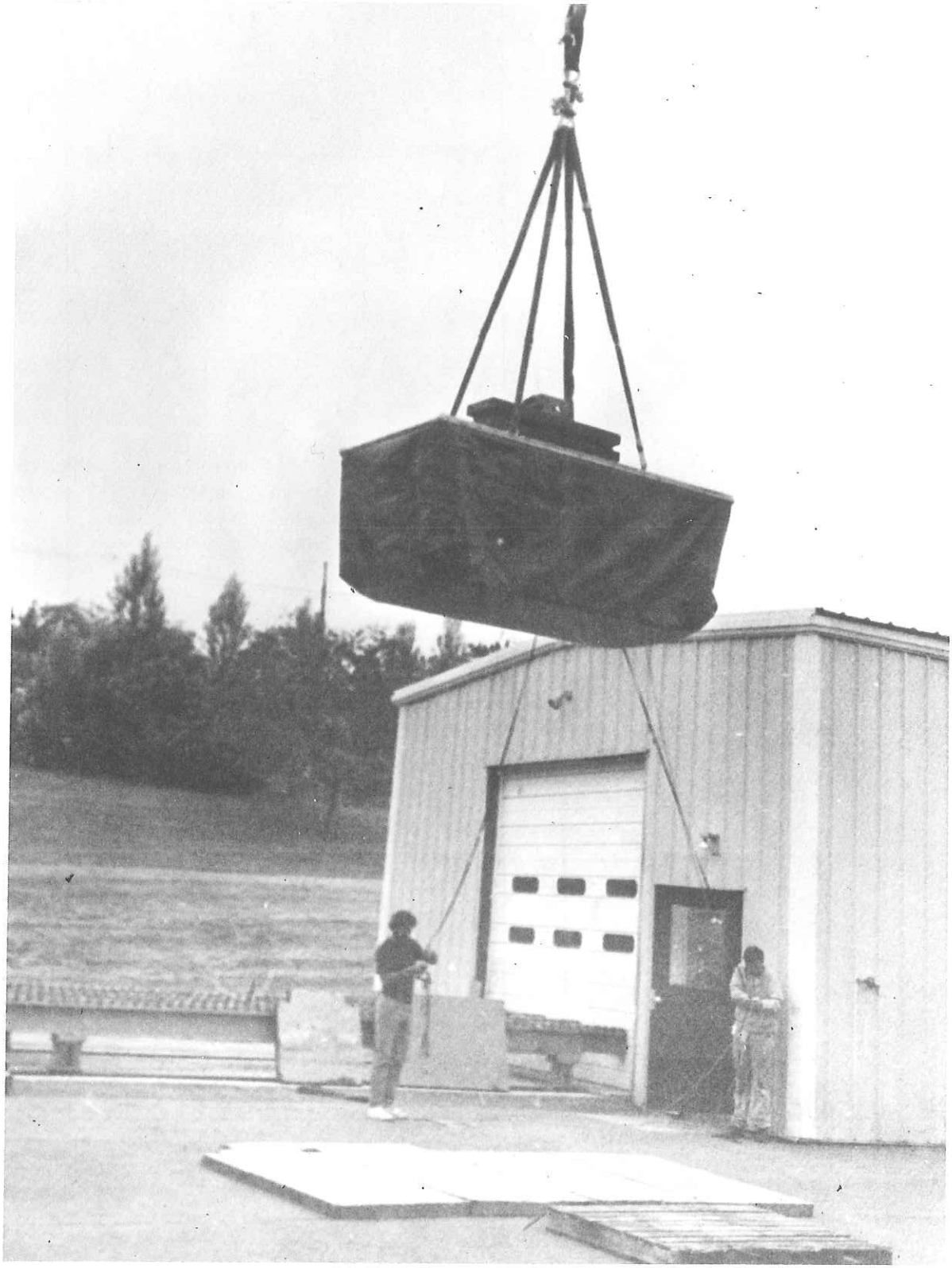

Figure 20. Photograph Showing the 9' x 4' x 4' Simple Airbag at 13' above Ground before a Drop Test

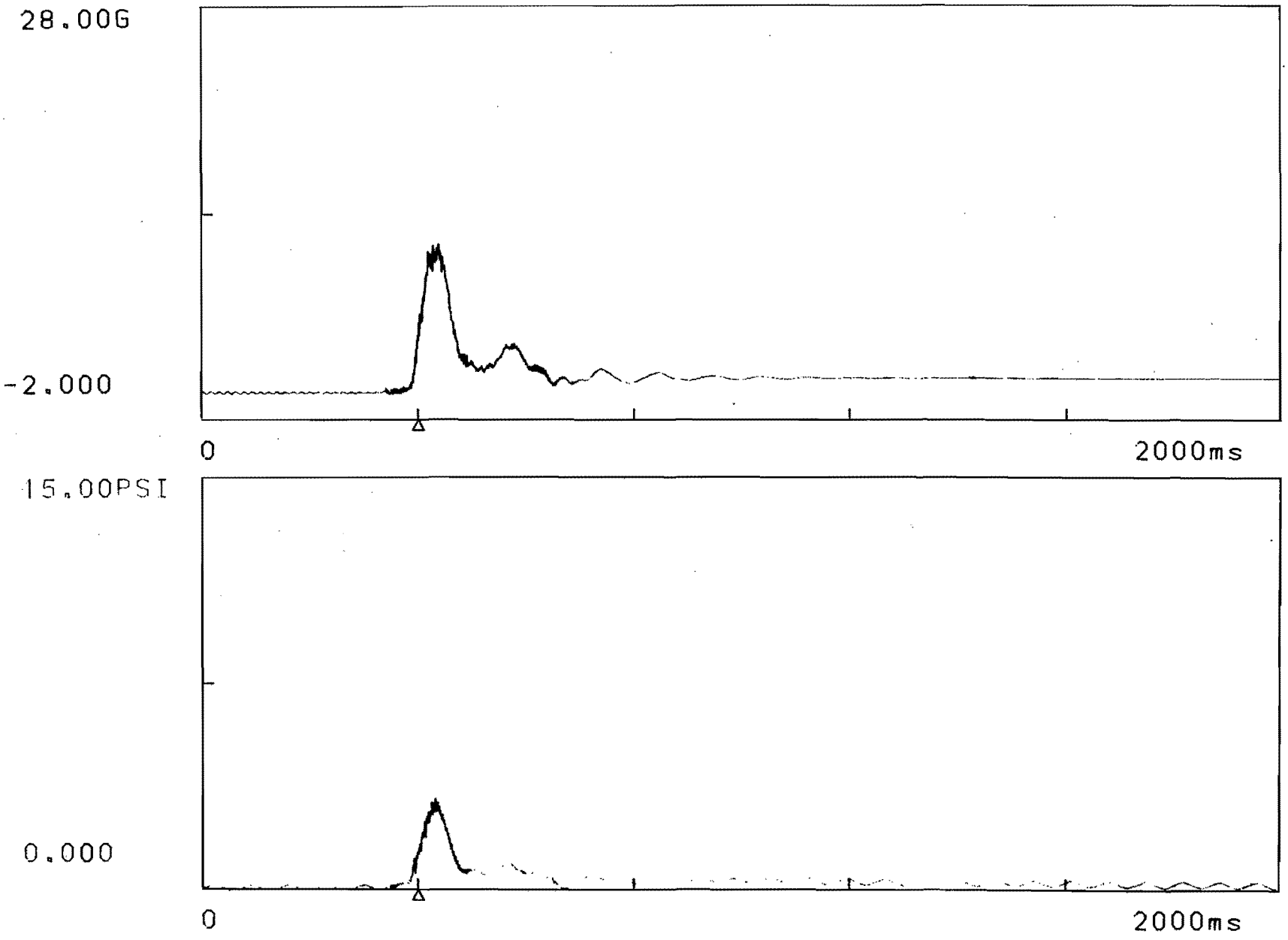

50

Experimental Results of the 9' x 4' x 4' Simple Airbag
Figure 21. H = 7', M = 1490 lbs, A_v = 1.78 ft^2

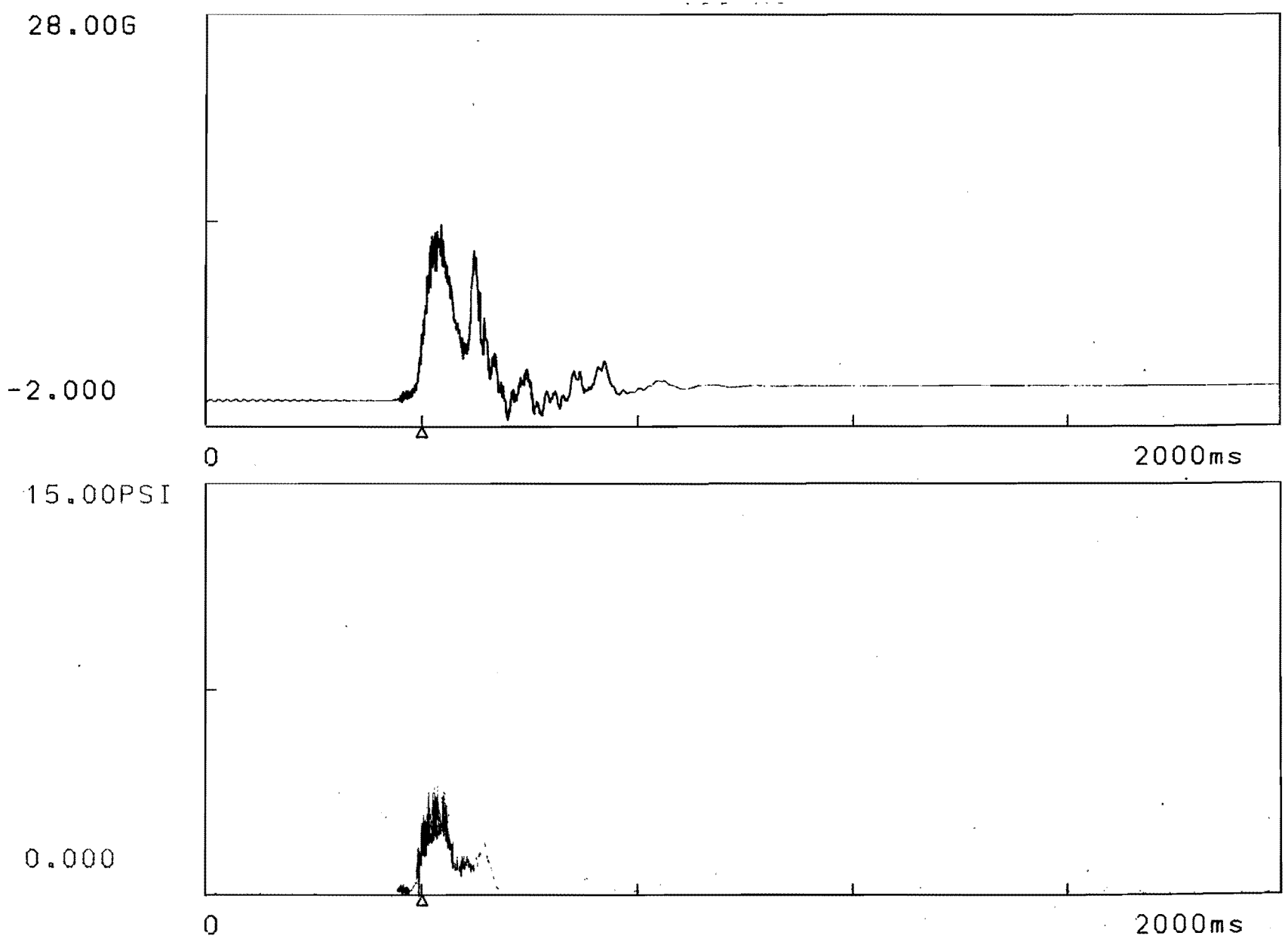

Experimental Results of the 9' x 4' x 4' Simple Airbag
Figure 22. H = 9', M = 1490 lbs, A_v = 2.0 ft^2

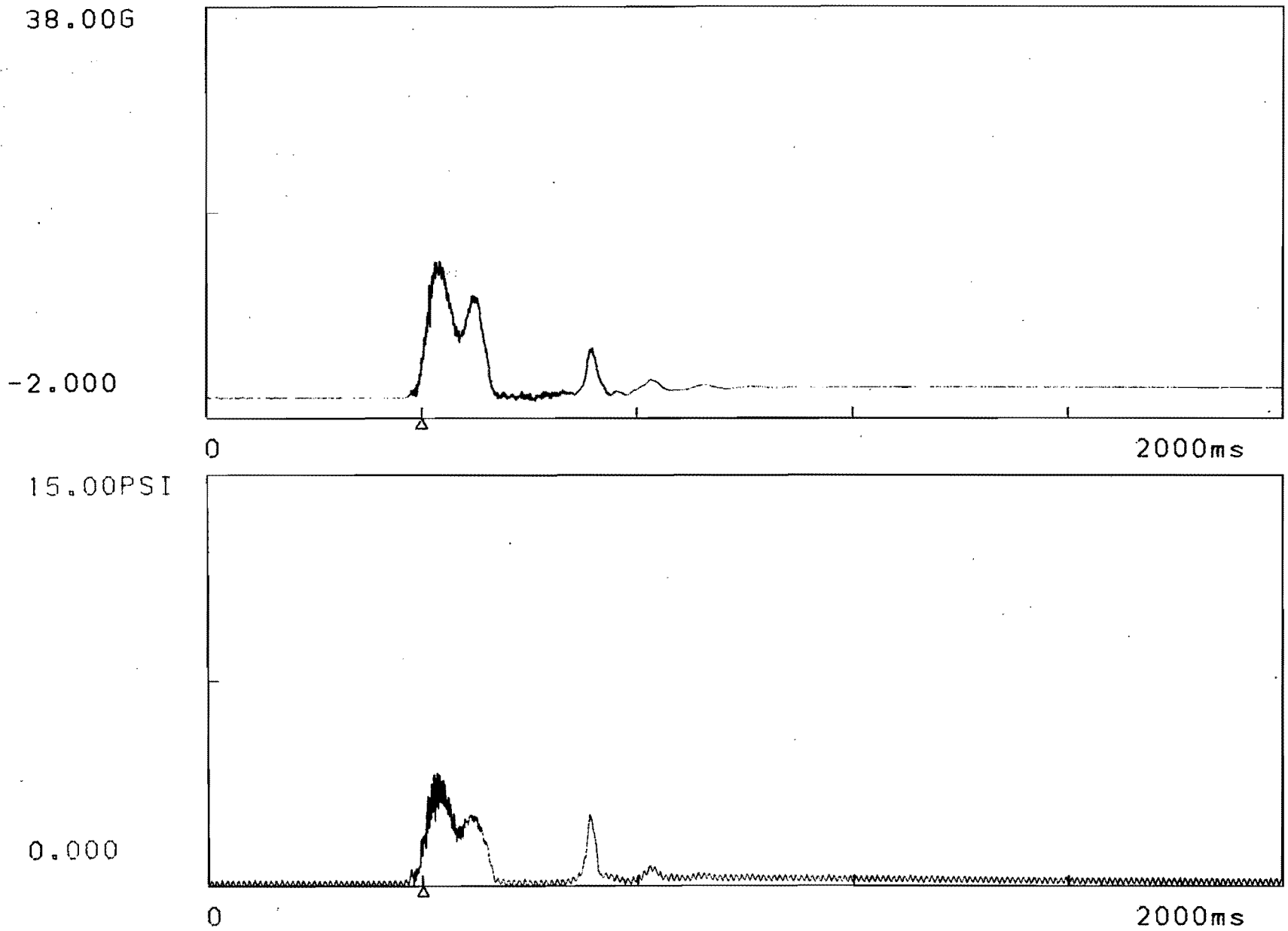

Experimental Results of the 9' x 4' x 4' Simple Airbag
Figure 23. H = 11', M = 1490 lbs, A_v = 2.22 ft^2

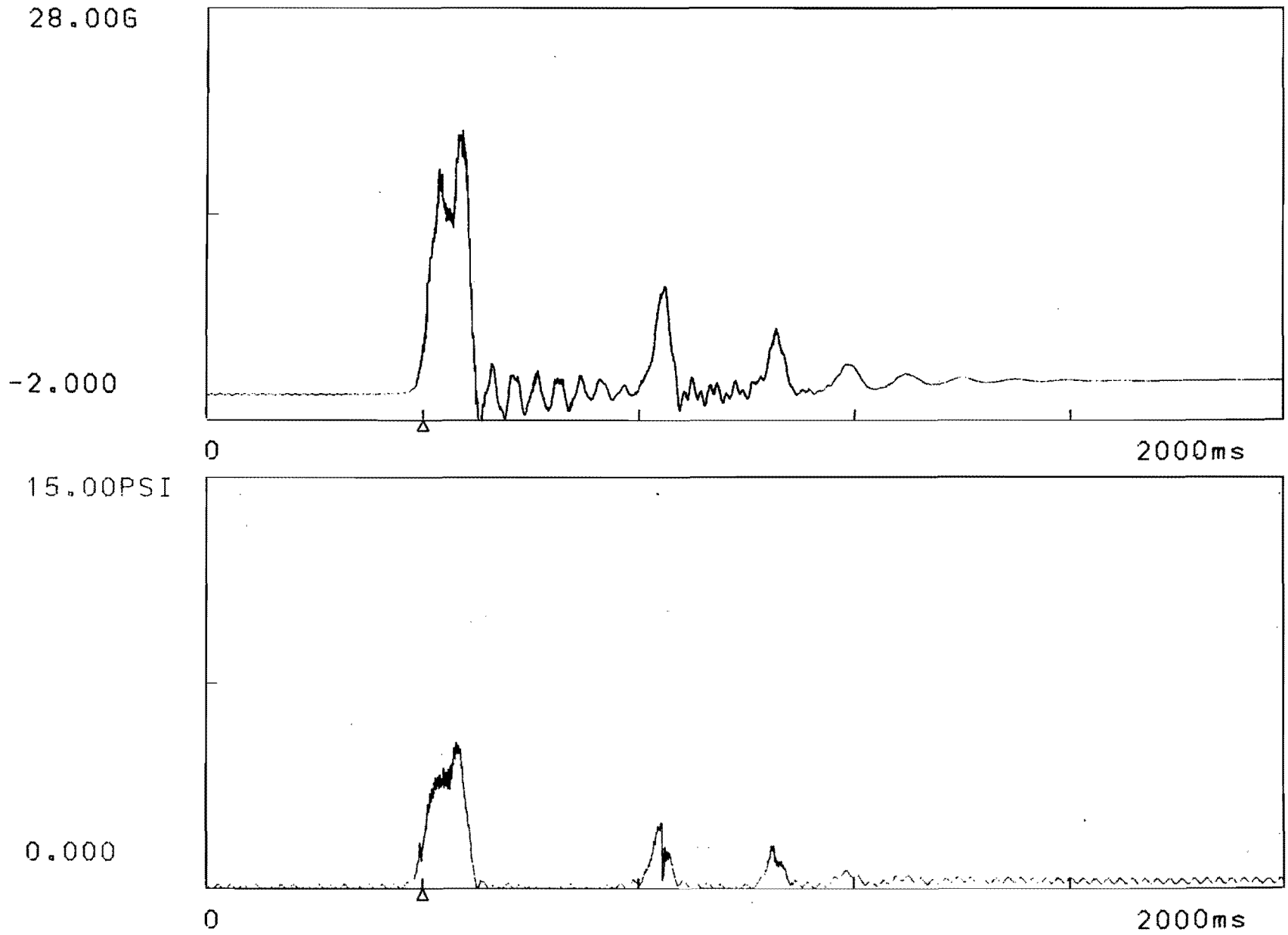

Experimental Results of the 9' x 4' x 4' Simple Airbag
Figure 24. H = 13', M = 1490 lbs, A_v = 2.22 ft^2

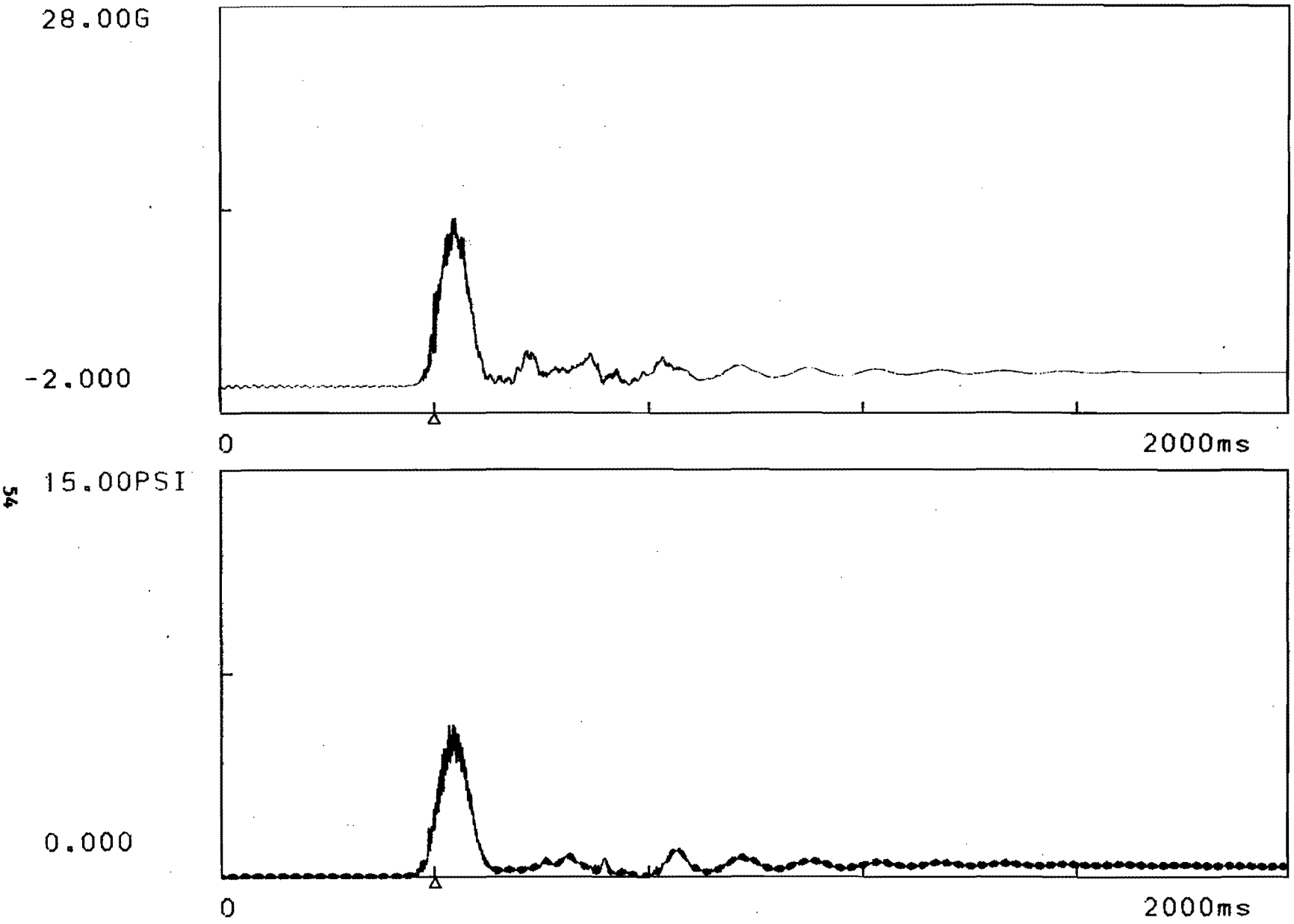

Experimental Results of the 9' x 4' x 4' Simple Airbag
Figure 25. H = 7', M = 2490 lbs, A_v = 1.22 ft^2

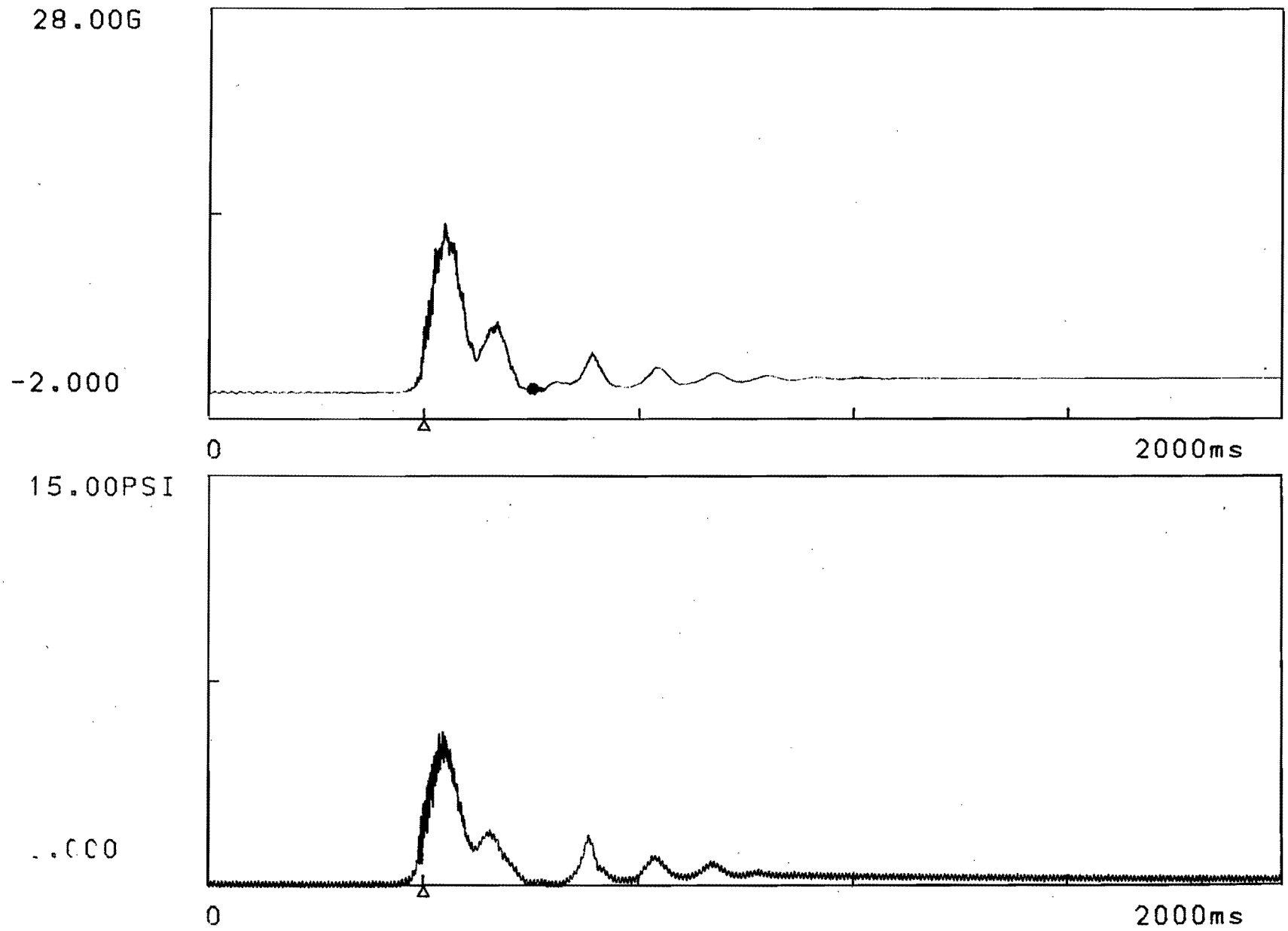

Experimental Results of the 9' x 4' x 4' Simple Airbag
Figure 26. H = 9', M = 2490 lbs, A_v = 1.56 ft^2

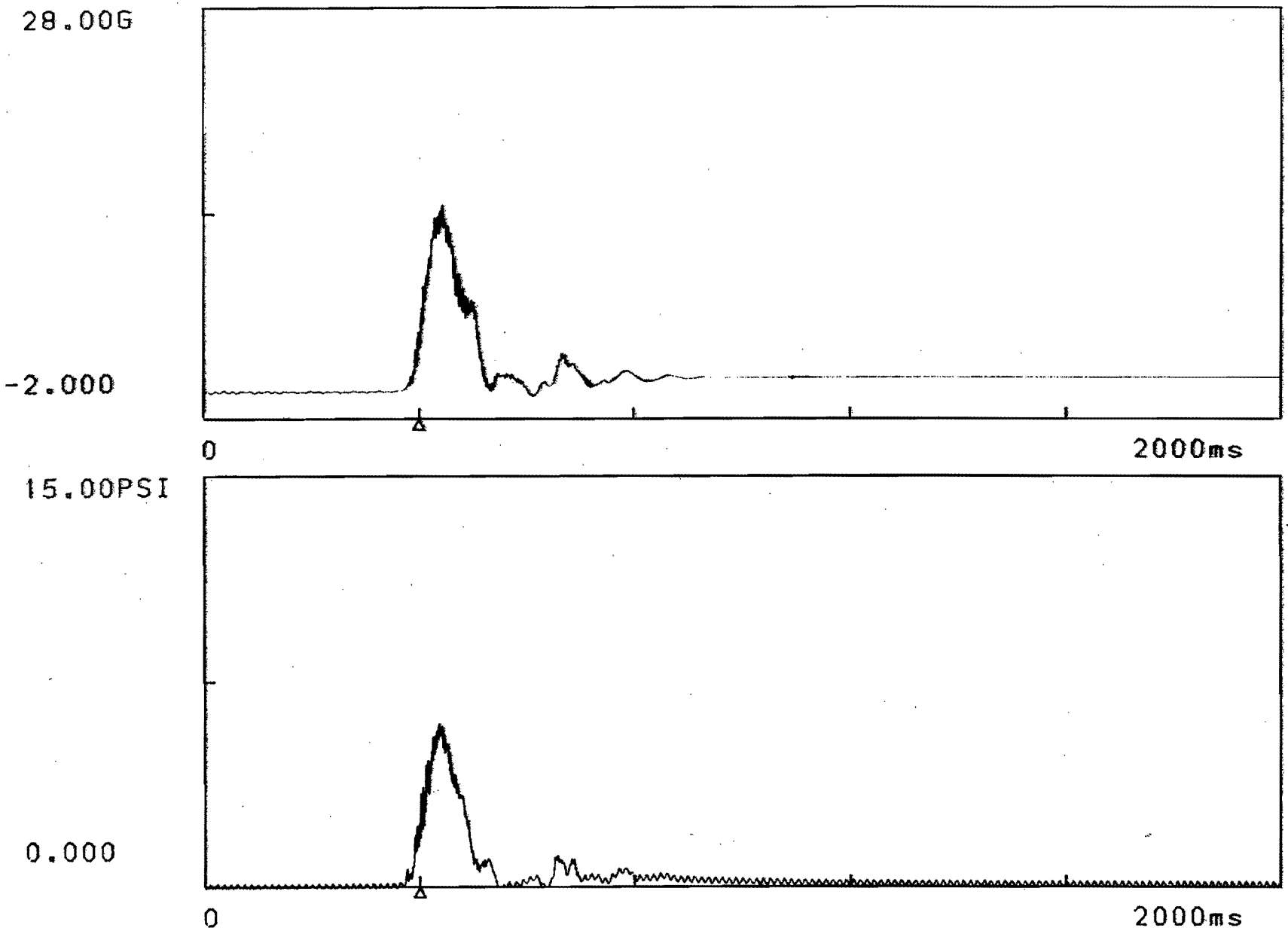

Experimental Results of the 9' x 4' x 4' Simple Airbag
Figure 27. H = 11', M = 2490 lbs, A_v = 1.56 ft^2

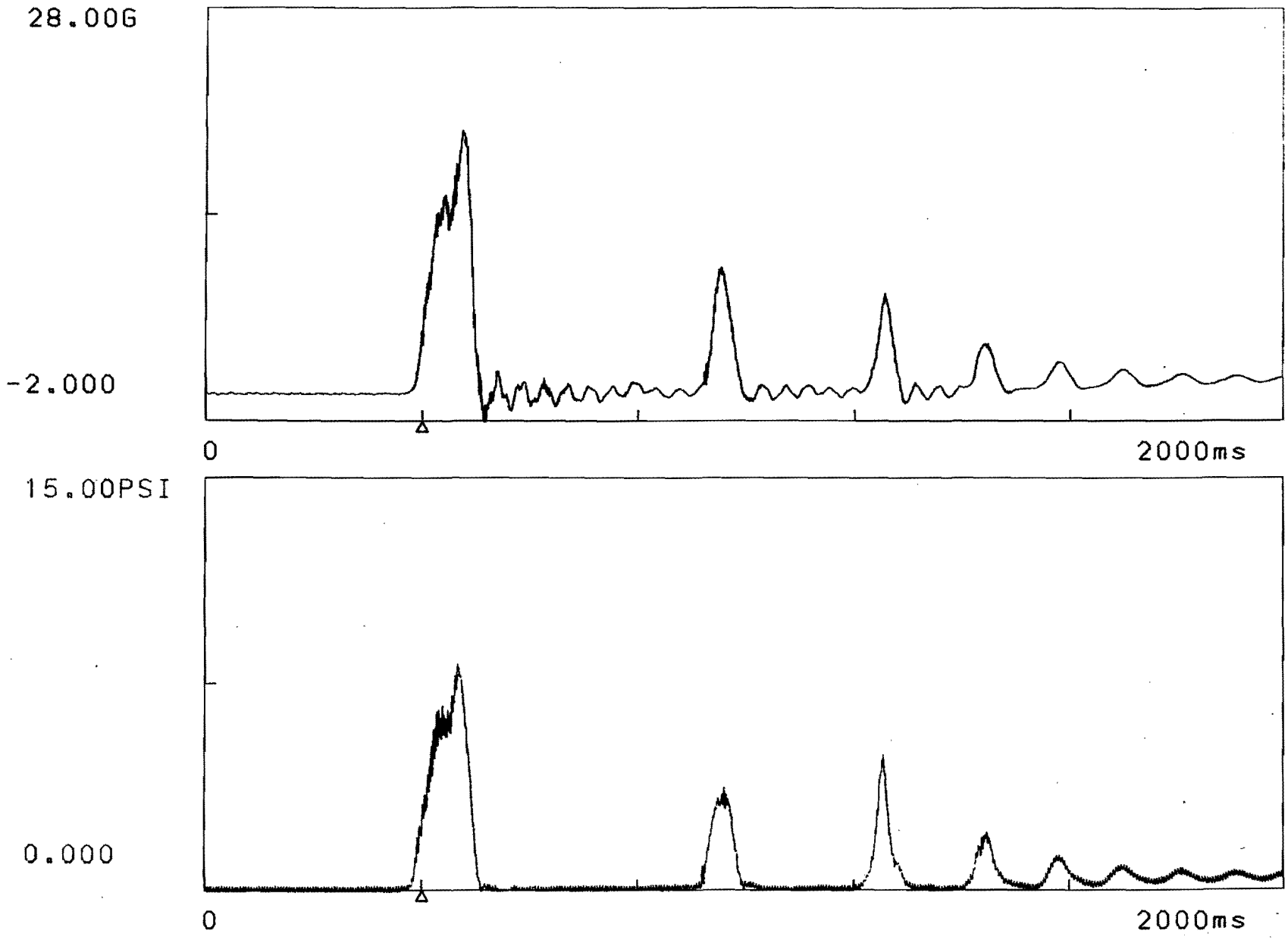

Experimental Results of the 9' x 4' x 4' Simple Airbag
Figure 28. H = 13', M = 2490 lbs, A_v = 1.78 ft^2

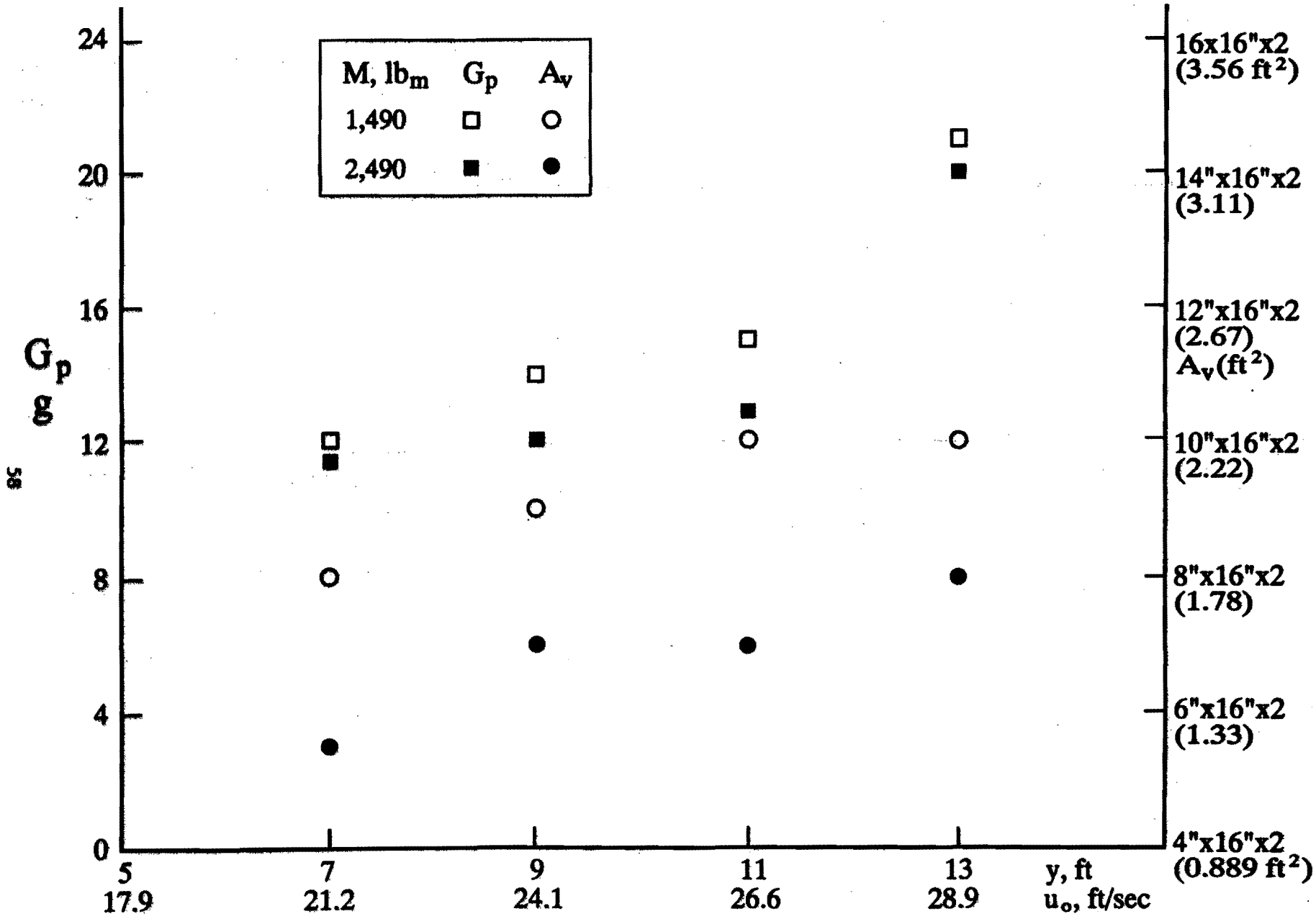

Figure 29. Peak G Force as a Function of Drop Height and Payload Weight for the 9' x 4' x 4' Simple Airbag

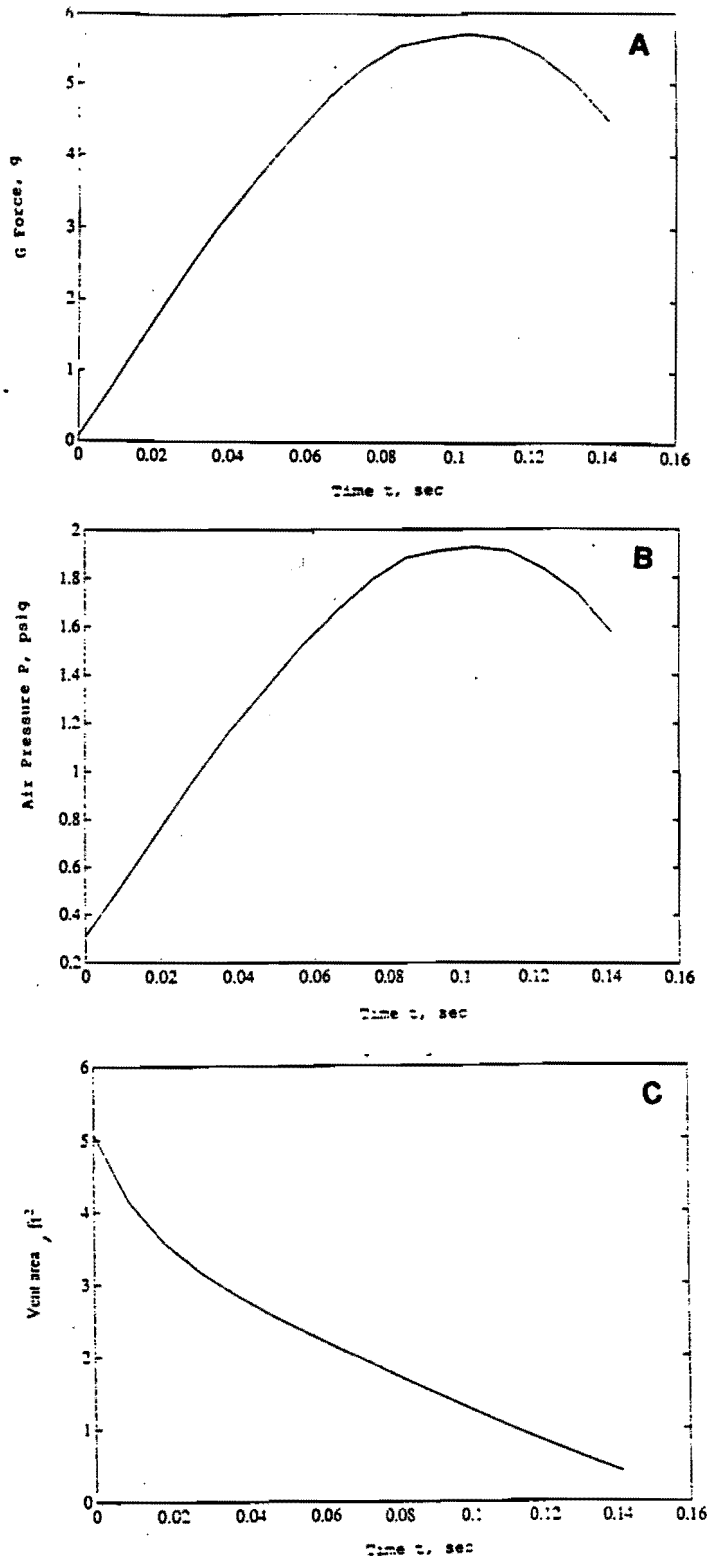

Analytical Results of Vent-Control Complex Airbags
Figure 30. 9' x 4' x 2', H = 7', M = 1490 lbs; A. G Force, B. Air Pressure, C. Vent Area

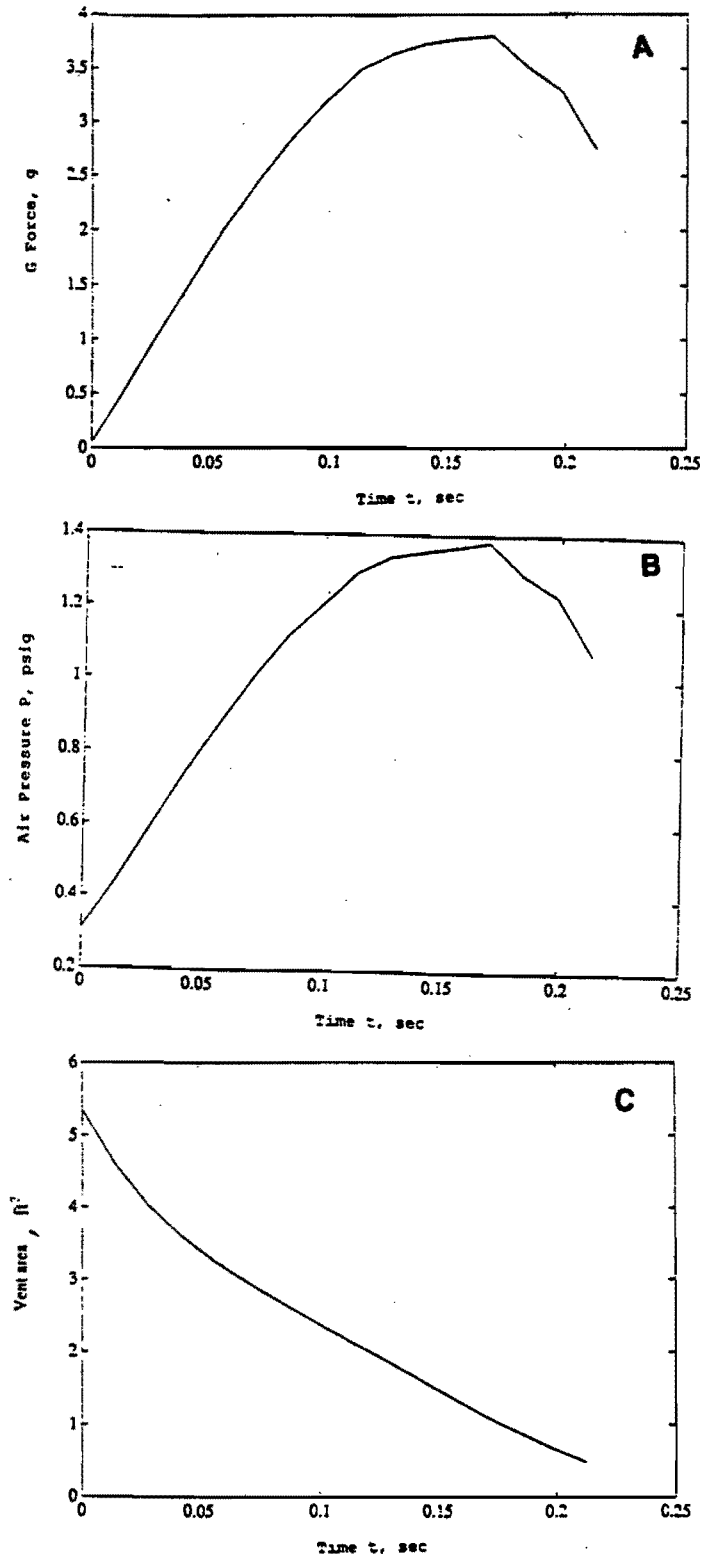

Analytical Results of Vent-Control Complex Airbags
Figure 31. 9' x 4' x 3', H = 7', M = 2490 lbs; A. G Force, B. Air Pressure, C. Vent Area

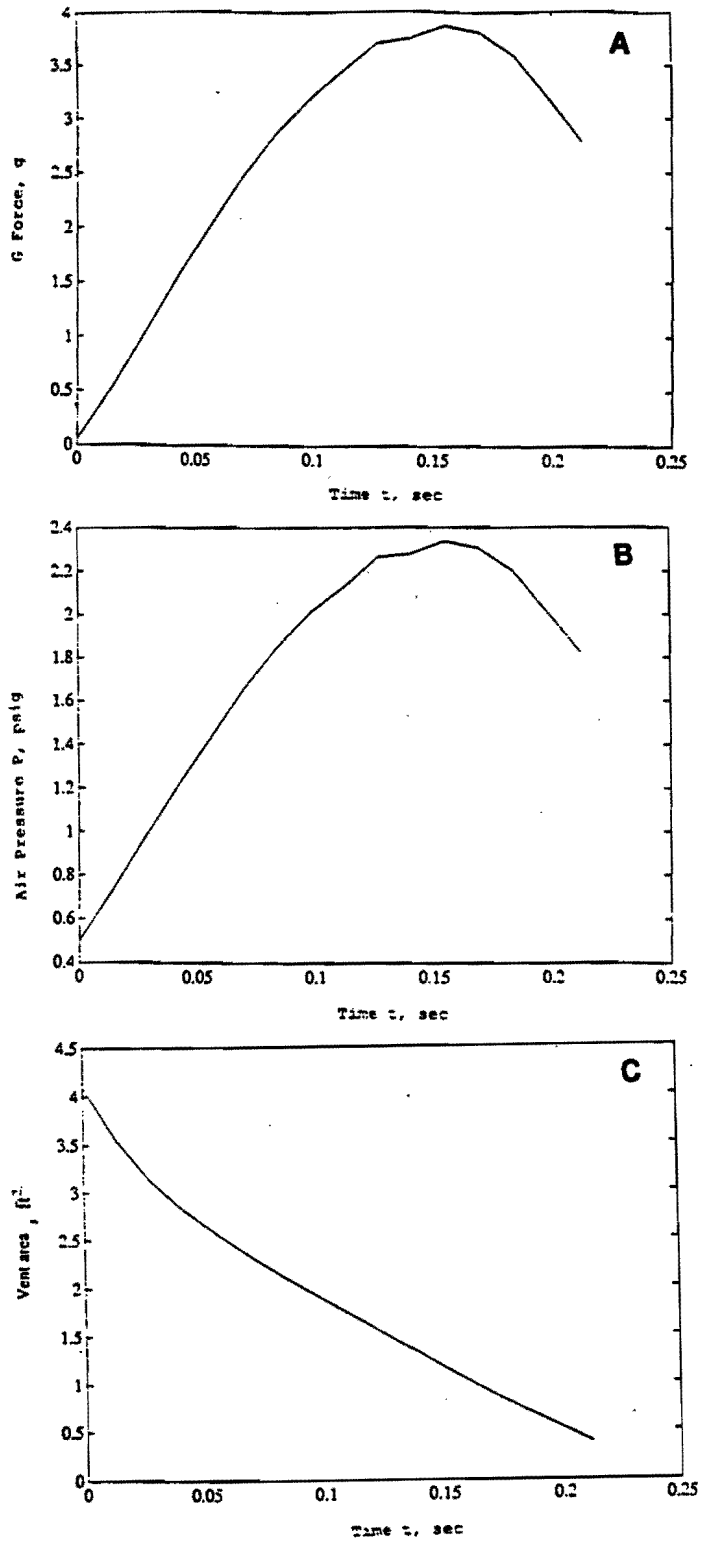

Analytical Results of Vent-Control Complex Airbags
Figure 32. 9' x 4' x 3', H = 7', M = 2490 lbs; A. G Force, B. Air Pressure, C. Vent Area

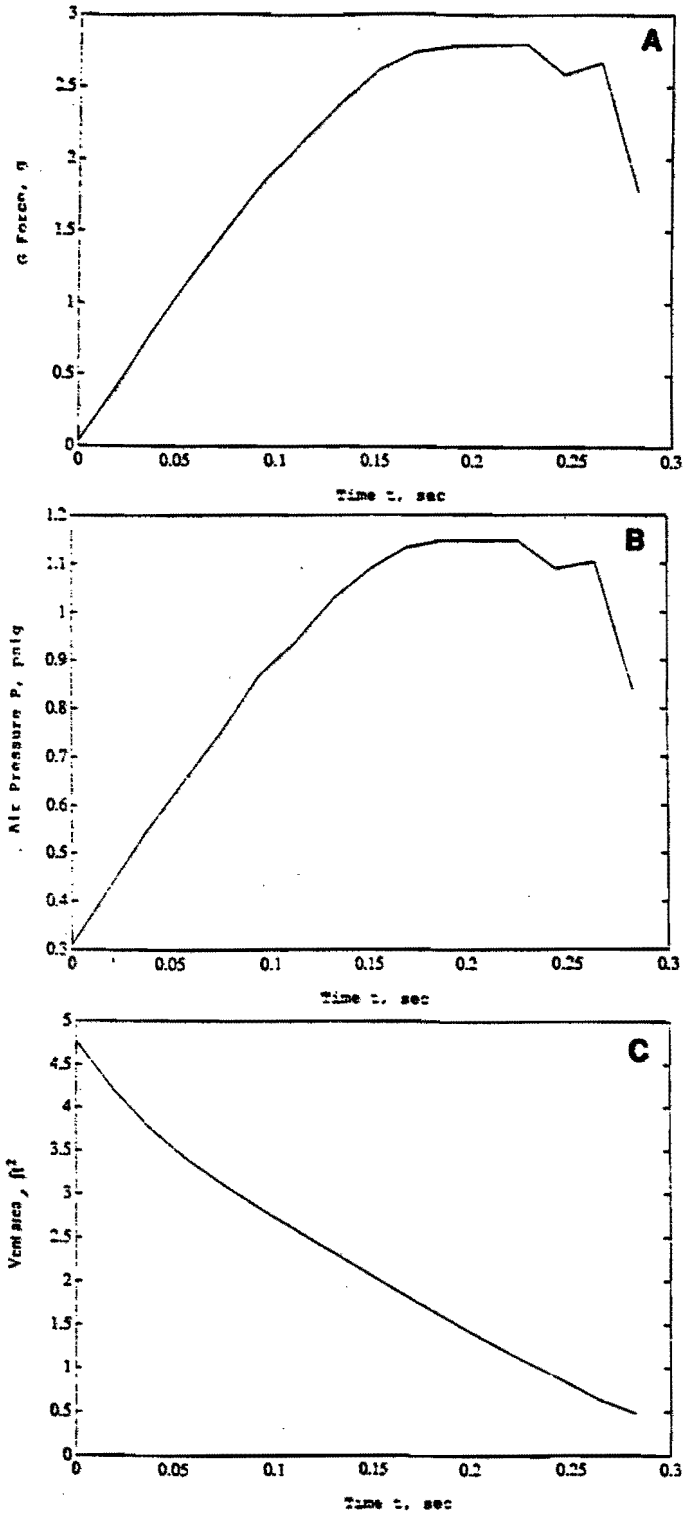

Analytical Results of Vent-Control Complex Airbags
Figure 33. 8' x 4' x 4', H = 7', M = 1390 lbs; A. G Force, B. Air Pressure, C. Velocity

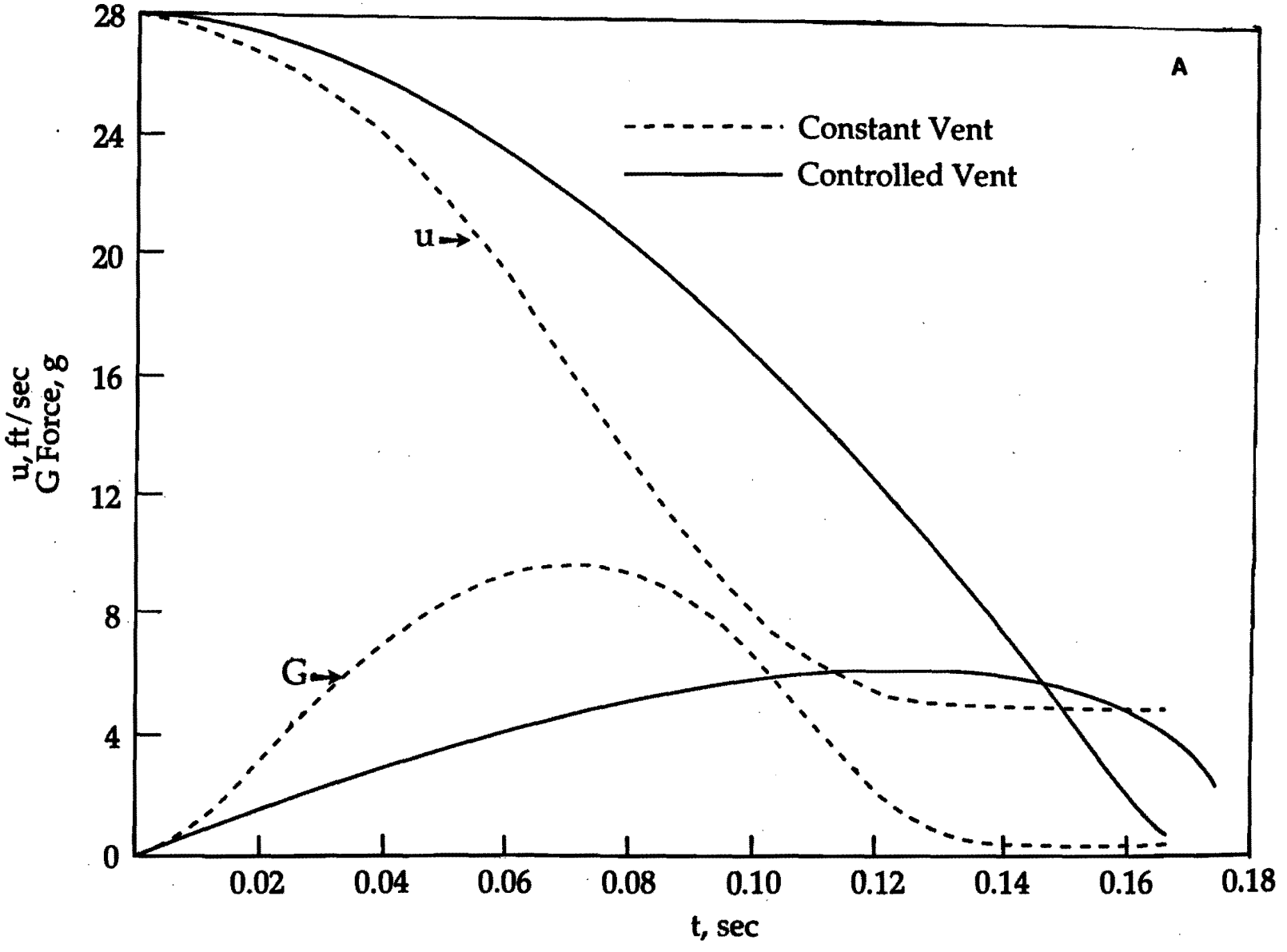

Analytical Results of Vent-Control Complex Airbags
Figure 34. 8' x 4' x 3', H = 13', M = 4000 lbs; A. G Force and Velocity

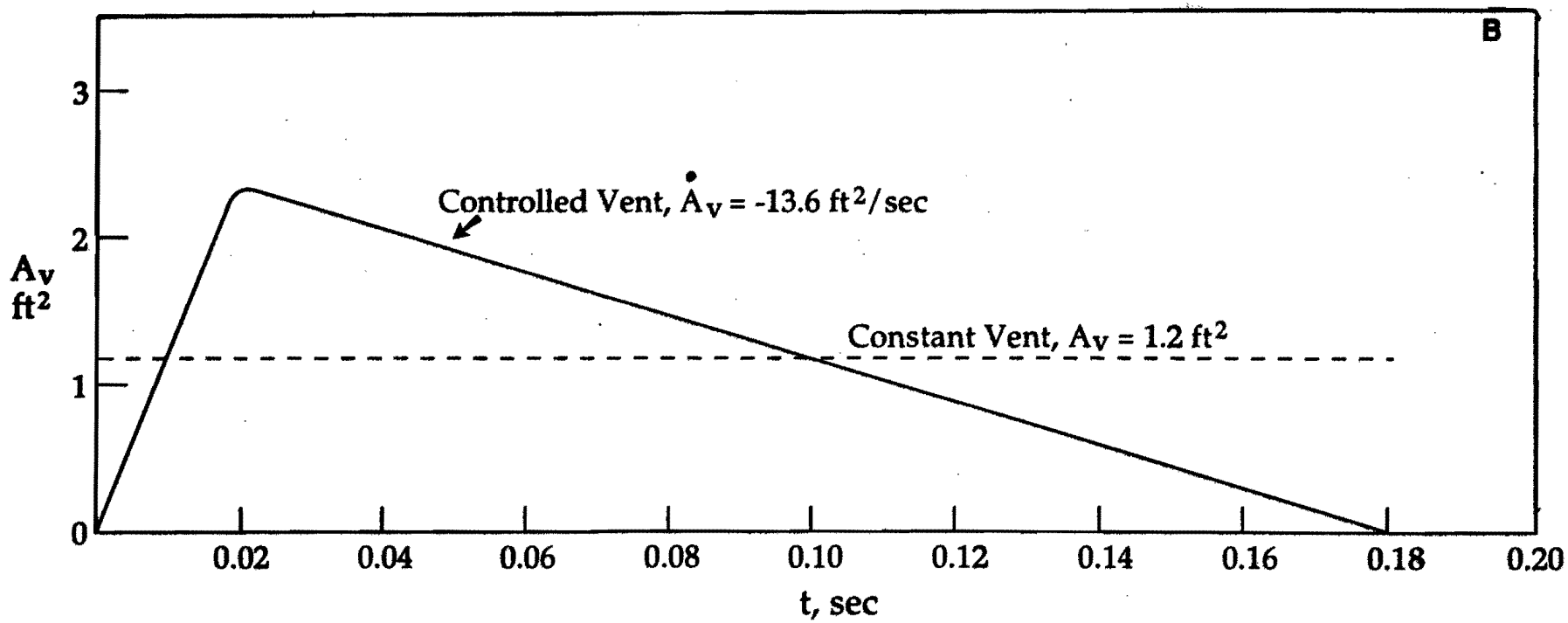

Analytical Results of Vent-Control Complex Airbags
Figure 34. 8' x 4' x 3', H = 13', M = 4000 lbs;
B. Vent Area

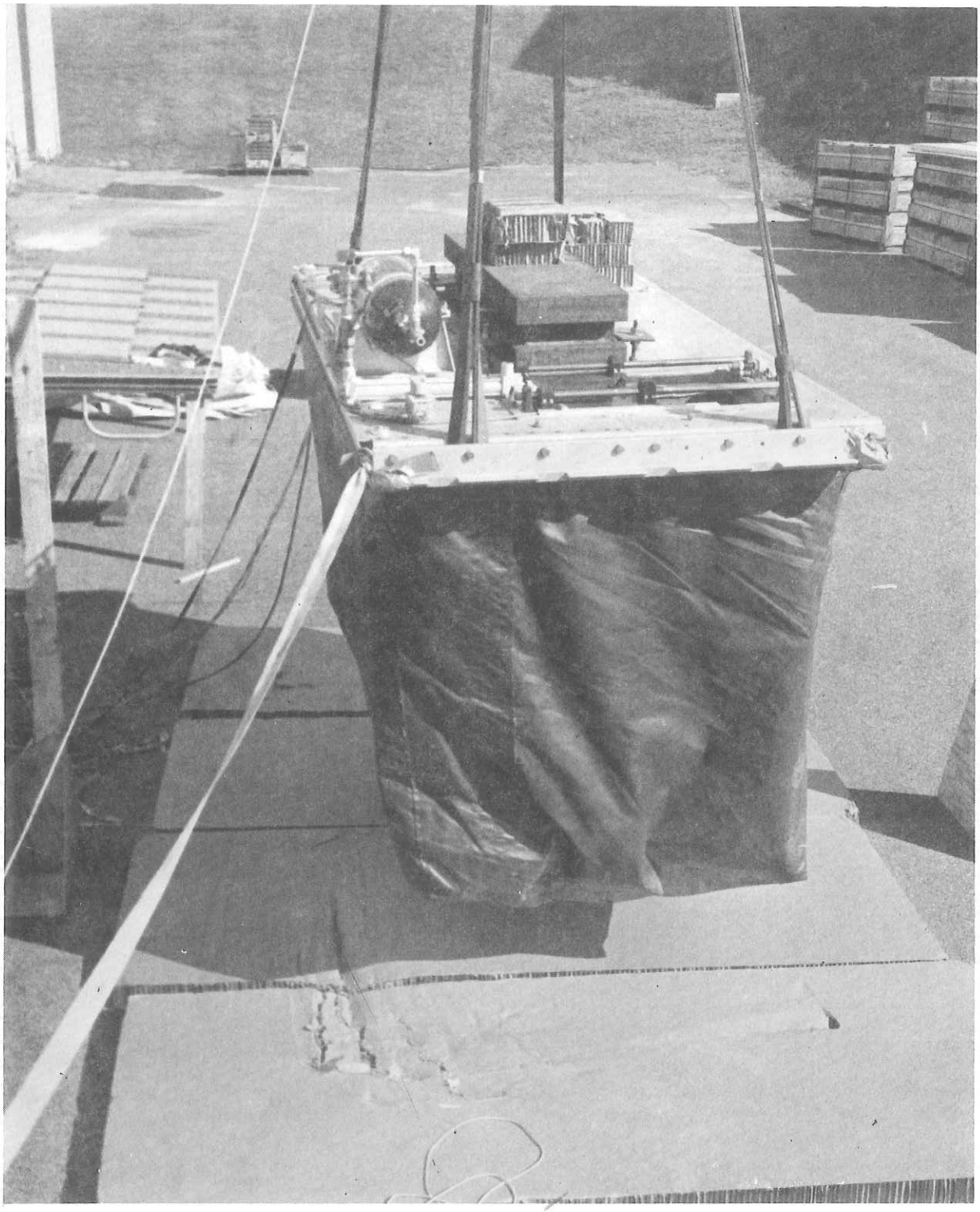

Figure 35. Photograph Showing the Overview of the 8' x 4' x 4' Vent-Control Complex Airbag

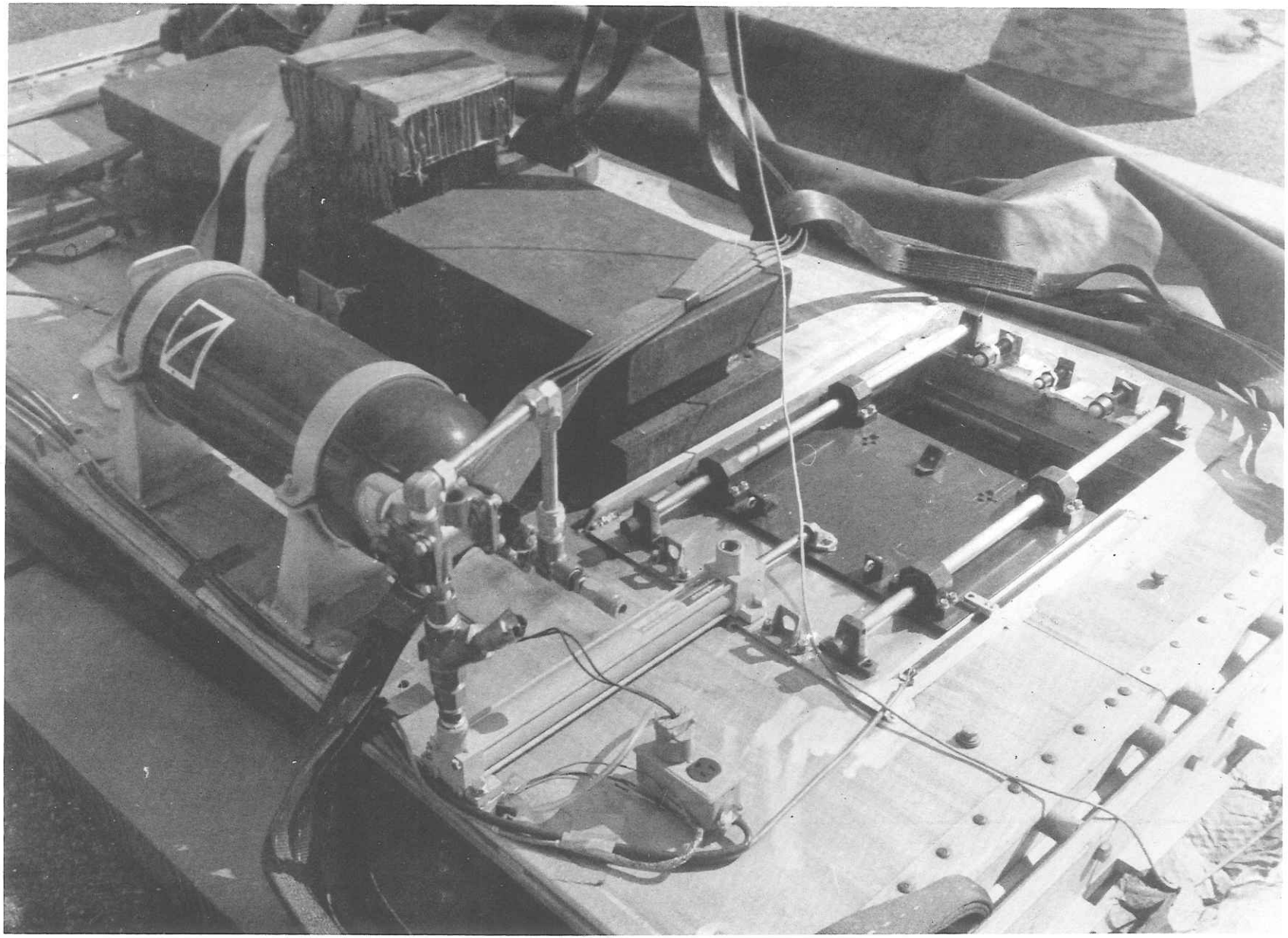

Figure 36. Photograph Showing the Components of the Vent-Control Mechanism

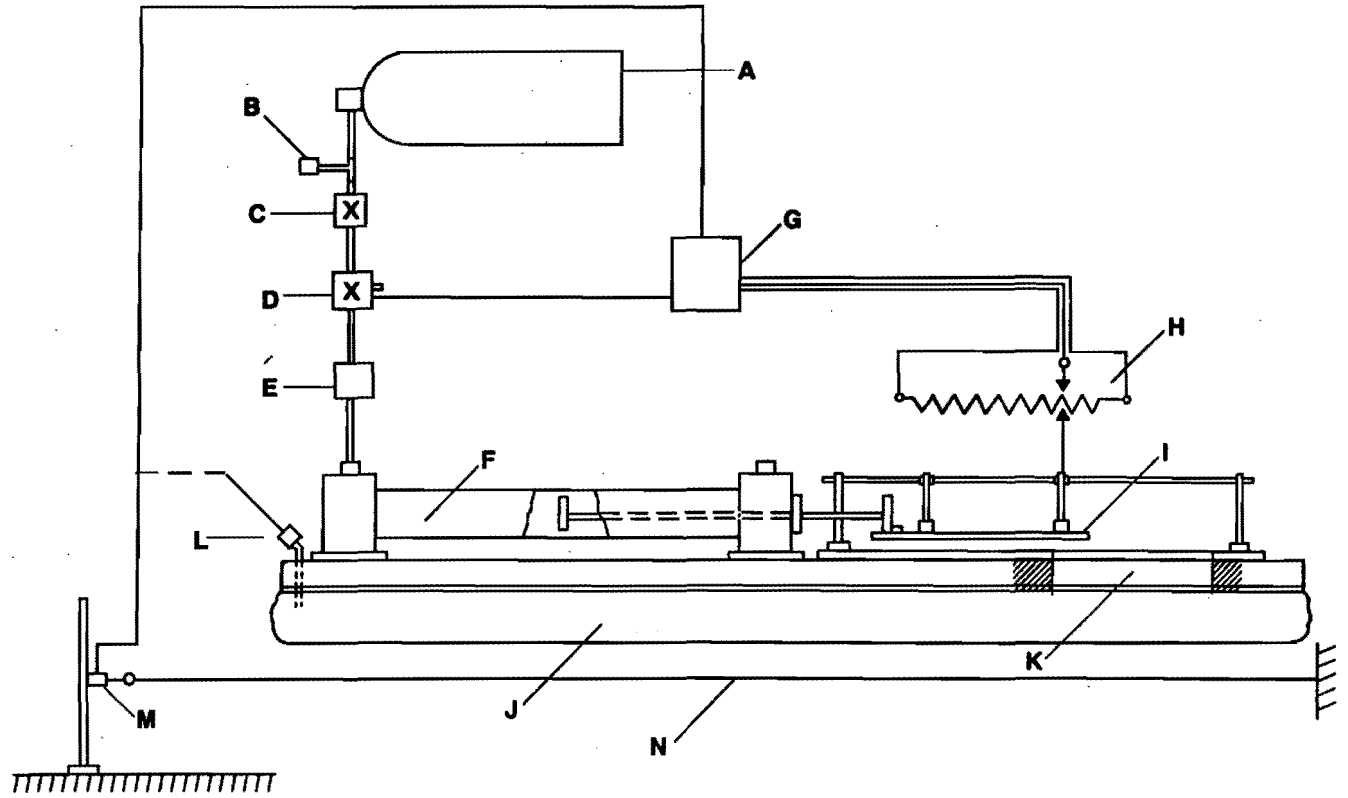

A. AIR SUPPLY TANK
B. SYSTEM FILL CONNECTION
C. TANK SHUT-OFF VALVE
D. AC OPERATED, NORMALLY CLOSED, 3-WAY SOLINOID VALVE
E. BALL CHECK SPEED VALVE (METERED FLOW & FREE FLOW)
F. AIR CYLINDER
G. SYSTEM CONTROL CIRCUITS
H. VALVE POSITION FEEDBACK POT
I. SLIDING GATE
J. AIRBAG
K. PLATFORM'S RECTANGULAR AIR VENT
L. BAG PRESSURE TRANSDUCER
M. MID-AIR TRIGGER SWITCH

Figure 37. Schematic Showing the Components of the Vent-Control Complex Airbag System

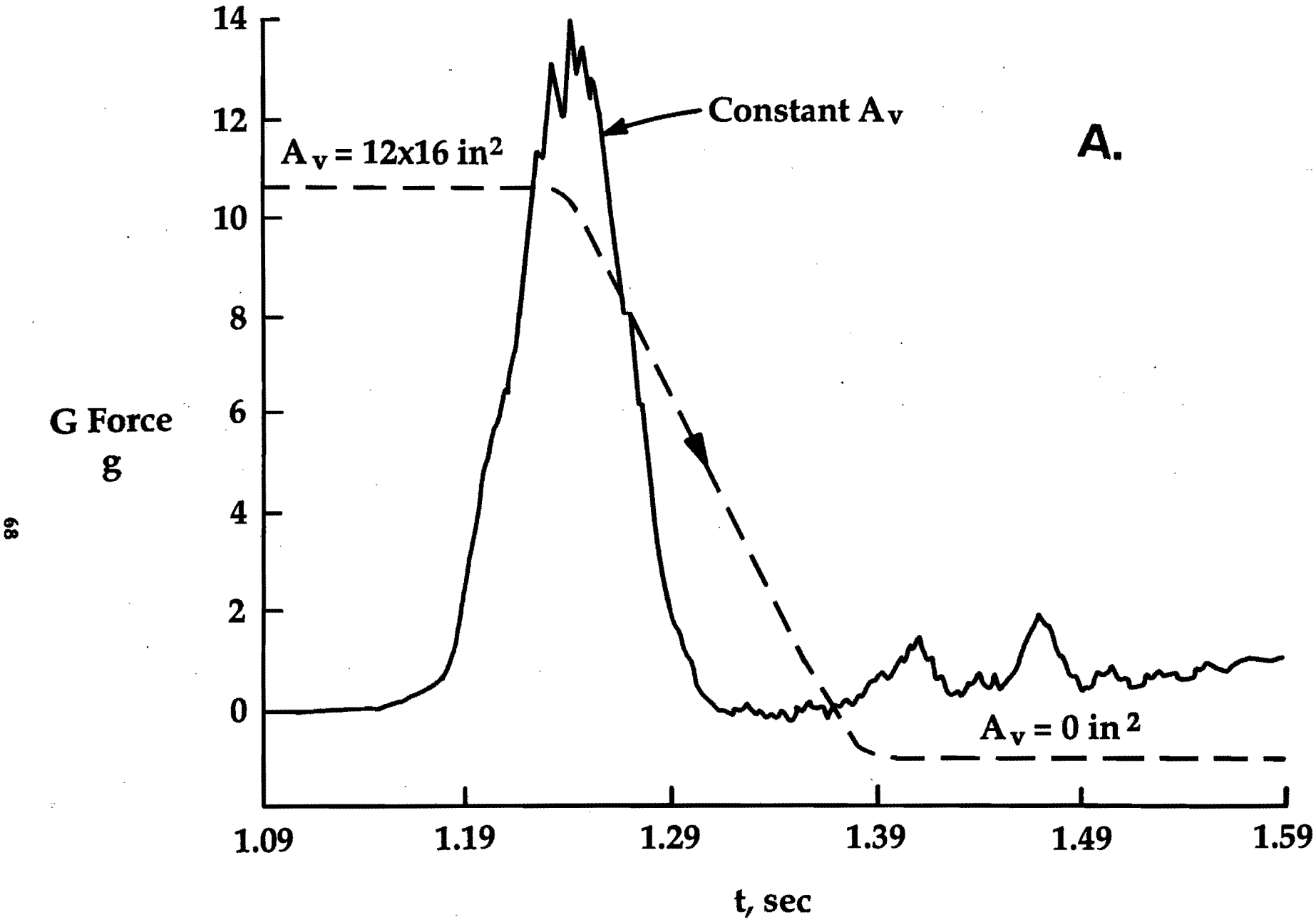

Figure 38. Performance of the 8' x 4' x 4' Airbag Operated with a Constant Vent: H = 7', M = 1390 lbs, A_v = 1.33 ft^2; A. G Force,

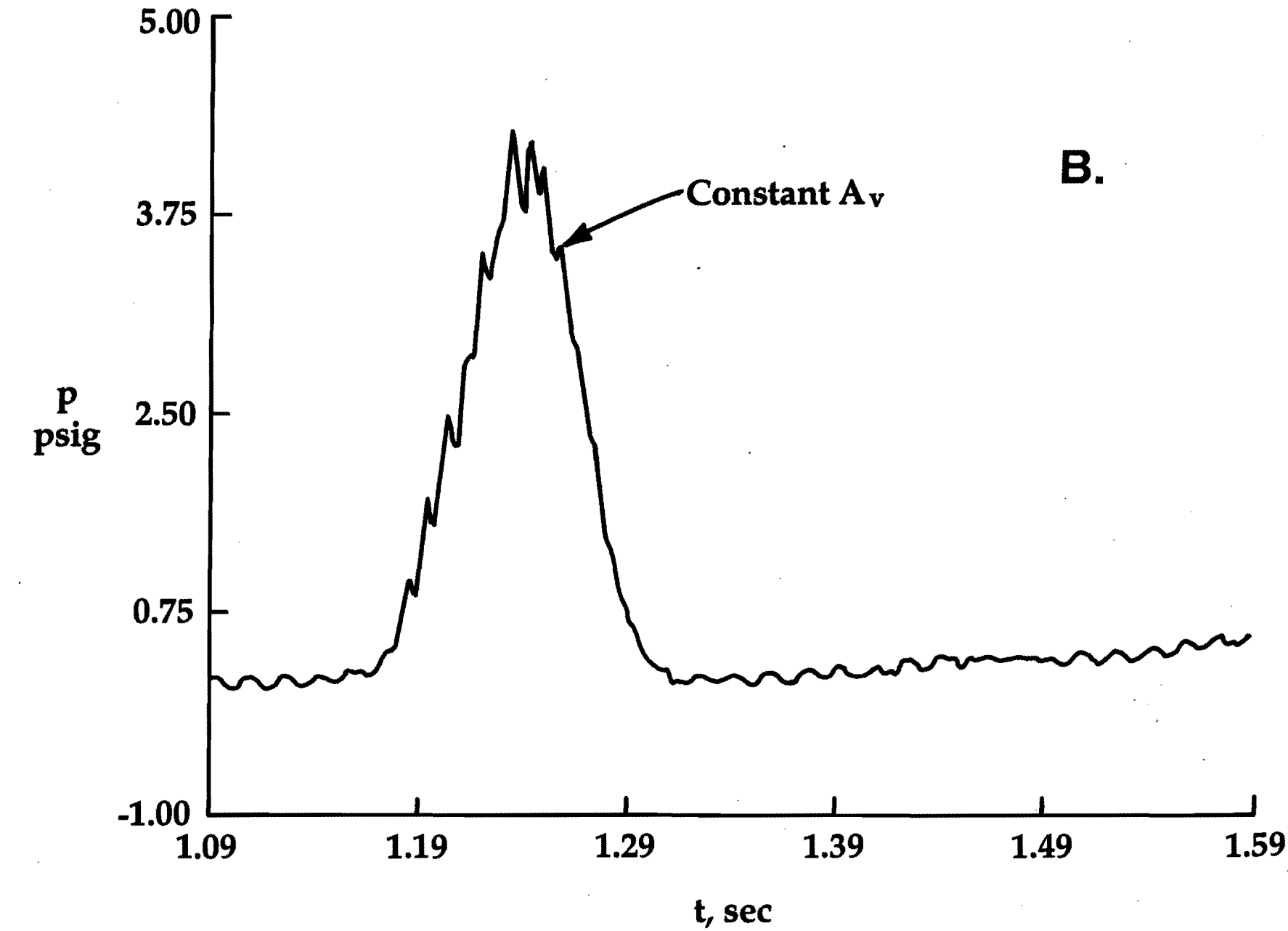

Figure 38. Performance of the 8' x 4' x 4' Airbag Operated with a Constant Vent: H = 7', M = 1390 lbs, A_v = 1.33 ft^2; B. Air Pressure

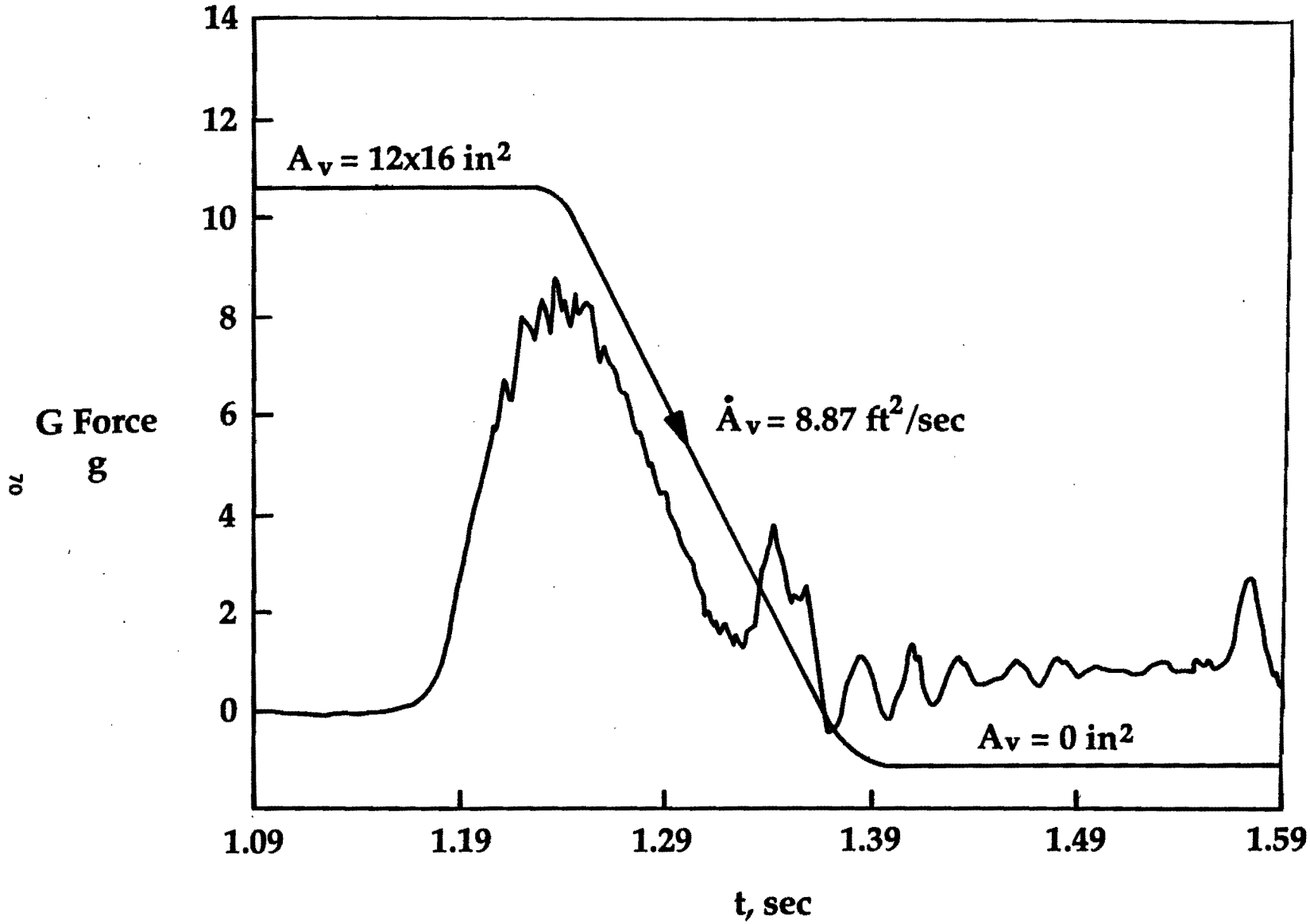

Figure 39. G Force Measurement of the 8' x 4' x 4' Airbag Operated with Vent-Control: H = 7', M = 1390 lbs

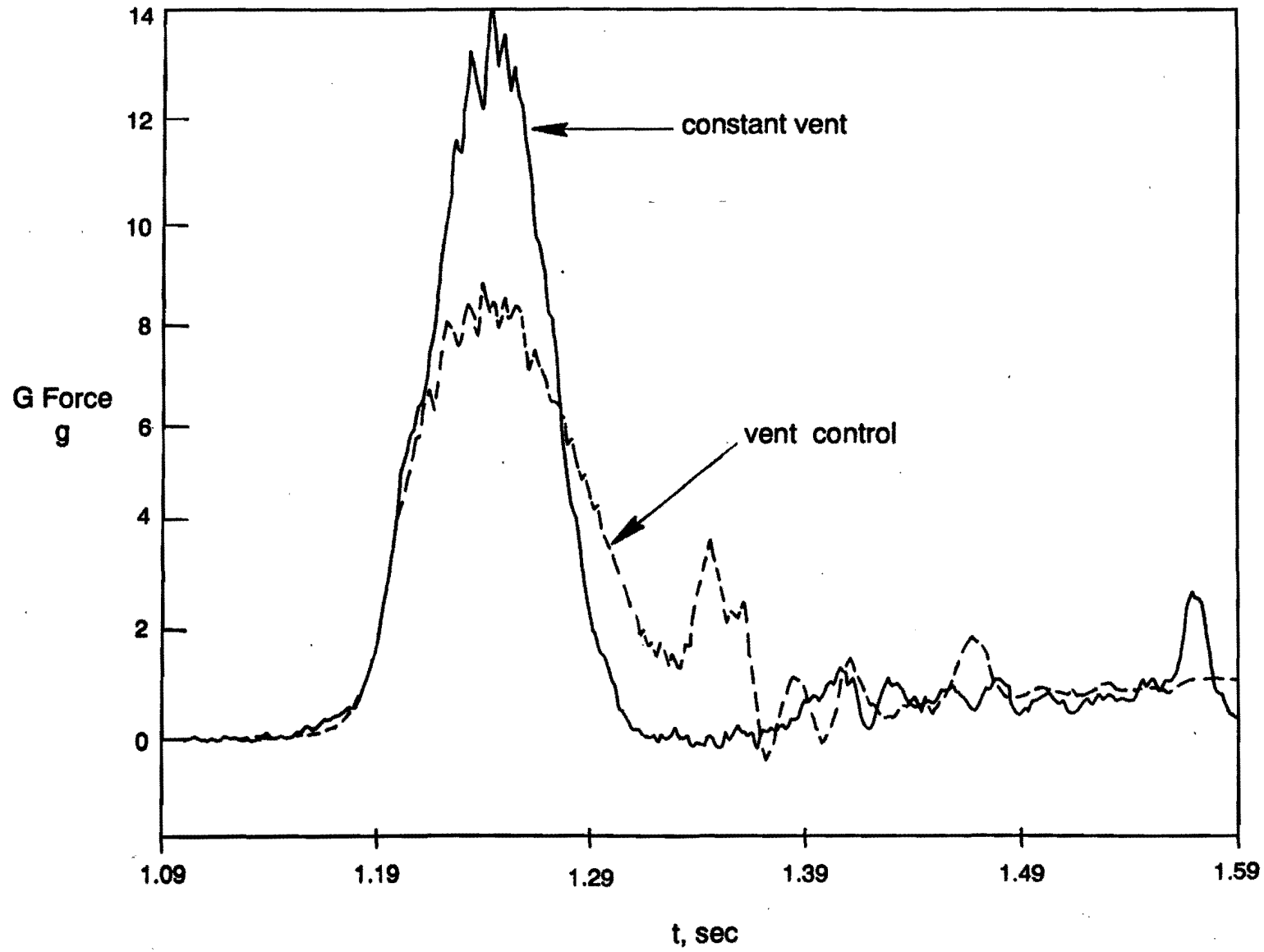

Figure 40. G Force Comparison of the 8' x 4' x 4' Airbag Operated with a Constant Vent (1.33 ft^2) and a Controlled Vent: H = 7', M = 1390 lbs

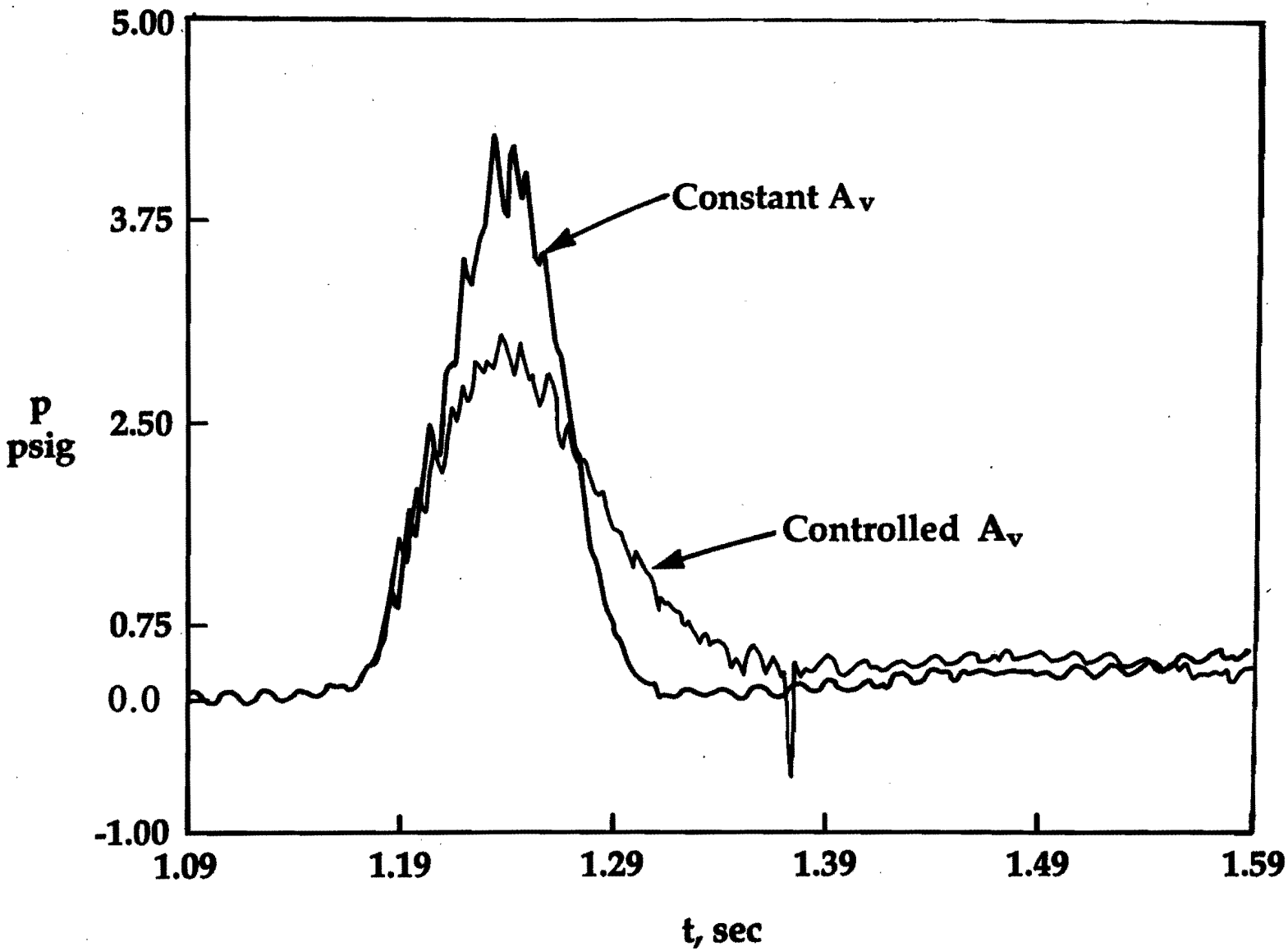

Figure 41. Air Pressure Comparison of the 8' x 4' x 4' Airbag Operated with a Constant Vent (1.33 ft^2) and a Controlled Vent: H = 7', M = 1390 lbs

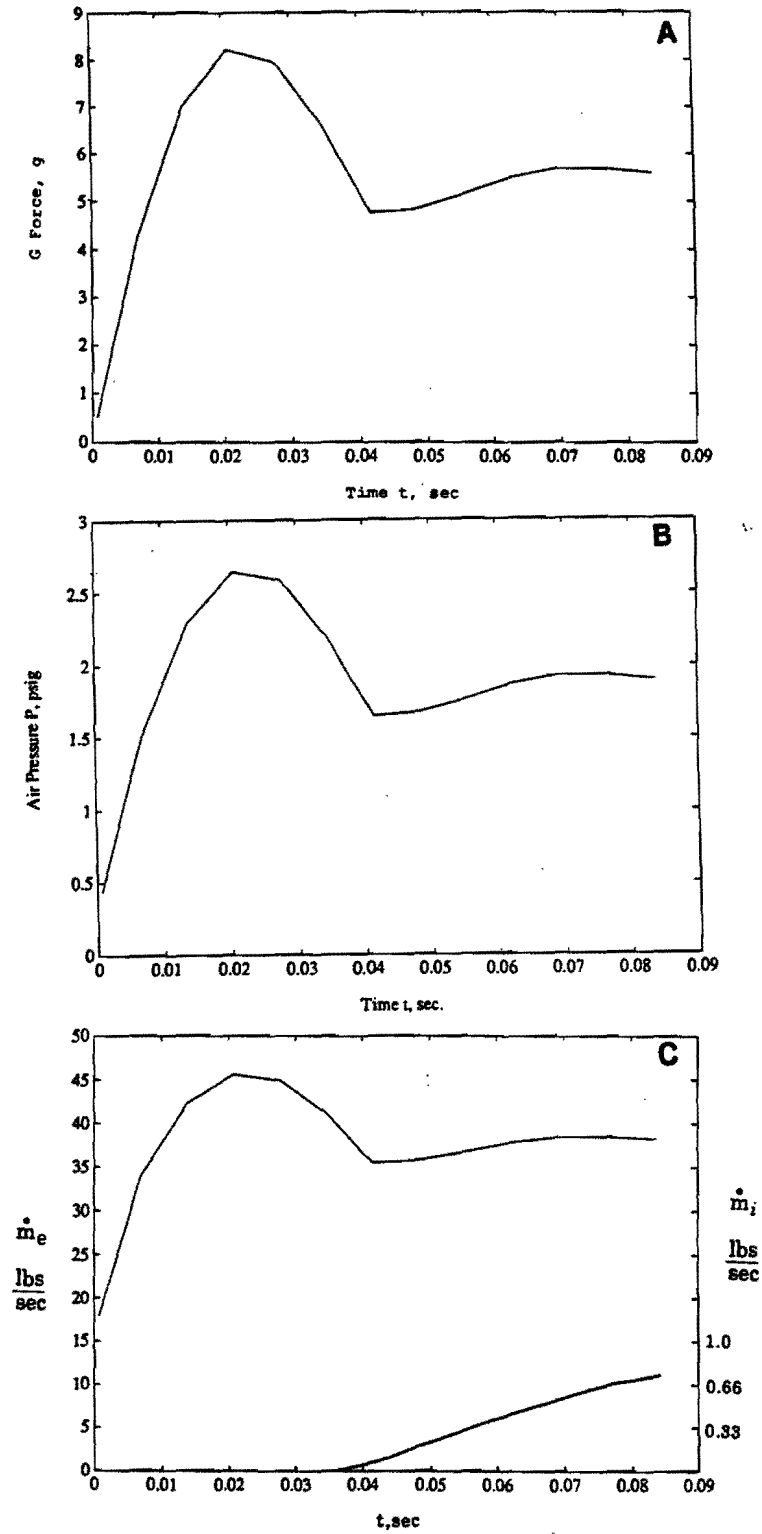

Analytical Results of Gas-Injection Airbags

Figure 42. 9' x 4' x 2', H = 7', M = 1490 lbs, A_v = 1.74 ft^2; A. G Force, B. Air Pressure, C. Air Flow Rates

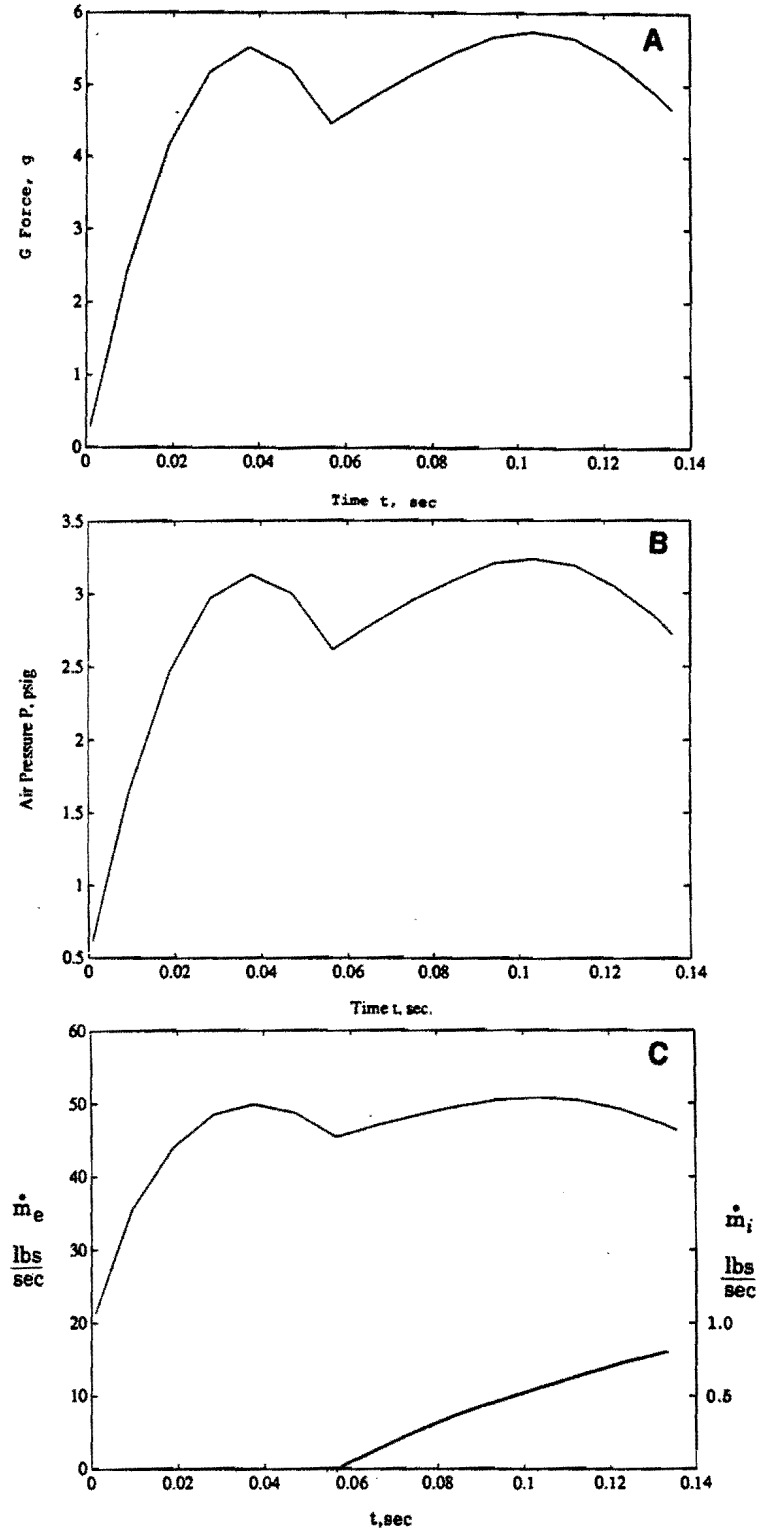

Analytical Results of Gas-Injection Airbags

Figure 43. 9' x 4' x 2', H = 7', M = 2490 lbs, A_v = 1.74 ft^2; A. G Force, B. Air Pressure, C. Air Flow Rates

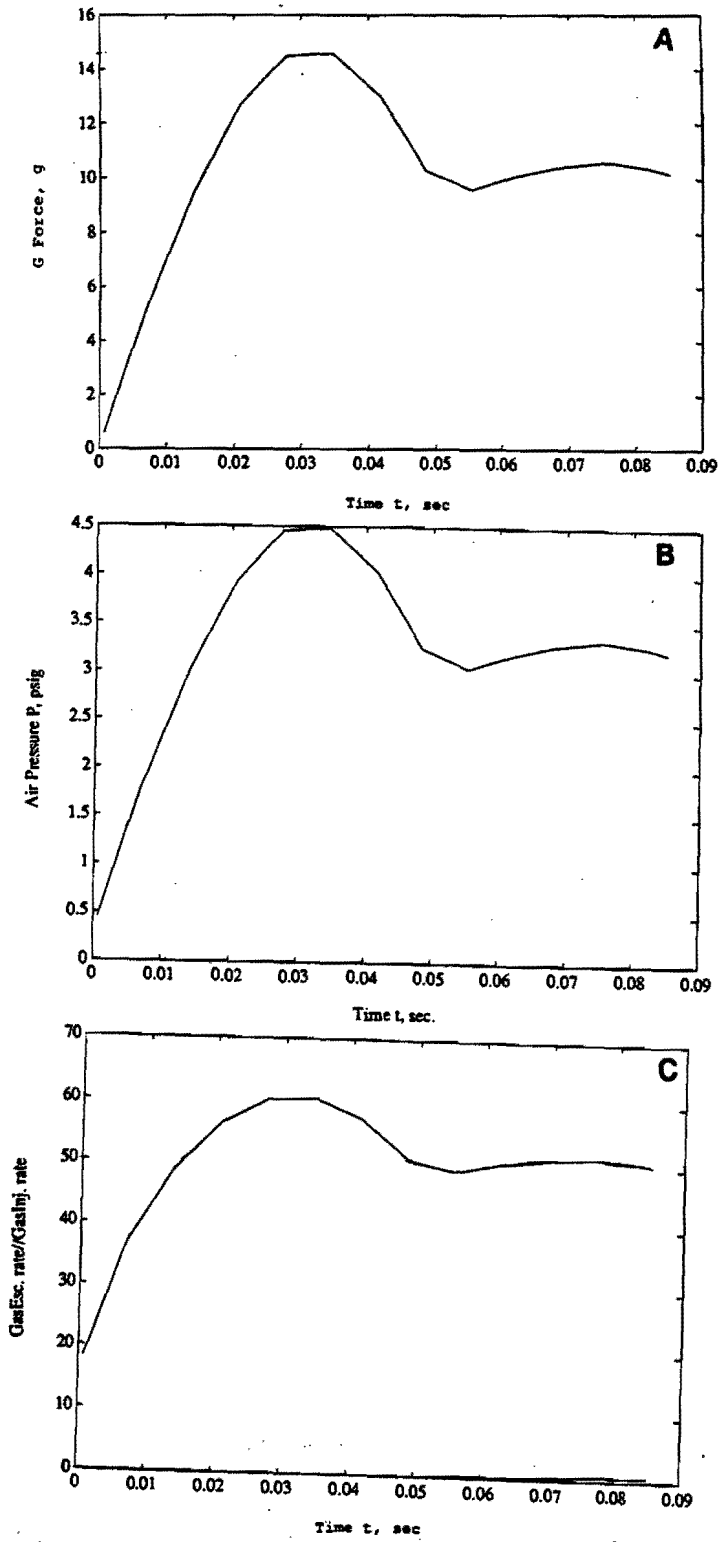

Analytical Results of Gas-Injection Airbags

Figure 44. 9' x 4' x 2', H = 13', M = 1490 lbs, A_v = 1.74 ft^2; A. G Force, B. Air Pressure, C. Air Flow Rates

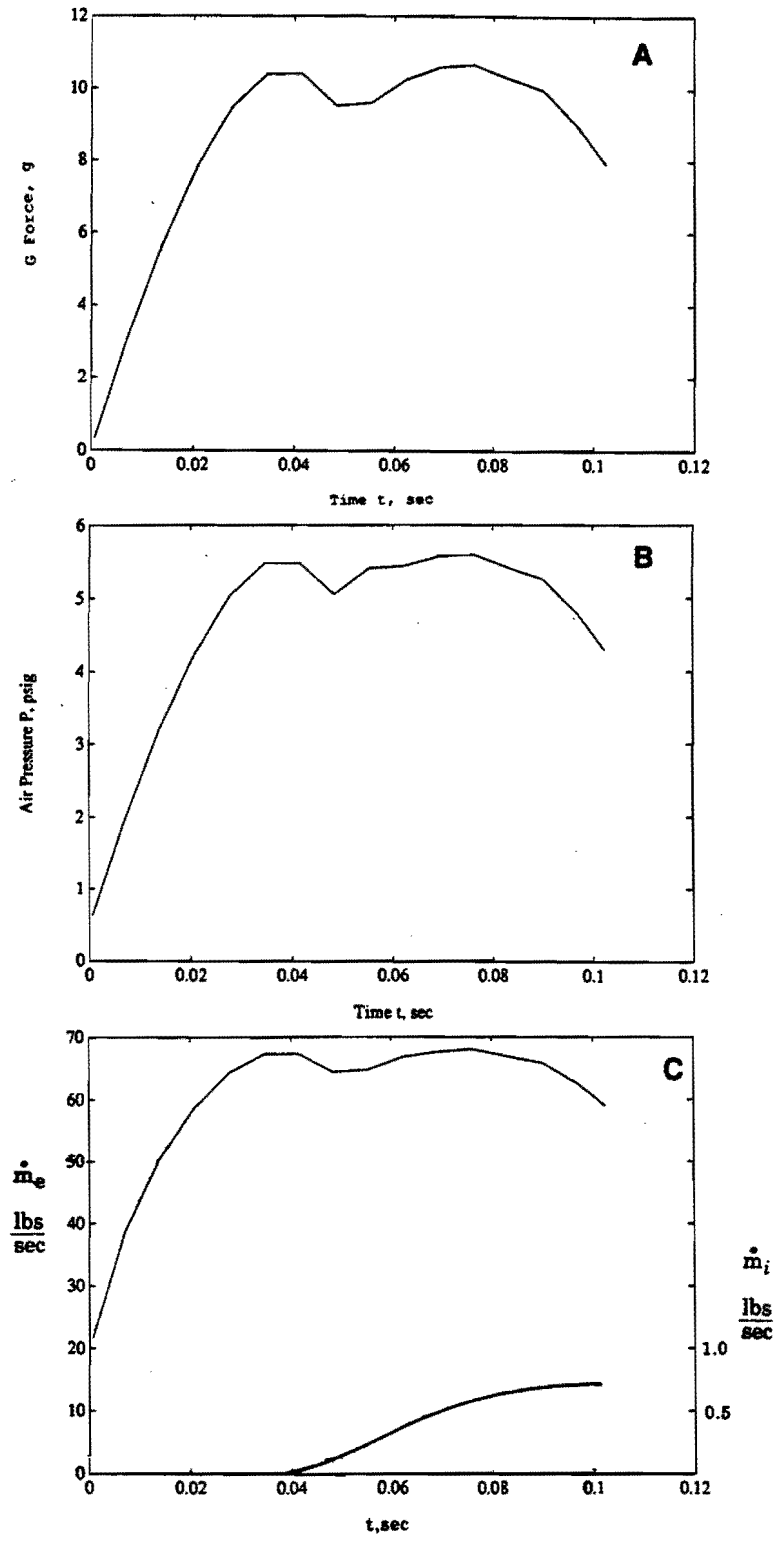

Analytical Results of Gas-Injection Airbags
Figure 45. 9' x 4' x 2', H = 13', M = 2490 lbs, A_v = 1.74 ft^2; A. G Force
B. Air Pressure, C. Air Flow Rates

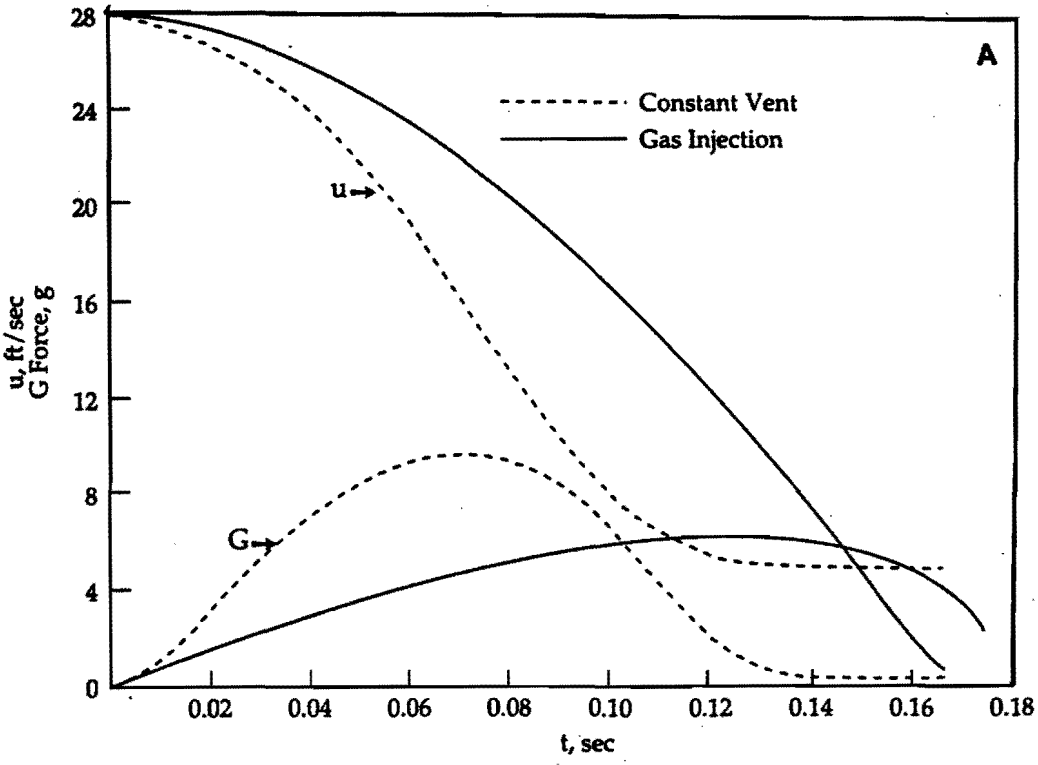

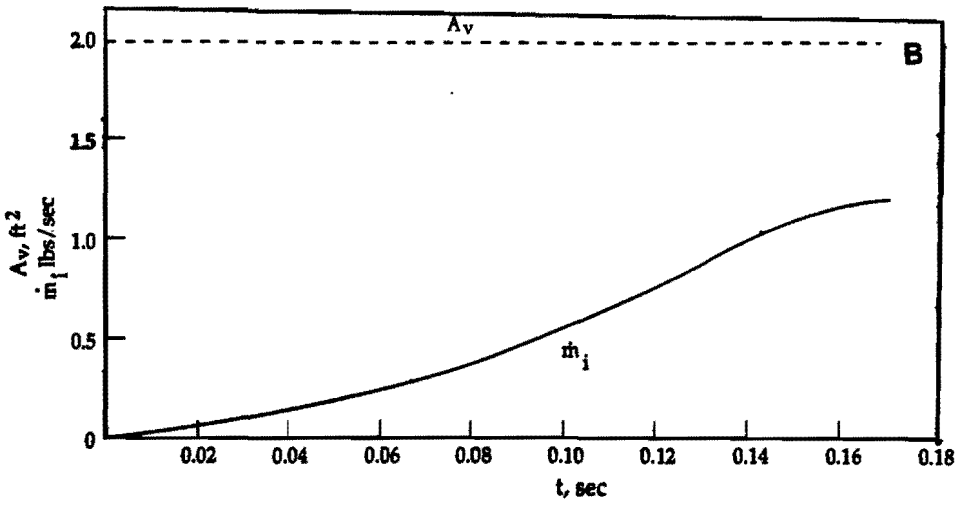

Analytical Results of Gas-Injection Airbags
Figure 46. 8' x 4' x 3', H = 13', M = 4000 lbs, A_v = 2.0 ft²; A. G Force and Velocity, B. Air Injection Rate

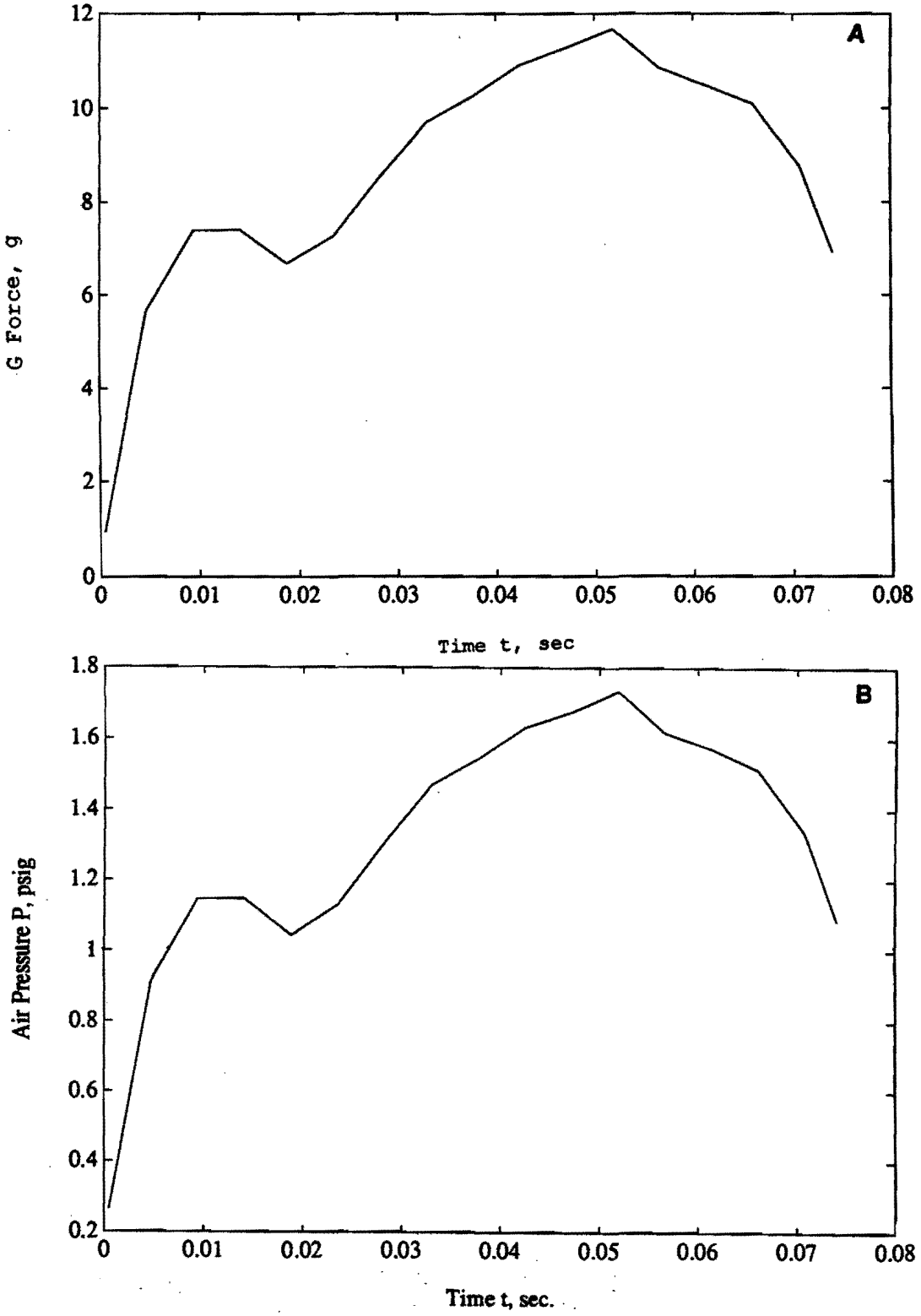

Analytical Results of Gas-Injection Airbags
Figure 47. 4' x 4' x 1', H = 7', M = 315 lbs, A_v = 1.32 ft^2;
A. G Force, B. Air Pressure

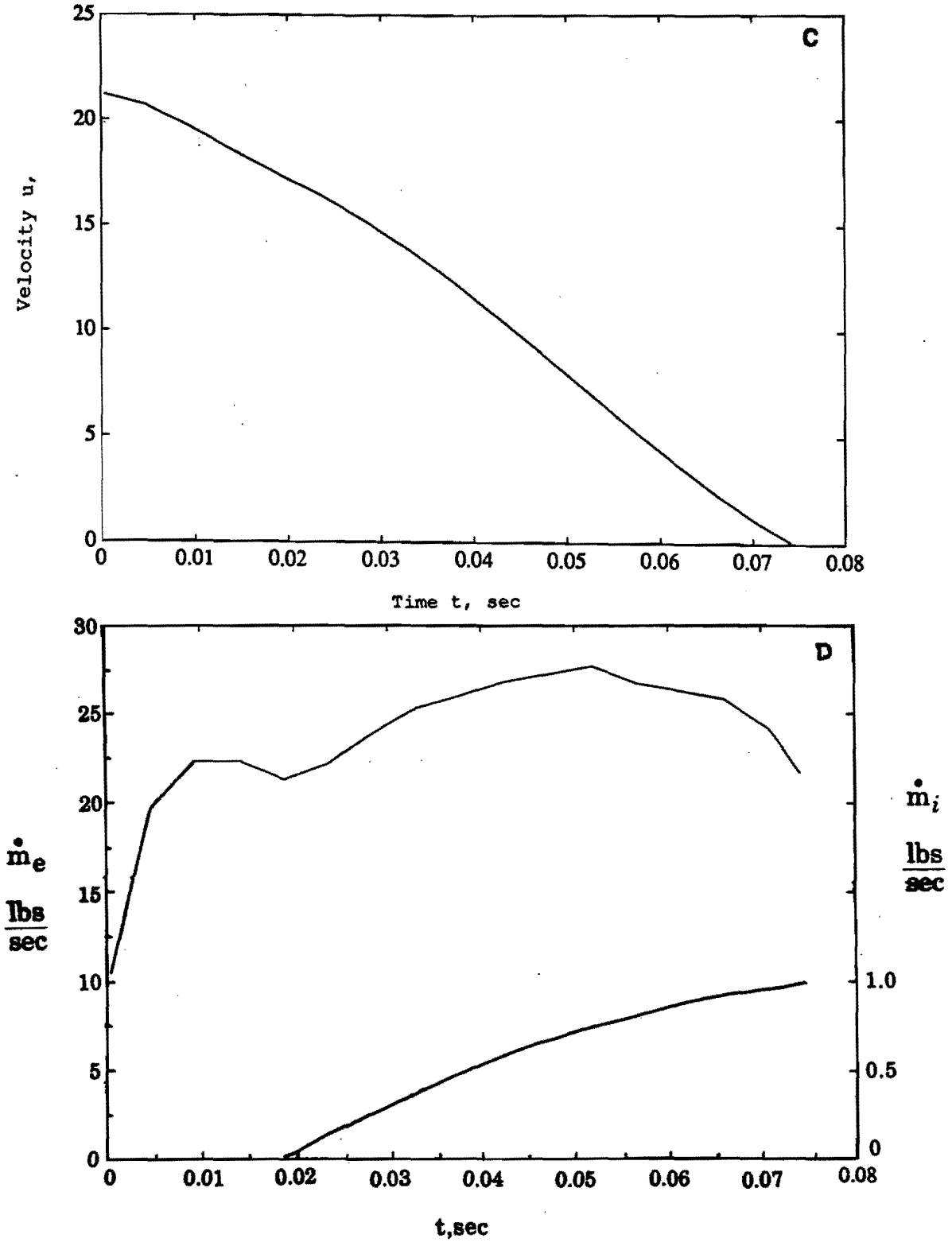

Analytical Results of Gas-Injection Airbags
Figure 47. 4' x 4' x 1', H = 7', M = 315 lbs, A_v = 1.32 ft^2;
C. Velocity, D. Air Flow Rates

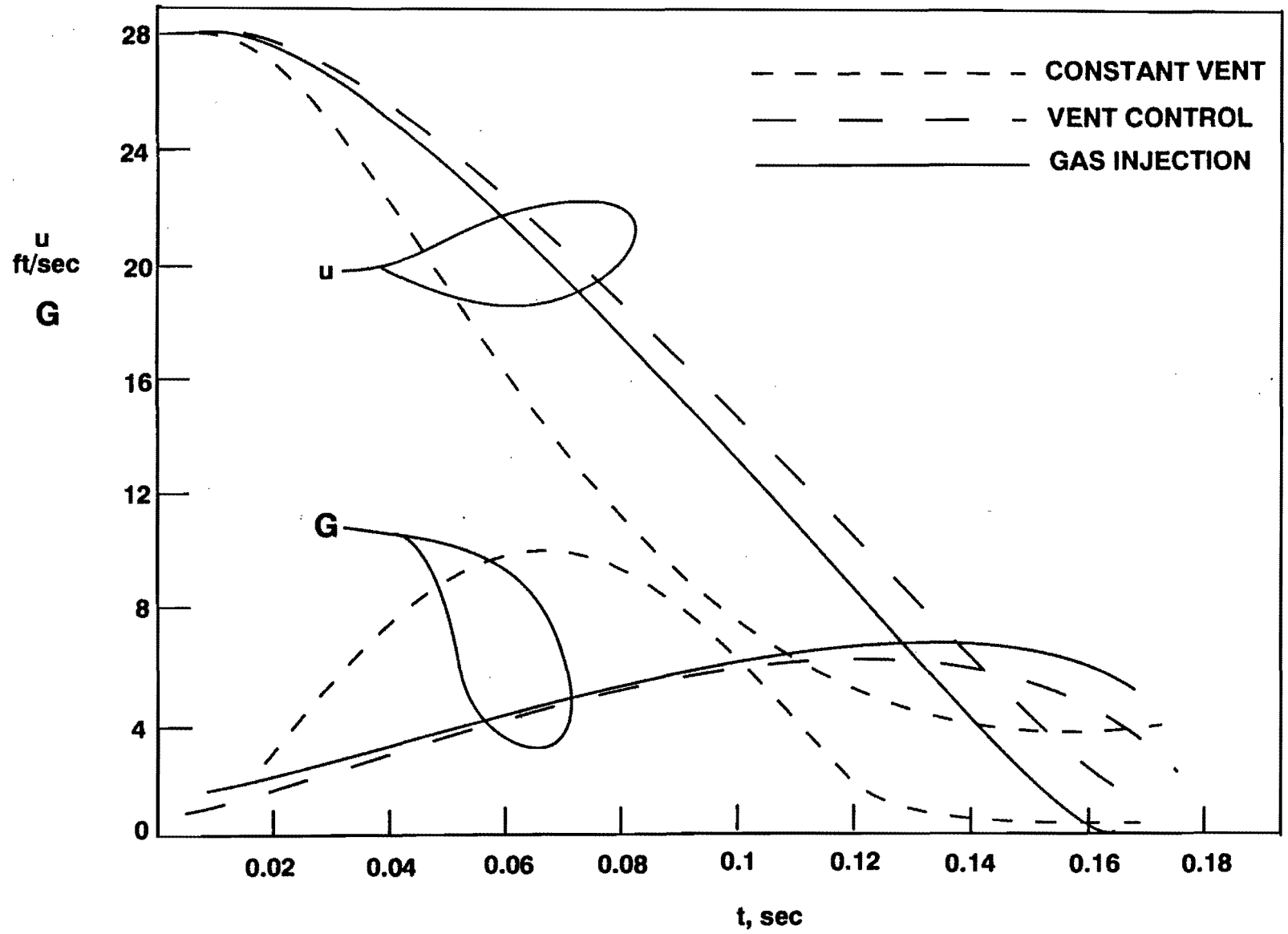

Figure 48. Comparison of a 8' x 4' x 3' Airbag Operated with a Constant Vent, Controlled Vent, and Gas-Injection: H = 13', M = 4000 lbs

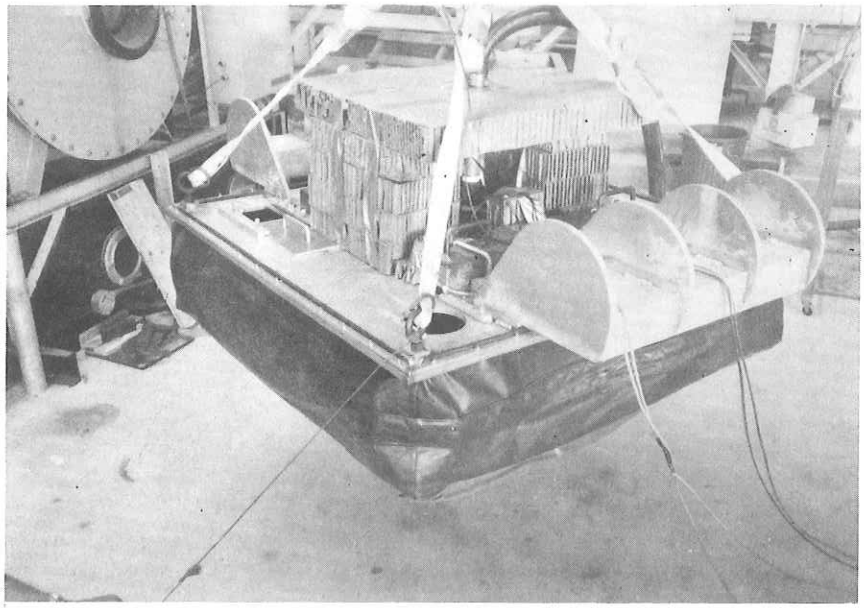

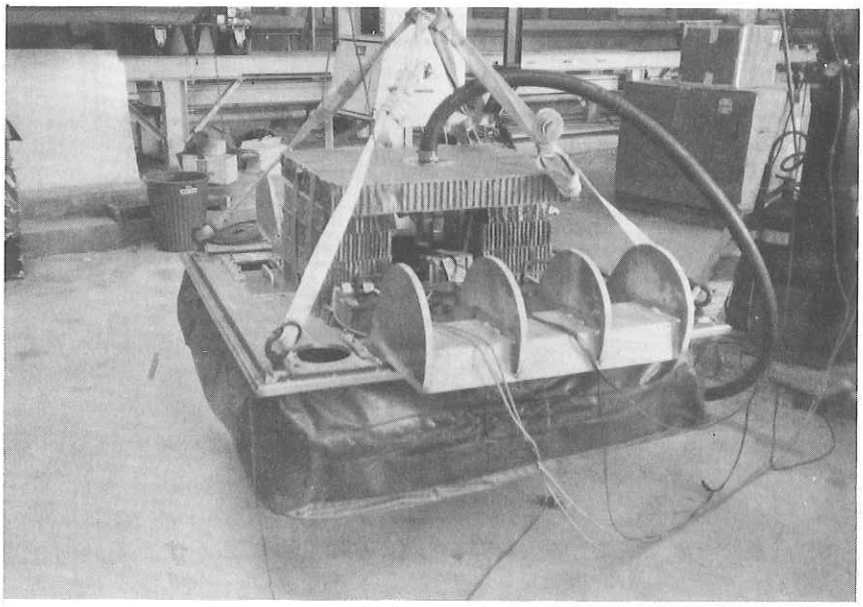

Figure 49. Photographs Showing the 4' x 4' x 1' Air-Injection Complex Airbag

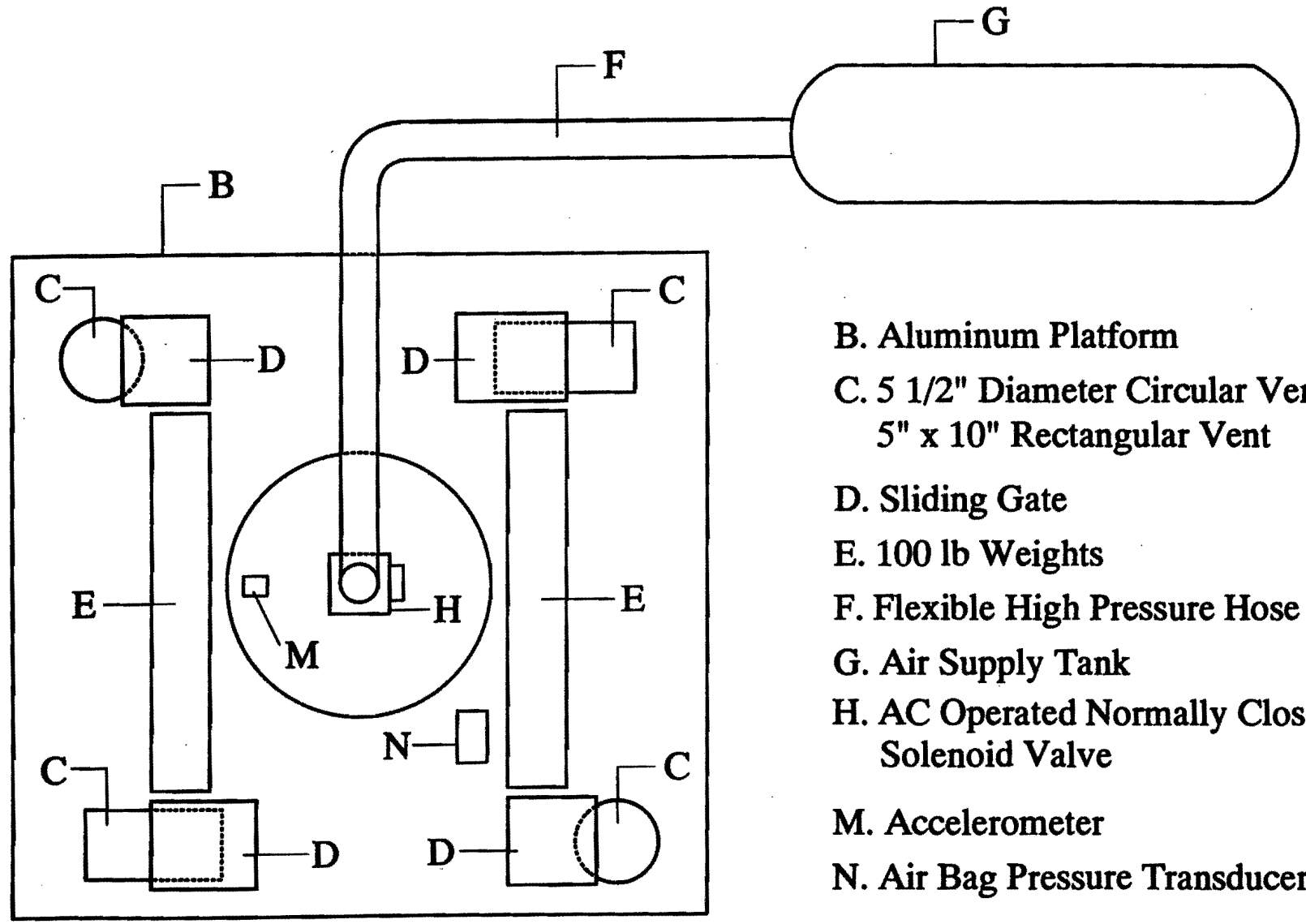

Figure 50. Schematics Showing the Components of the 4' x 4' x 1' Air-Injection Complex Airbag: A. Plan View

A. Airbag
B. Aluminum Platform
C. 5 1/2" diameter Circular Vent
5" x 10" Rectangular Vent
D. Sliding Gate
E. 100 lb Weight
F. Flexible High Pressure Hose
G. Air Supply Tank
H. AC Operated Normally Closed Solenoid Valve
I. Metal Pipe
J. Timing-control Circuit
K. Solenoid Valve
L. Mechanical Release Device
M. Accelerometer
N. Airbag Pressure Transducer

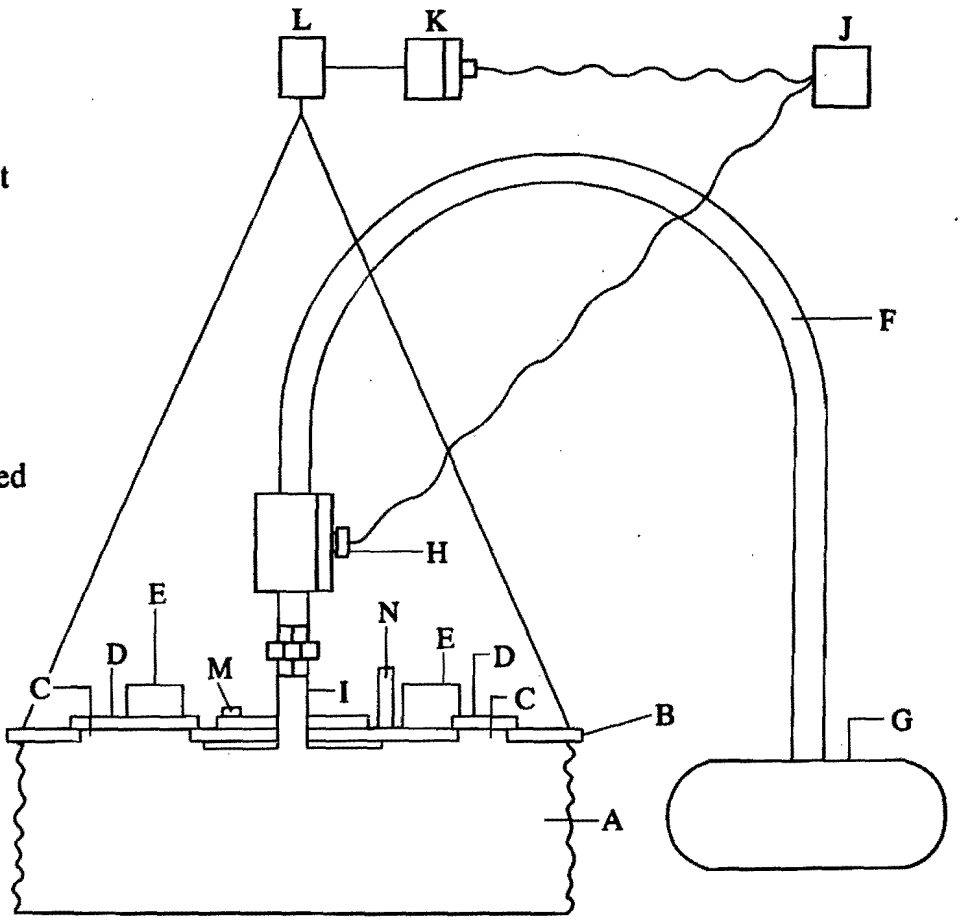

Figure 50. Schematics Showing the Components of the 4' x 4' x 1' Air-Injection Complex Airbag: B. Side View

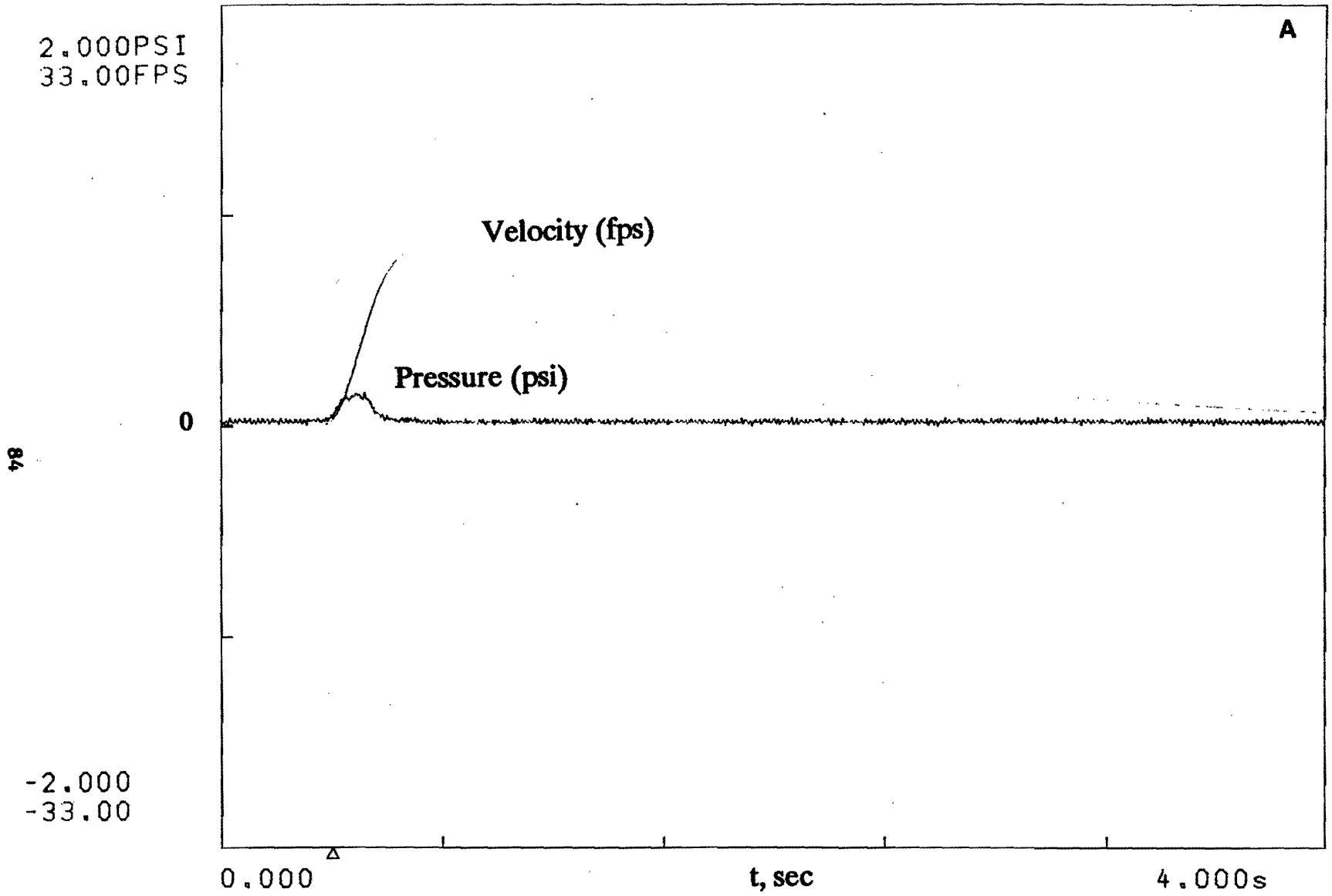

Figure 51. Air Velocity Measurements at the 5.5"-Diameter Air Vent and Air Pressure Measurements of the 4' x 4' x 1' Air-Injection Complex Airbag: A. P_i = 70 psig, t_i = 0.2 sec

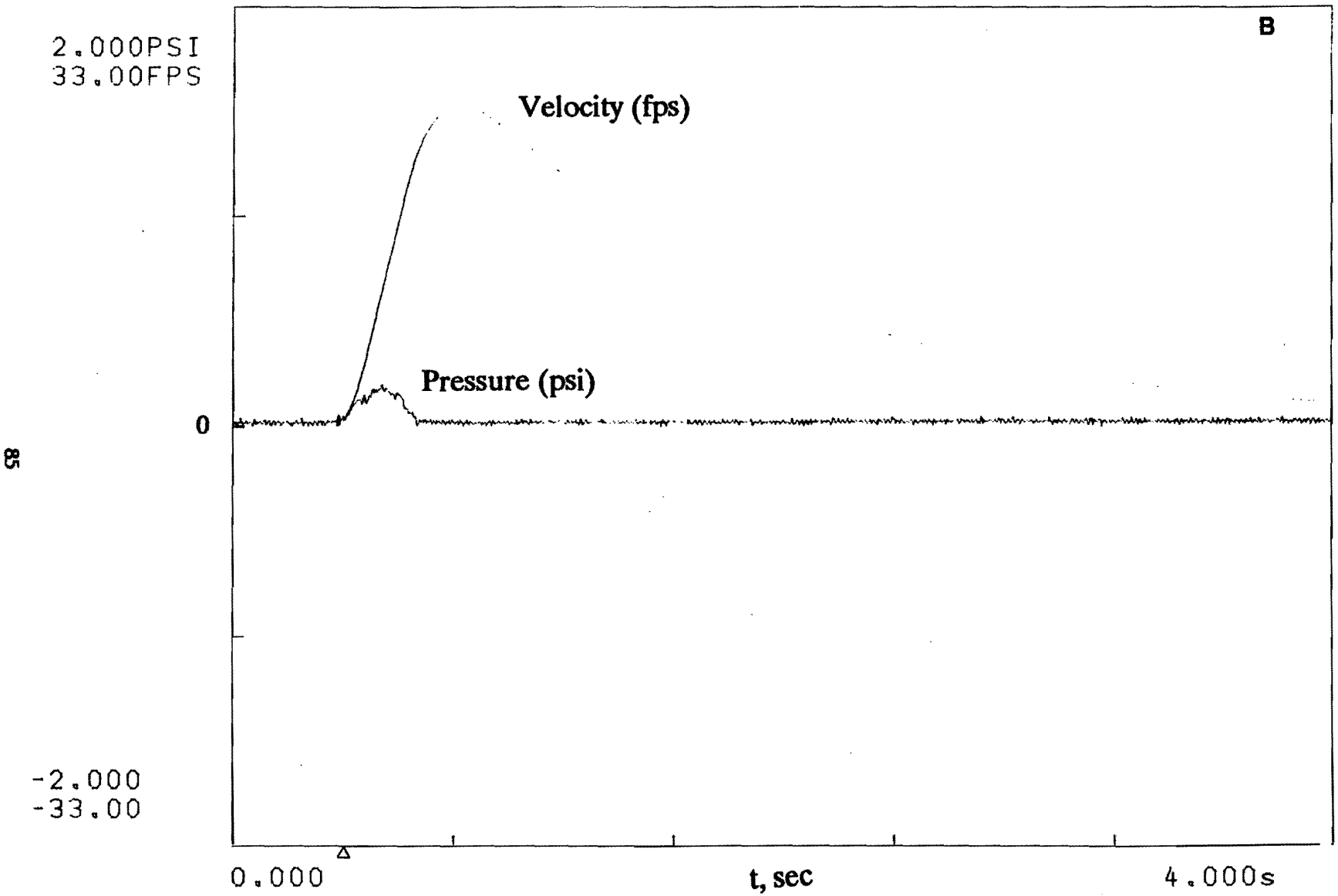

Figure 51. Air Velocity Measurements at the 5.5"-Diameter Air Vent and Air Pressure Measurements of the 4' x 4' x 1' Air-Injection Complex Airbag: B. P_i = 70 psig, t_i = 0.3 sec

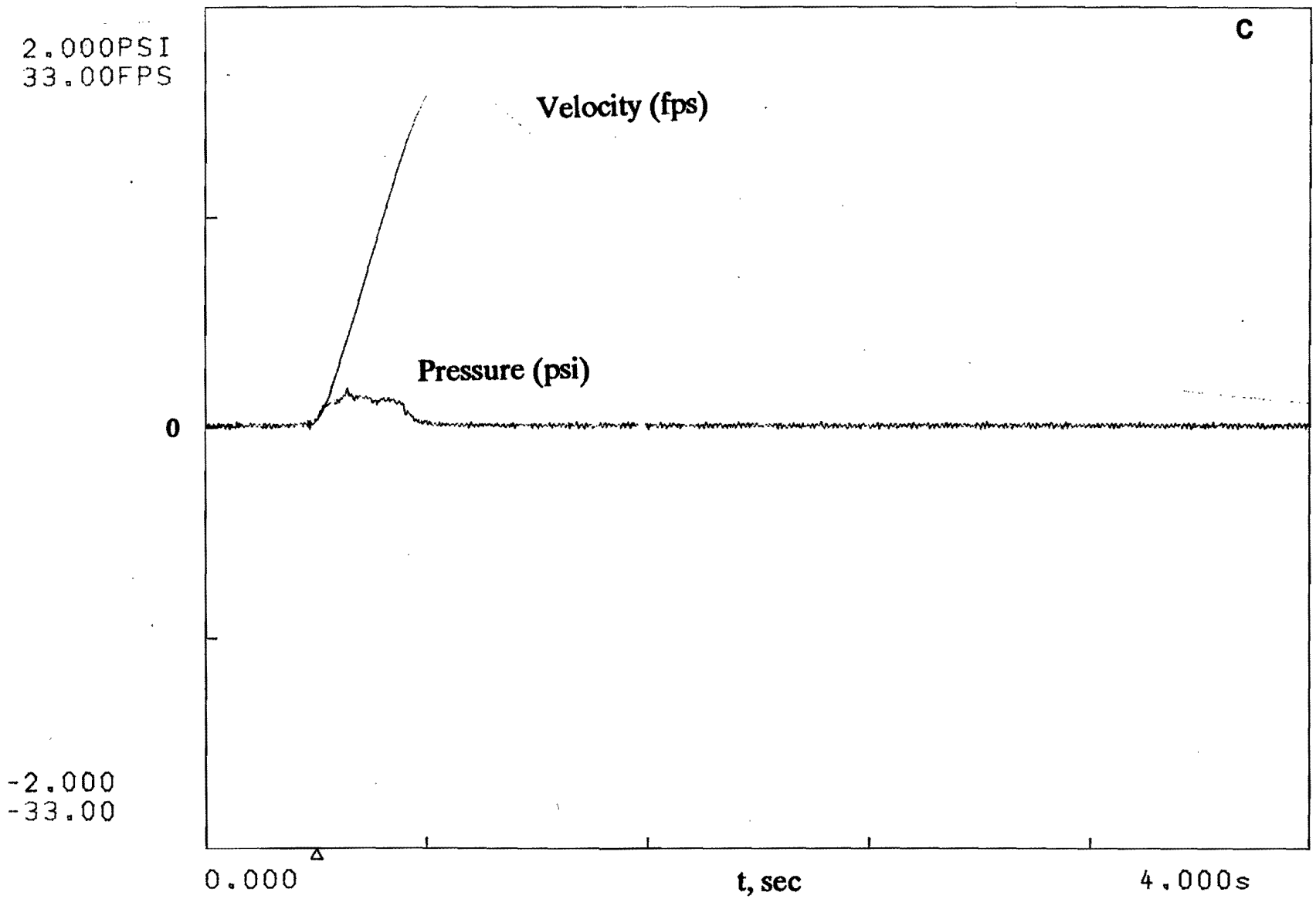

Figure 51. Air Velocity Measurements at the 5.5"-Diameter Air Vent and Air Pressure Measurements of the 4' x 4' x 1' Air-Injection Complex Airbag: C. P_i = 70 psig, t_i = 0.4 sec

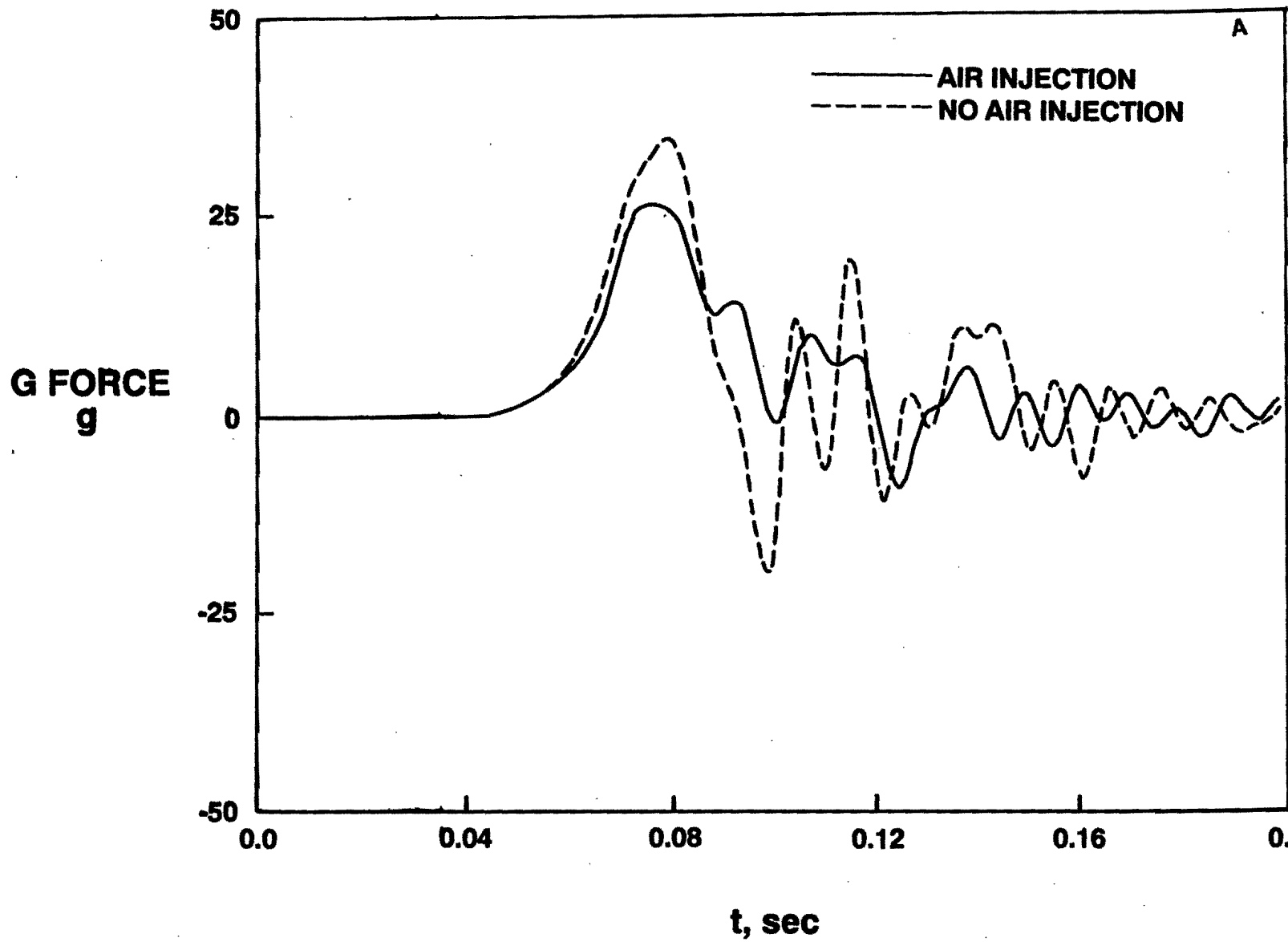

Figure 52. Performance of the 4' x 4' x 1' Airbag Operated with a Constant Vent (0.903 ft^2) with and without Air-Injection: A. G Force

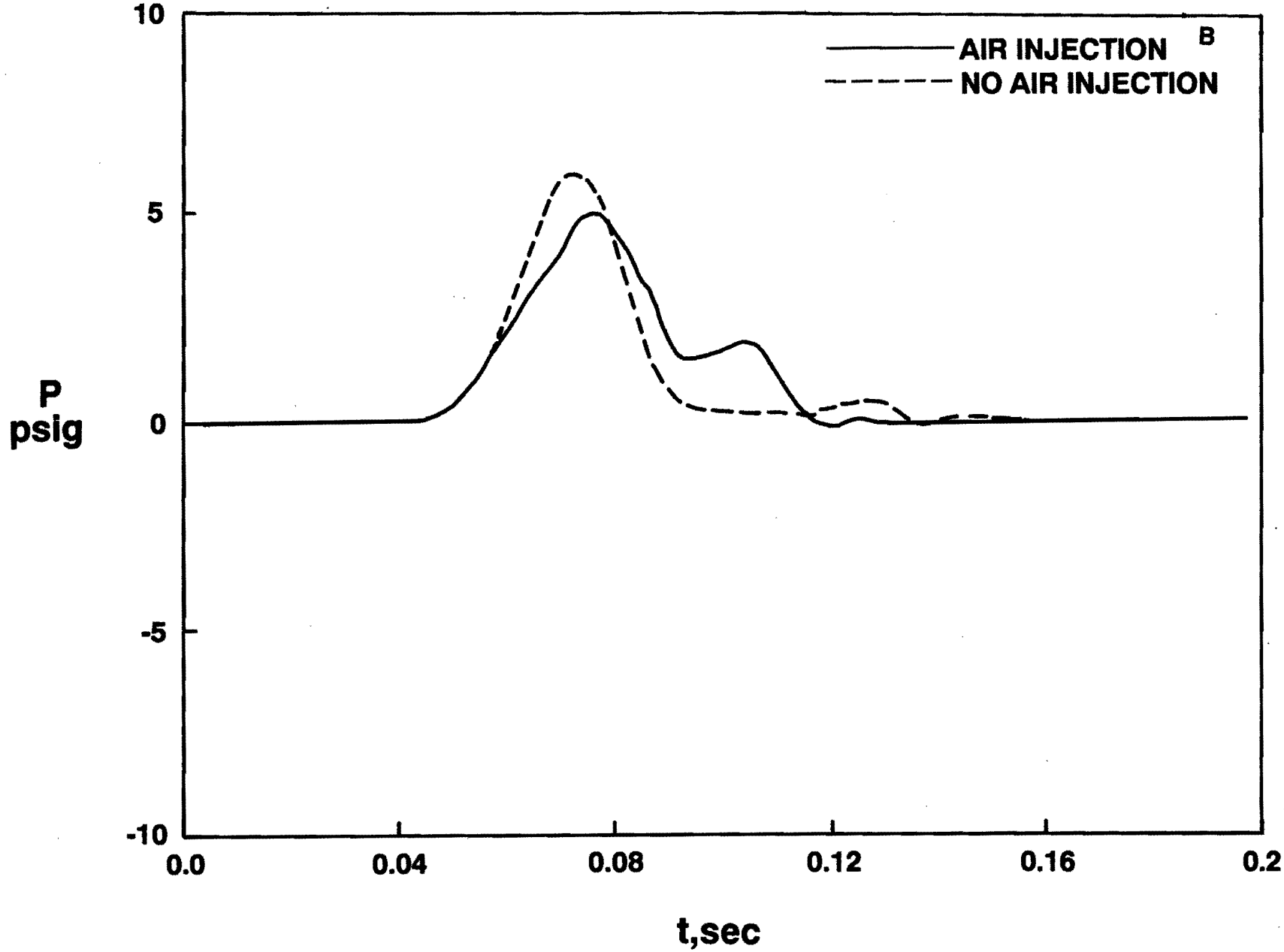

Figure 52. Performance of the 4' x 4' x 1' Airbag Operated with a Constant Vent (0.903 ft^2) with and without Air-Injection: B. Air Pressure

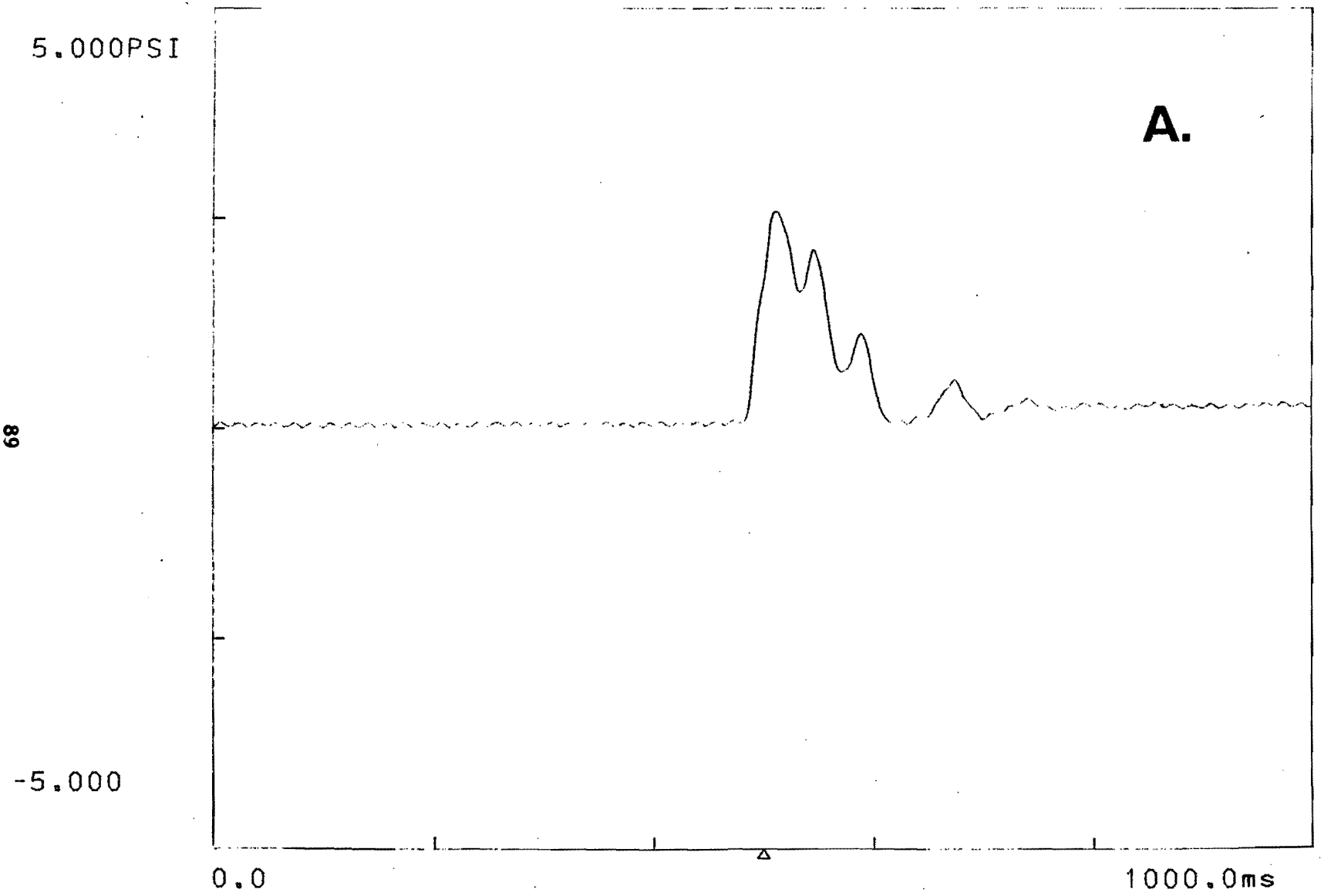

Figure 53. Comparison of Air Pressure of the 4' x 4' x 1' Airbag Operated without Air-Injection (A)

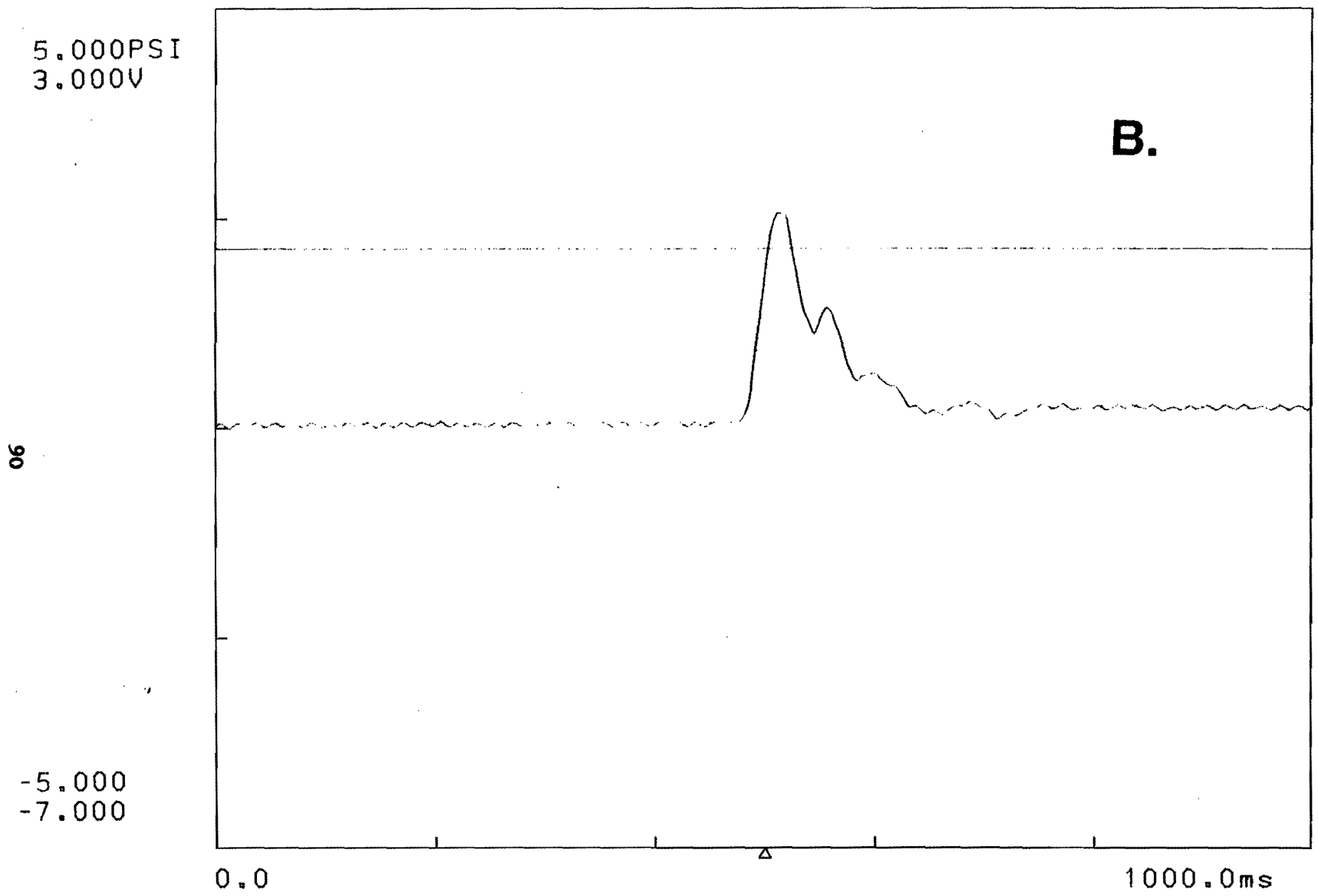

Figure 53. Comparison of Air Pressure of 4' x 4' x 1' Airbag Operated with Air Injection during Airbag Compression (B)

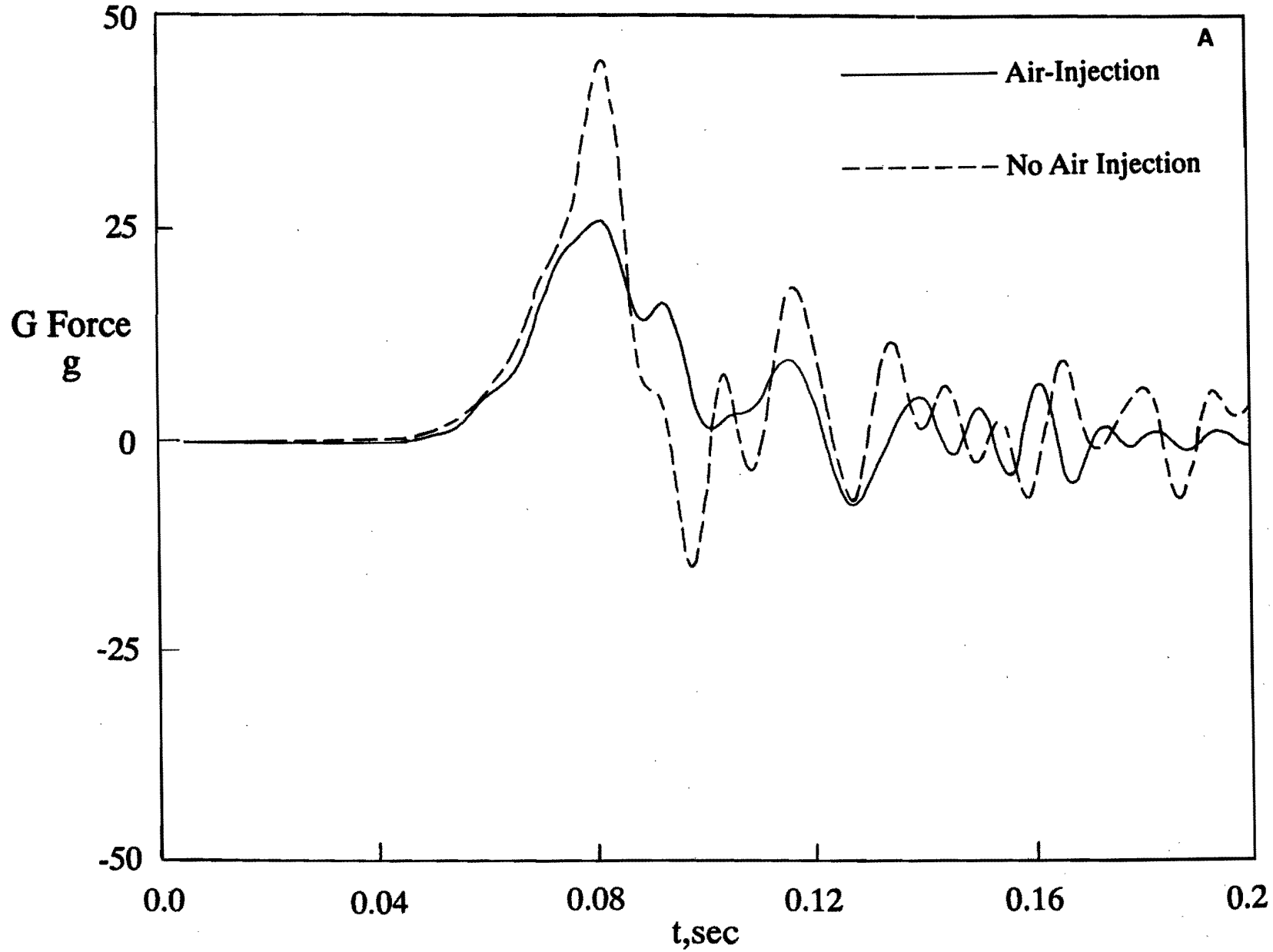

Figure 54. Comparison of the 4' x 4' x 1' Airbag Performance Operated without Air-Injection: A. G Force

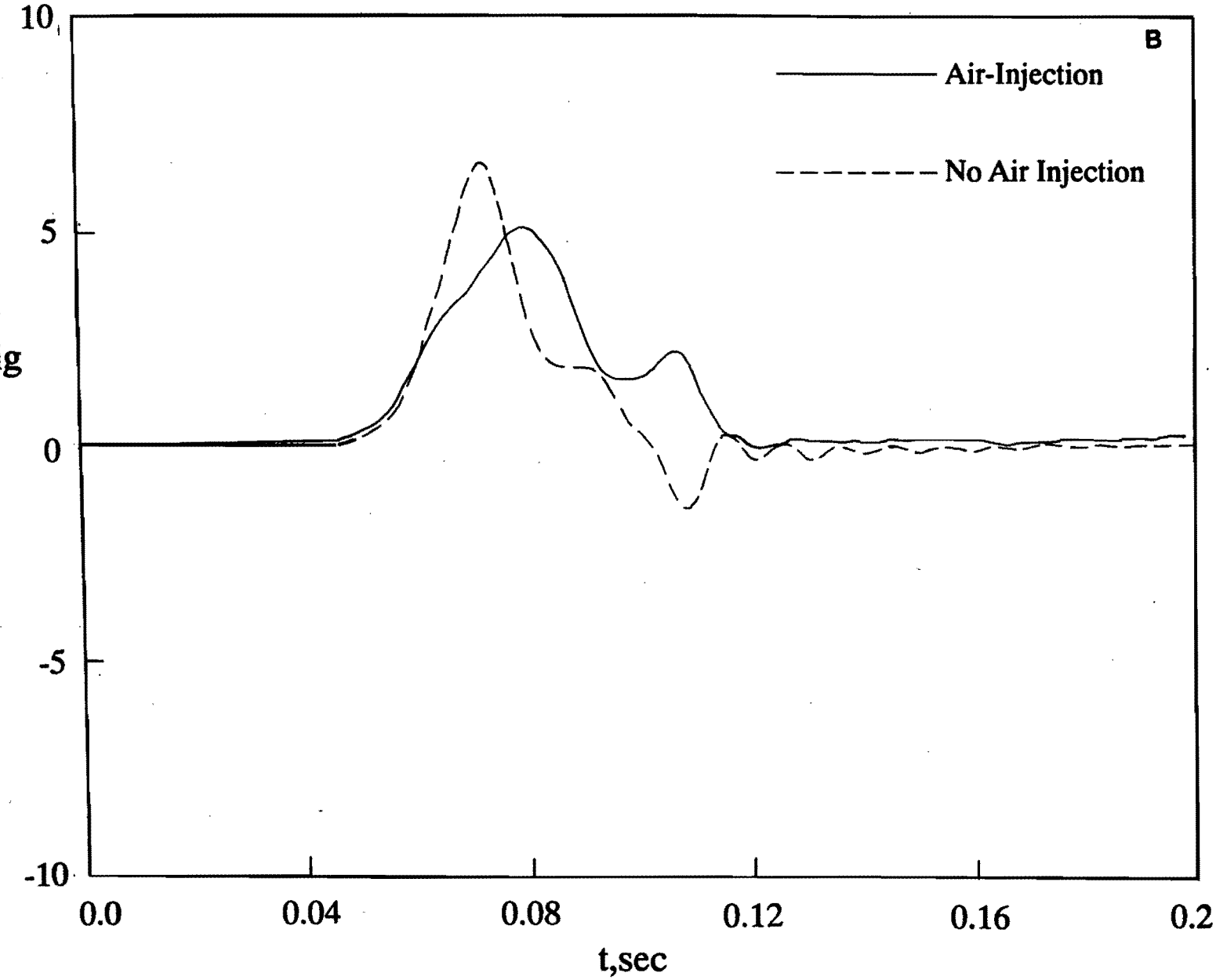

Figure 54. Comparison of the 4' x 4' x 1' Airbag Performance Operated with Air-Injection: B. Air Pressure

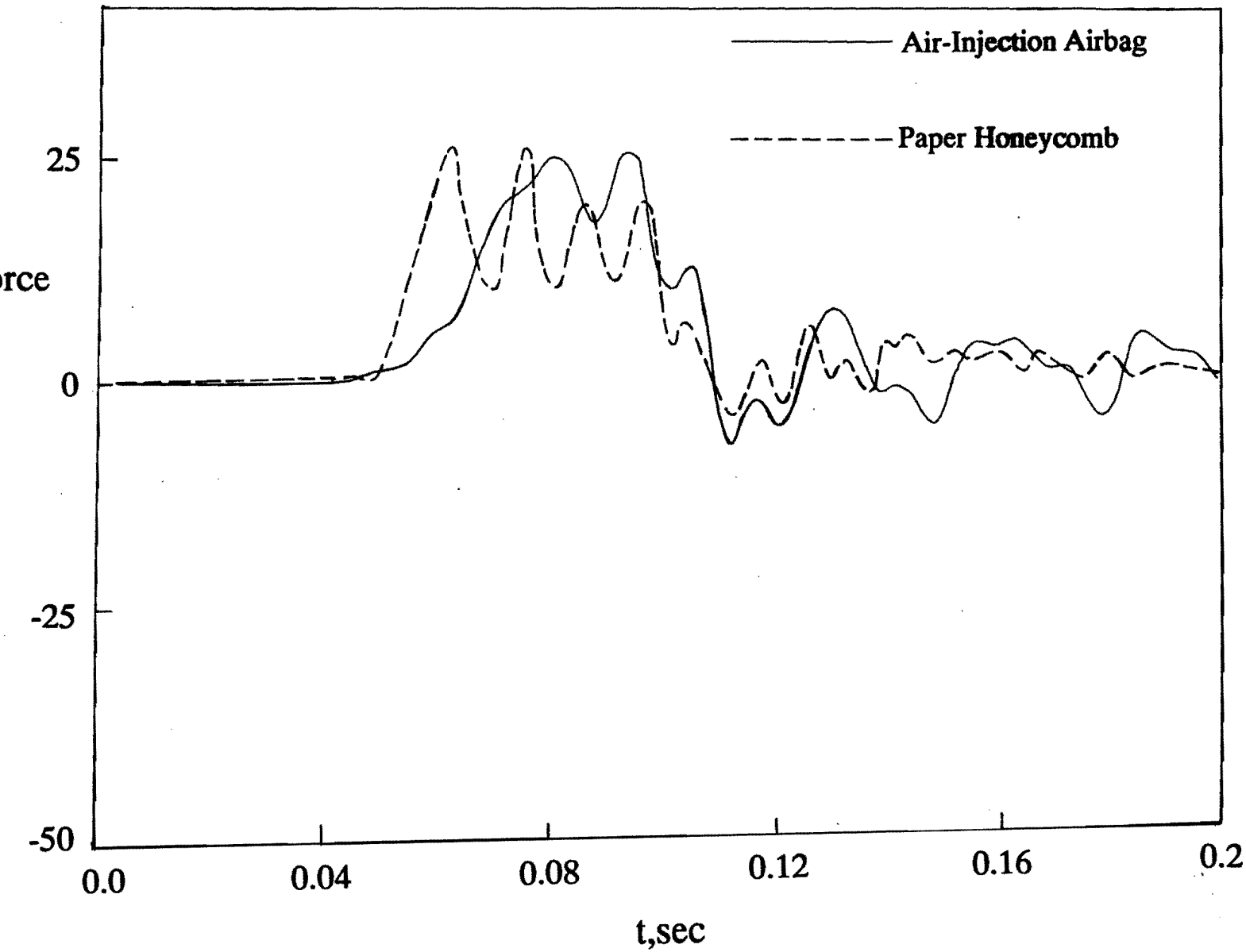

Figure 55. G Force Comparison of the 4' x 4' x 1' Air-Injection Airbag and paper honeycomb

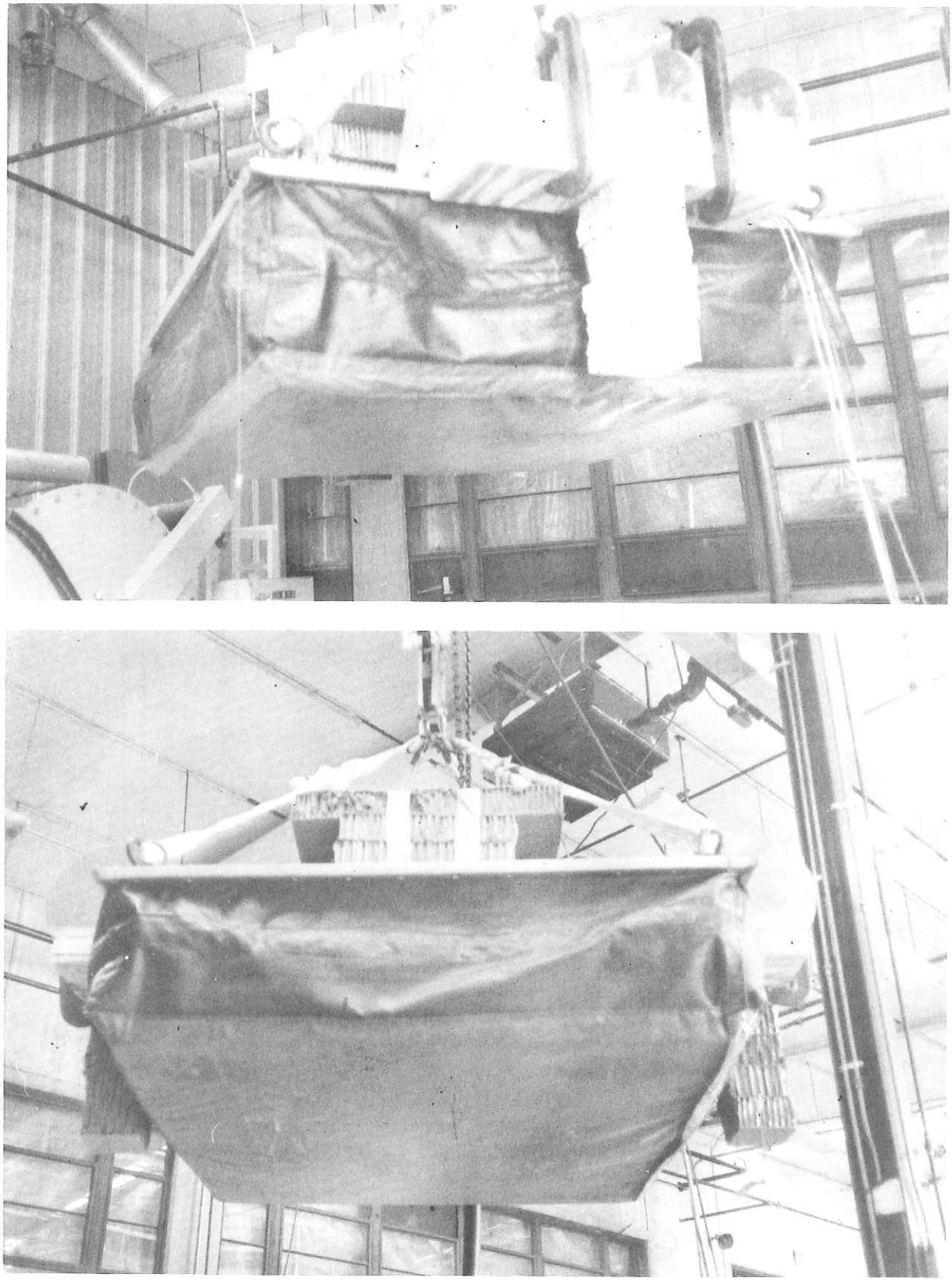

Figure 56. Photographs Showing the 4' x 4' x 1' Augmented Airbag Using Paper Honeycomb

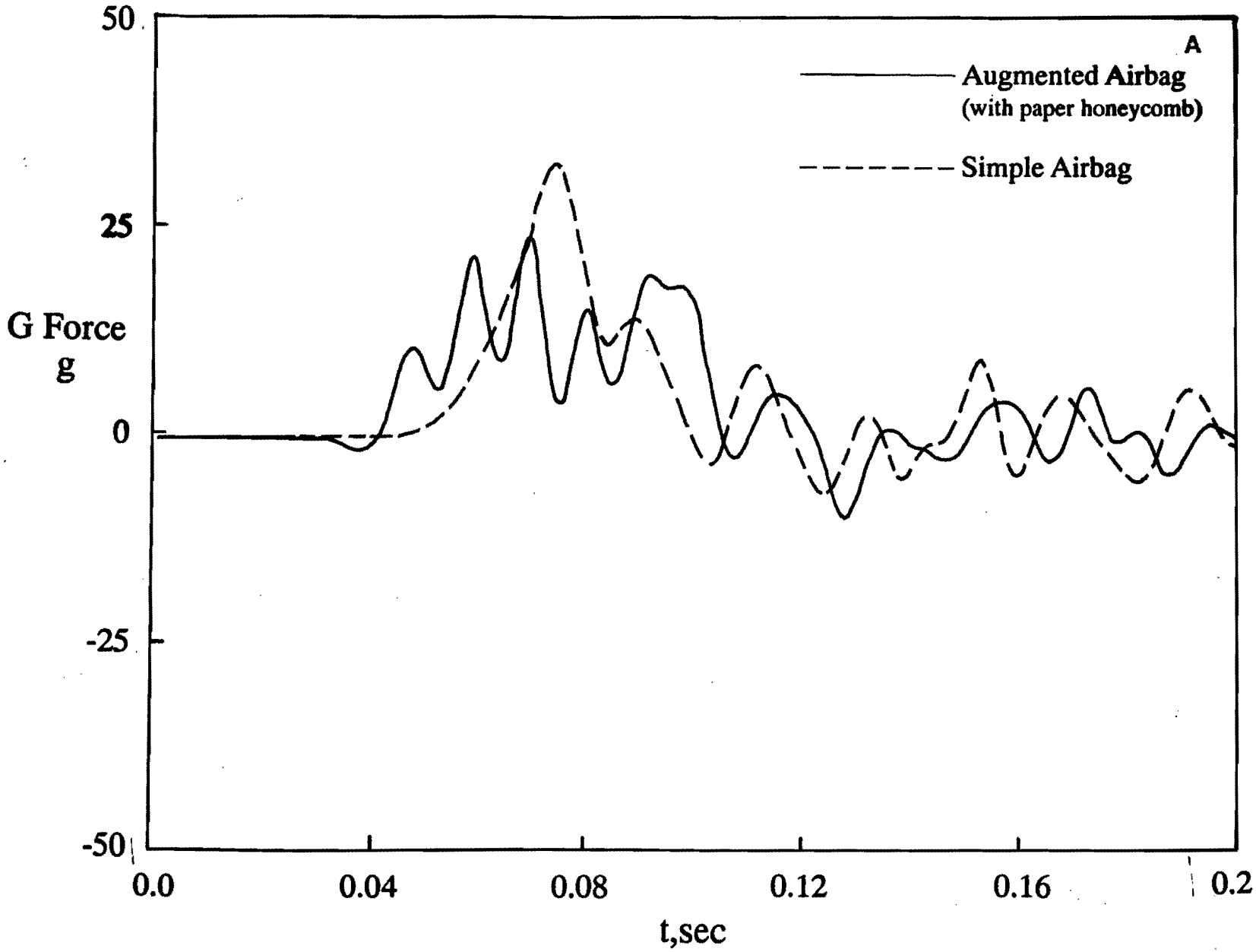

Figure 57. Performance Comparison (Two Tests) of the 4' x 4' x 1' Augmented Airbag and Simple Airbag: A. G Force

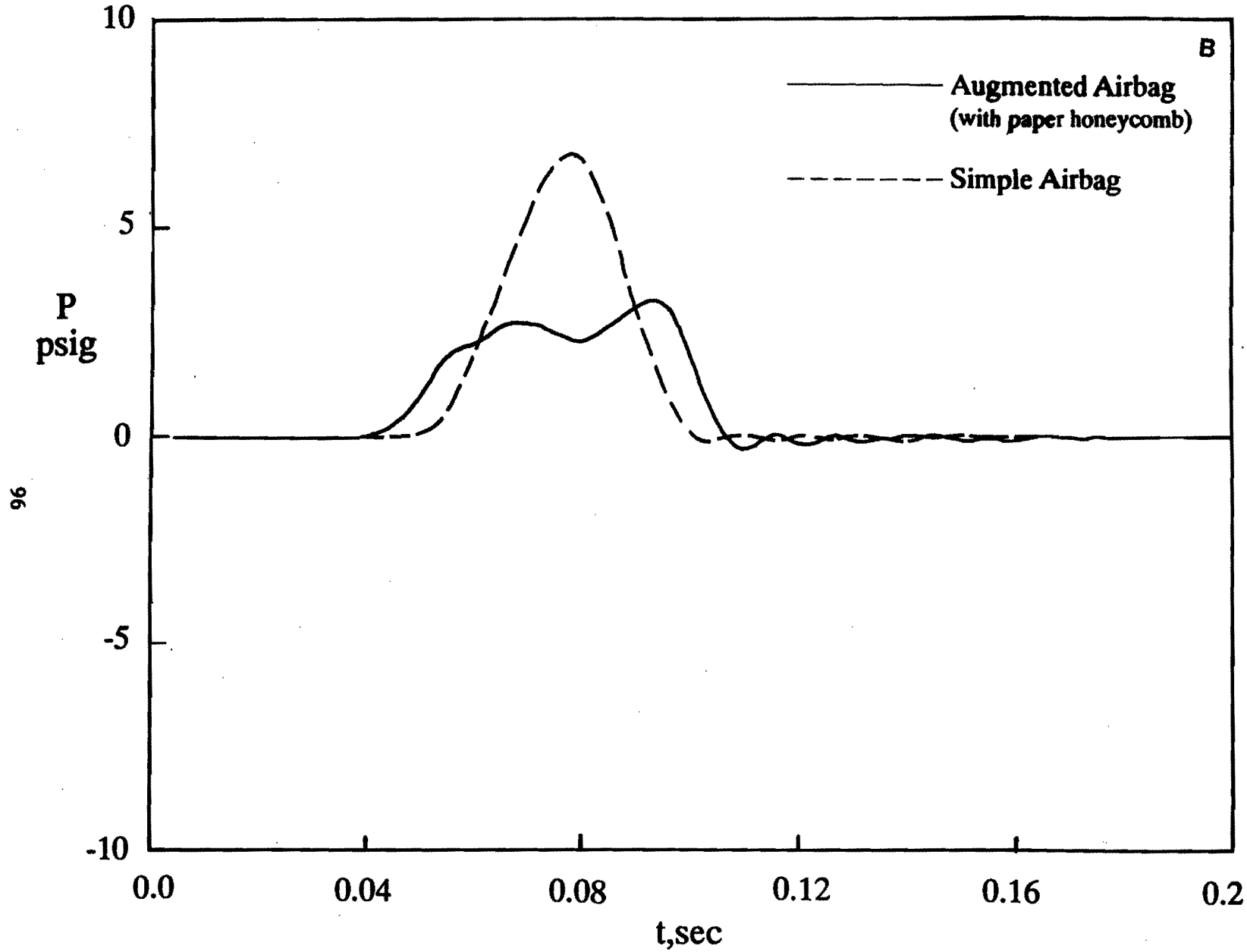

Figure 57. Performance Comparison (Two Tests) of the 4' x 4' x 1' Augmented Airbag and Simple Airbag: B. Air Pressure

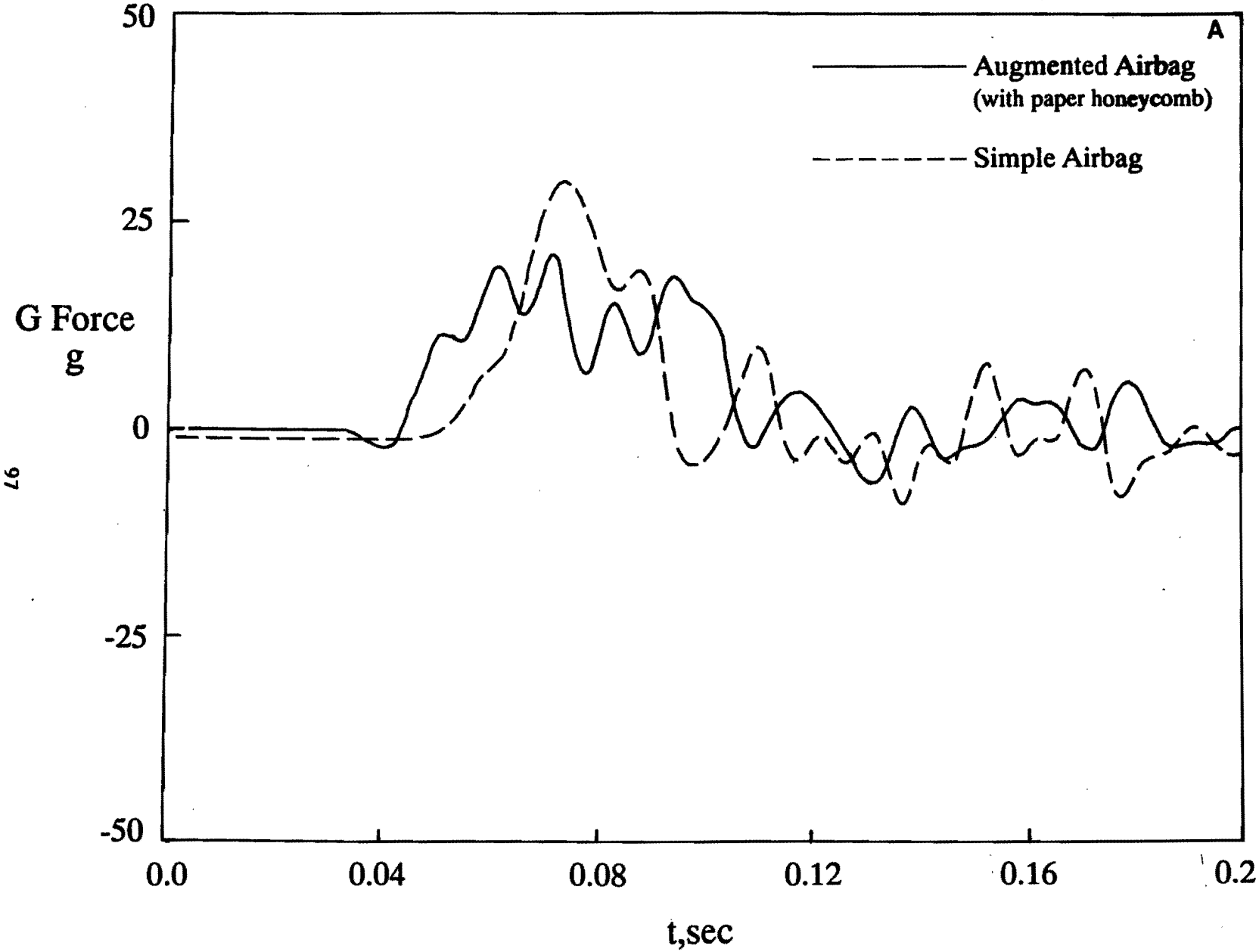

Figure 58. Performance Comparison (Two Tests) of the 4' x 4' x 1' Augmented Airbag and Simple Airbag: A. G Force

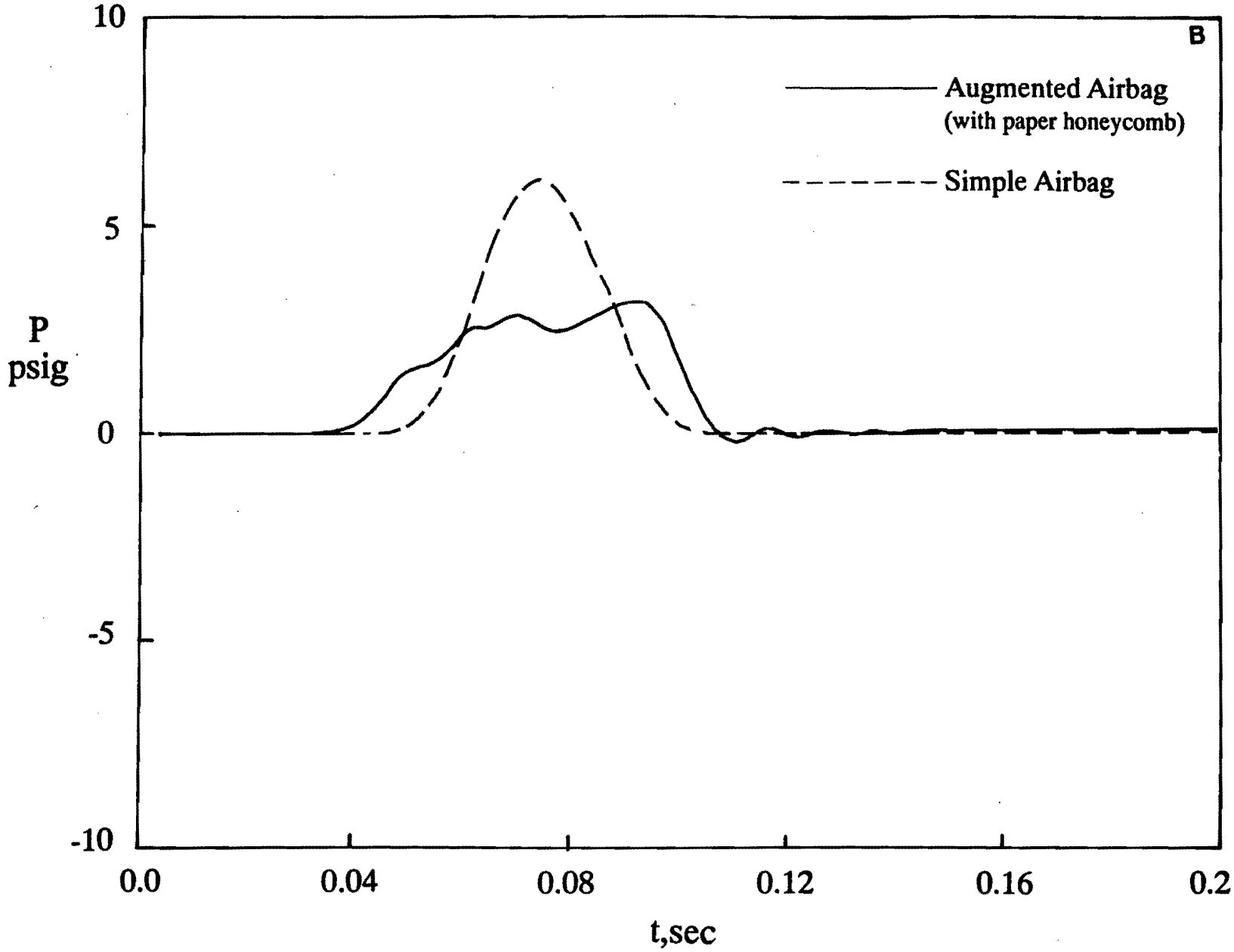

Figure 58. Performance Comparison (Two Tests) of the 4' x 4' x 1' Augmented Airbag and Simple Airbag: B. Air Pressure

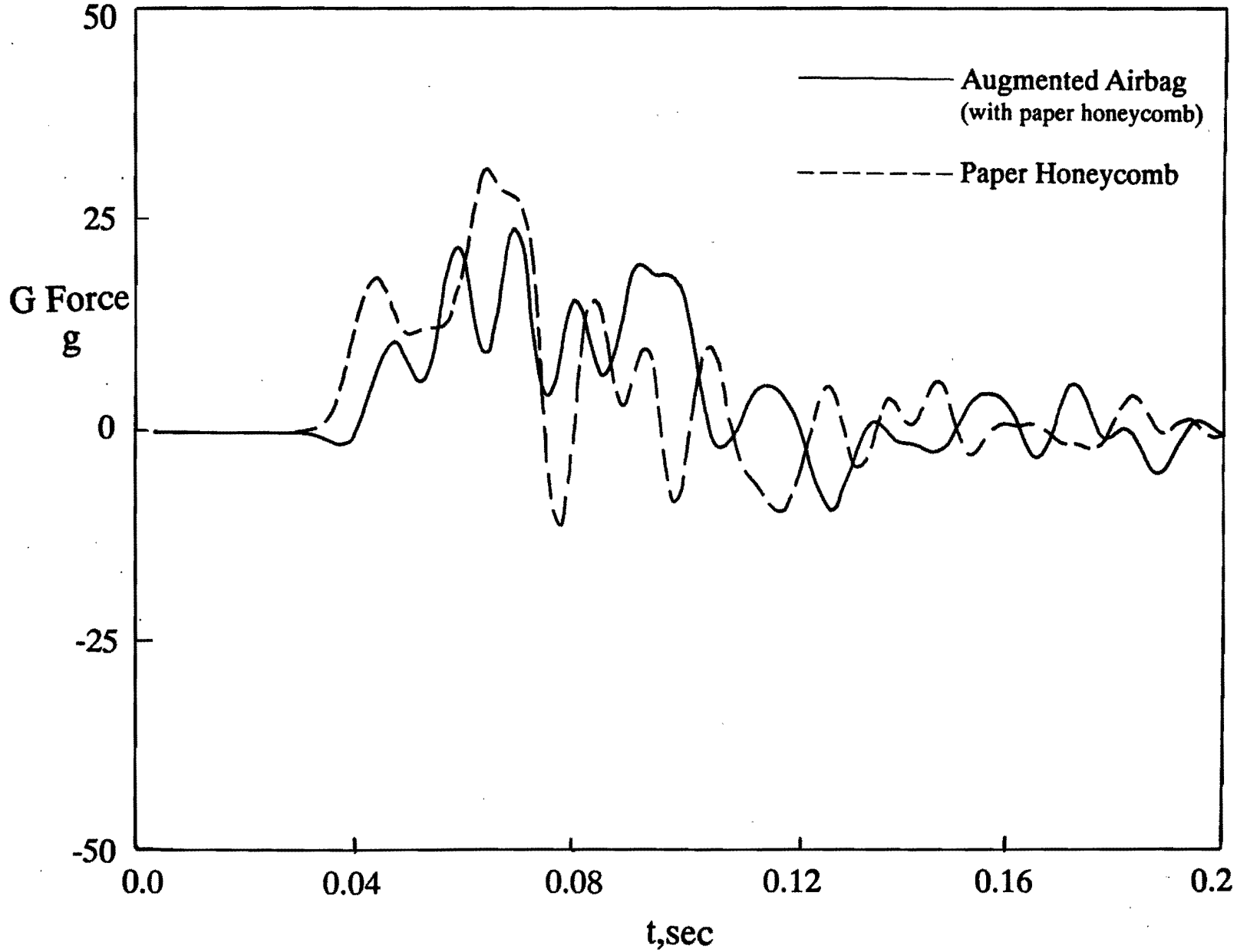

Figure 59. G Force Comparison of the 4' x 4' x 1' Augmented Airbag and Paper Honeycomb

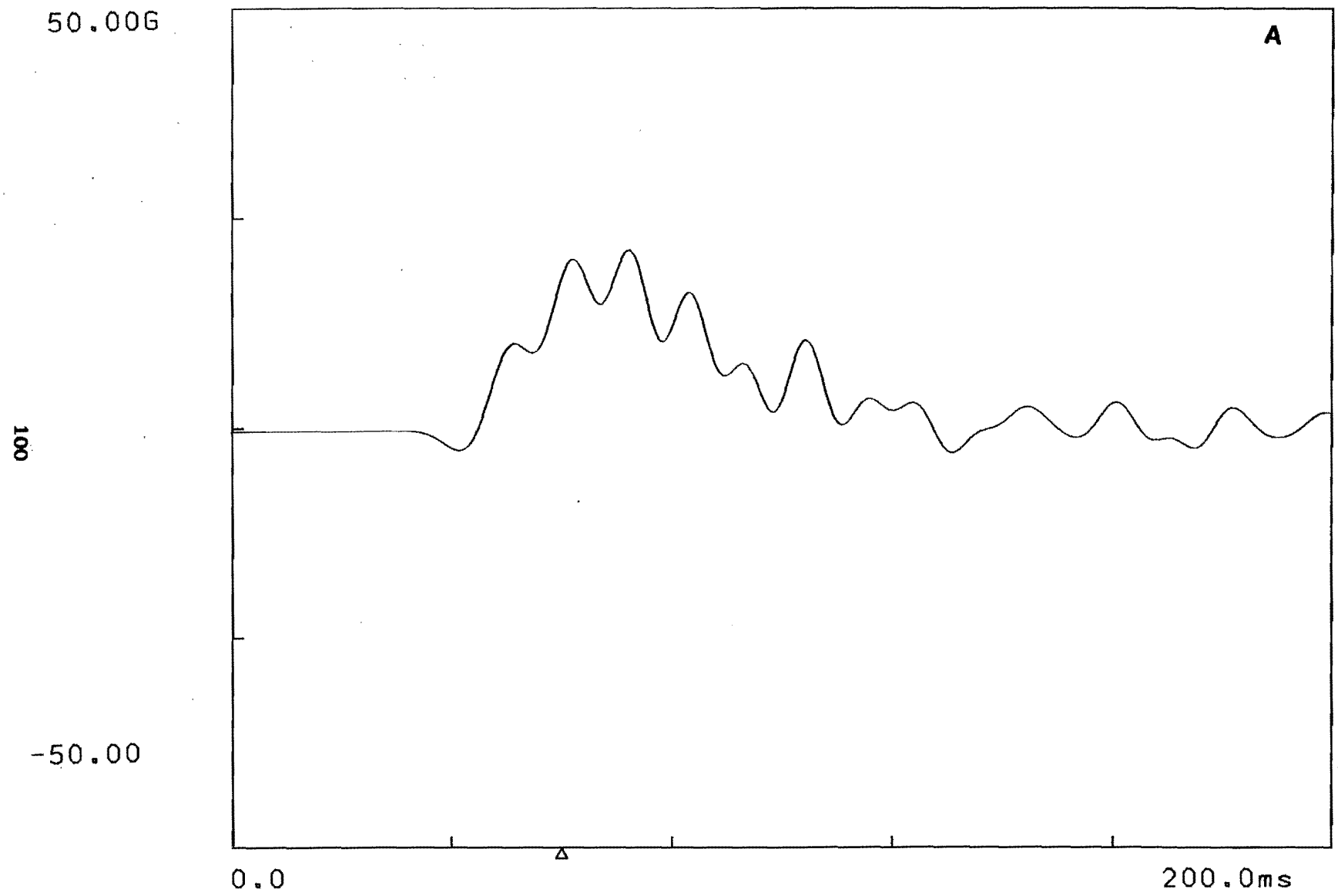

Figure 60. Performance of the 4' x 4' x 1' Augmented Airbag with Air-Injection: A. G Force

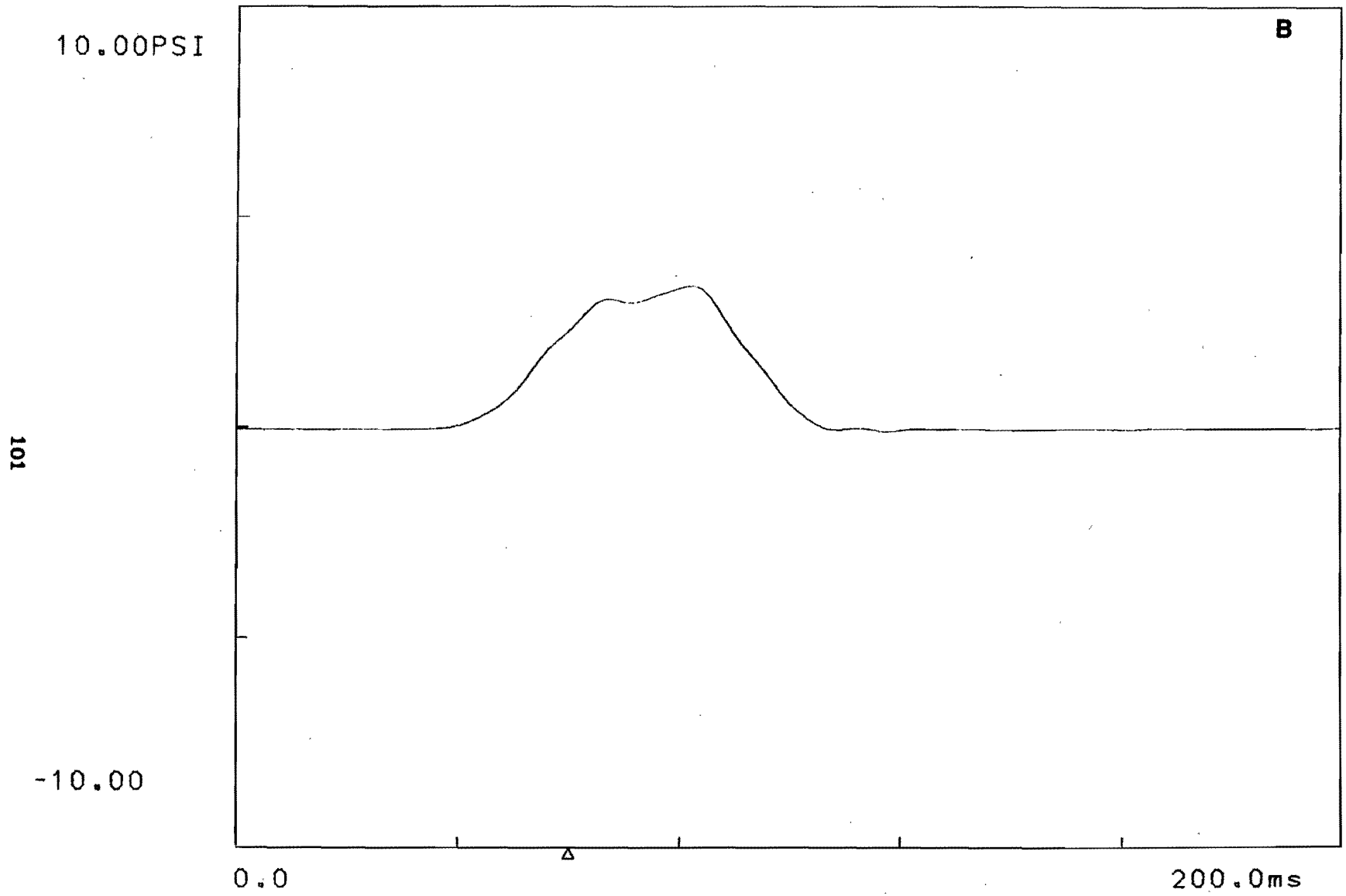

Figure 60. Performance of the 4' x 4' x 1' Augmented Airbag with Air-Injection: B. Air Pressure

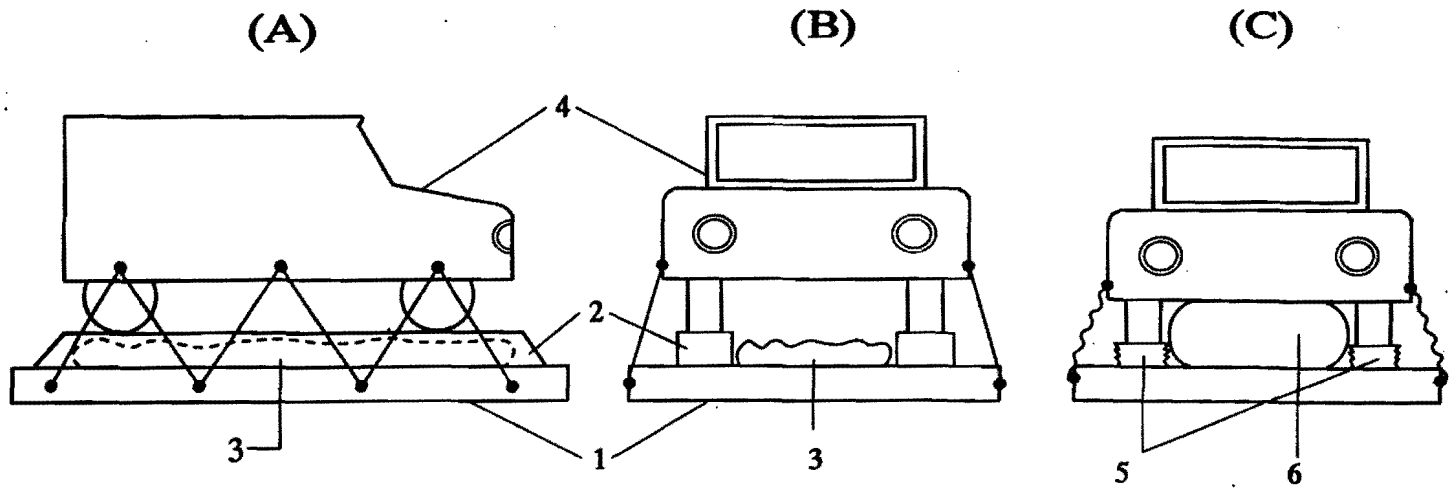

1. Platform
2. Paper Honeycomb
3. Deflated Airbag
4. Vehicle
5. Crushed Paper Honeycomb
6. Inflated Airbag

Figure 61. Schematics Showing the Concept of Using Air-Injection Airbags Augmented by Paper Honeycomb for Airdrop of a Vehicle